Dissertation

submitted to the

Combined Faculty of Natural Sciences and Mathematics

of the Ruperto Carola University Heidelberg, Germany

for the degree of

Doctor of Natural Sciences

Presented by

Elisabeth Drucker, M.Sc.

born in: Vienna, Austria

Oral examination: 05/15/2019

FUNCTIONAL AND MECHANISTIC CHARACTERIZATION OF THE NUCLEAR IMPORT RECEPTOR KARYOPHERIN-α2 IN LIVER CANCER

Referees:

Prof. Dr. Ursula Klingmüller

Prof. Dr. Kai Breuhahn

For my mom,

a woman who cherished the merit of wisdom.

ABBREVIATIONS

AASLD	American Association for the Study of Liver Diseases
AFLD	Alcoholic fatty liver disease
ASH	Alcoholic steatohepatitis
ATF-2	Activating transcription factor 2
BCLC	Barcelona Clinic Liver Cancer
BSA	Bovine serum albumin
CAS	Cellular apoptosis susceptibility (also XPO2)
CDC2	Cell division cycle protein 2 homolog (gene, also CDK1 (protein))
ChIP	Chromatin immunoprecipitation
ChIP-Seq	ChIP (DNA) sequencing
CoIP	Co-immunoprecipitation
CTNNB1	β-catenin
COX2	Cyclooxygenase 2
CRM1	Chromosomal maintenance 1 (also XPO1)
ctrl	Control
DMEM	Dulbecco's Modified Eagle Medium
DMSO	Dimethyl sulfoxide
EASL	European Association for the Study of the Liver
EDTA	Ethylenediaminetetraacetic acid
FBP-1/2	Fuse binding protein 1/2
FCS	Fetal calf serum
FFPE	Formalin-fixed paraffin-embedded
FIR	FBP-interacting repressor
GMPS	Guanosine monophosphate synthetase
GTSF1	Gametocyte-specific factor 1

ABBREVIATIONS

HBV	Hepatitis B virus
HCV	Hepatitis C virus
HCC	Hepatocellular carcinoma
HGF	Hepatocyte growth factor
HMOX1	Heme oxygenase 1
H&E	Hematoxylin and eosin
IgG	Immunoglobulin G
IHC	Immunohistochemistry
IP	Immunoprecipitation
KPNA	Karyopherin-alpha
KPNB	Karyopherin-beta
LC-MS/MS	Liquid chromatography tandem mass spectrometry
LIHC	Liver hepatocellular carcinoma
MAPK	Mitogen-activated protein kinase
MCM2	Mini-chromosome maintenance protein 2
MDM2	Mouse double minute 2 homolog
MDM9	Melanoma differentiation-associated gene 9 (also Syntenin-1)
MT	Microtubule
Mut	Mutated
NAFLD	Non-alcoholic fatty liver disease
NASH	Non-alcoholic steatohepatitis
NCT	National Center for Tumor Diseases
NES	Nuclear export signal
NLS	Nuclear localization signal
NPC	Nuclear pore complex
NSCLC	Non-small cell lung cancer
NT	Non-tumor
NTS	Nuclear transport system

Nup	Nucleoporin
PARP	Poly (ADP-ribose) polymerase
PBS	Phosphate Buffered Saline
PCR	Polymerase chain reaction
PMSF	Phenylmethylsulphonyl fluoride
P/S	Penicillin-Streptomycin
qRT-PCR	Quantitative reverse transcription polymerase chain reaction
RIPA	Radioimmunoprecipitation assay
RPL32	Ribosomal protein L32 (gene)
RPMI	Roswell Park Memorial Institute
SD	Standard deviation
SRSF6	Serine and arginine rich splicing factor 6
STMN1	Stathmin (gene)
TCGA	The Cancer Genome Atlas
TFDP1	Transcription factor DP1
TMA	Tissue microarray
TPX2	Targeting protein for *Xenopus* kinesin-like protein 2
TRACE	Transcatheter arterial chemoembolization
UPLC	Ultra performance liquid chromatography
wt	Wildtype
XPO1	Exportin-1 (also CRM1)
XPO2	Exportin-2 (also CAS)

ABSTRACT

Exchange of macromolecules between the nucleo- and cytoplasm is provided by the nuclear transport system (NTS). Karyopherins represent essential components of NTS) by serving as nuclear transport receptors/adaptor proteins. Dysregulation of karyopherins in (hepato-) carcinogenesis, including the pivotal nuclear import factor karyopherin-α2 (KPNA2), has been previously reported. However, the functional and regulatory role of KPNA2 in hepatocellular carcinoma (HCC) remains incompletely understood. To further characterize KPNA2 in this context, mass spectrometry-based proteomics was combined with functional/mechanistic cell-based approaches and data derived from murine and human HCC samples. Quantitative mass spectrometry upon siRNA-mediated KPNA2 knockdown in HCC cells revealed the microtubule-related oncoprotein stathmin among the most downregulated proteins. KPNA2 depletion resulted in impaired colony formation and tumor cell migration in HCC cells, which could be recapitulated by direct knockdown of stathmin. Having identified stathmin as functional relevant "downstream" target of KPNA2 the underlying molecular mechanism of KPNA2-dependent stathmin regulation was dissected. Out of several candidates the transcription factors E2F1 and TFDP1 were identified as transport substrates of KPNA2 and to be retained in the cytoplasm upon KPNA2 ablation followed by reduced *STMN1* expression. Finally, significant correlations of *STMN1* with *E2F1/TFDP1* and *KPNA2* expression were found based on data derived from murine HCC models and human HCC cohorts with high *KPNA2* and *STMN1* expression being associated with poorer patient outcome.

Taken together, these data suggest that KPNA2 regulates *STMN1* by mediating nuclear import of E2F1/TFDP1 and thereby provide a functionally relevant link between the NTS and microtubule-interacting proteins in HCC. Though further studies are required, interfering with nuclear import factors such as KPNA2 could represent a promising therapeutic approach in liver cancer.

KURZDARSTELLUNG

Das Kerntransportsystem (*nuclear transport system*, NTS) gewährleistet den Austausch von Makromolekülen zwischen dem Nukleo- und Zytoplasma. Karyopherine stellen essentielle Komponenten des NTS dar, indem sie als nukleäre Transportrezeptoren bzw. Adapterproteine fungieren. Eine Dysregulation von Karyopherinen, einschließlich des wichtigen nukleären Importfaktors Karyopherin-α2 (KPNA2), in der (Hepato-) Karzinogenese, wurde bereits beschrieben. Allerdings sind die damit verbundenen funktionellen Effekte und deren Mechanismen bislang nur unzureichend aufgeklärt. Um in diesem Kontext KPNA2 näher zu charakterisieren, wurde Massenspektrometrie-basierte Analytik mit funktionellen/mechanistischen zell-basierten Ansätzen und Daten aus murinen und humanen HCC (hepatozelluläres Karzinom)-Proben kombiniert. Mit Hilfe der quantitativen Massenspektrometrie konnte nach siRNA-vermitteltem Knockdown von KPNA2 in HCC Zellen das Mikrotubuli (MT)-interagierende Onkoprotein Stathmin (STMN1) als eines der am stärksten herunterregulierten Proteine identifiziert werden. Der KPNA2-Knockdown führte ferner zu einer verringerte Klonogenität und einem verringerten Migrationsvermögen der HCC Zellen, welche auch nach direktem Knockdown von Stathmin beobachtet werden konnten. Da sich Stathmin somit als funktionell relevantes “downstream target” von KPNA2 darstellte, wurde der zu Grunde liegende Mechanismus genauer untersucht. Aus einer Gruppe von mehreren Kandidaten konnten die Transkriptionsfaktoren E2F1 und TFDP1 als Cargos von KPNA2 identifiziert werden, die nach KPNA2 Knockdown einen Importdefekt mit konsekutiver Verringerung der *STMN1* Expression aufwiesen. Darüber hinaus fanden sich signifikante Korrelationen zwischen der *STMN1* und der *E2F1/TFDP1* sowie der *KPNA2* Expression in den murinen HCC Proben und in HCC Patientenkollektiven, wobei eine hohe *KPNA2*- und *STMN1*-Expression mit einer schlechten Prognose verbunden war.

Zusammenfassend weisen die genannten Daten darauf hin, dass KPNA2 über den nukleären Import von E2F1/TFDP1 die *STMN1*-Expression reguliert und stellen damit eine funktionell relevante Verbindung zwischen dem NTS und MT-interagierenden Proteinen im HCC her. Vorbehaltlich noch weiterer erforderlicher Untersuchungen, könnten nukleäre Importfaktoren wie KPNA2 vielversprechende therapeutische Zielstrukturen im HCC darstellen.

TABLE OF CONTENTS

1 INTRODUCTION

1.1 Hepatocellular carcinoma

1.1.1 Etiology and prevalence of HCC

Liver cancer comprises several histologically different primary malignancies including hepatocellular carcinoma, cholangiocarcinoma (intrahepatic bile duct carcinoma) and hepatoblastoma [1, 2]. Hepatocellular carcinoma (HCC) is the most prevalent primary liver cancer with increasing incidence worldwide. With almost 800,000 new cases a year, HCC is the fifth most frequent cancer in men and the ninth most frequent cancer in women. Therapeutic options are limited making HCC the second most lethal malignancy after lung cancer [3–5].

HCC usually develops out of chronic liver disease. Around 85% of HCC cases arise from chronic hepatitis B or C viral infection (HBV/HCV), which increase the lifetime risk of developing HCC by 15-20 fold compared to the non-infected population [4, 6]. Both infections endorse the development of liver cirrhosis, which further promotes hepatocarcinogenesis [4]. Furthermore, alcoholic fatty liver disease (AFLD) and non-alcoholic fatty liver disease (NAFLD), which can progress to alcoholic steatohepatitis (ASH) and non-alcoholic steatohepatitis (NASH) [7–9], aflatoxin-B1-contaminated food and with lower frequency metabolic disorders like hereditary haemochromatosis can contribute to the development of HCC [8, 9]. Due to the high incidence rate of HBV and HCV infections along with the widespread contamination of agricultural products with aflatoxin-B1, HCC is especially prevalent in less developed regions such as the sub-Saharan Africa, and Eastern and South-Eastern Asia [3, 4, 10]. While HBV is usually vertically transmitted from mother to child in these high-risk areas, HBV in the western world and HCV in general are predominantly horizontally transmitted (e.g. by sexual intercourse, drug abuse) [4, 8]. HBV infections and therefore future HCC cases are decreasing in Asian countries due to the successful establishment of vaccination programs [11]. In contrast, the great number of HCV infections in the 1960s and 1970s and the raising number of lifestyle-related incidences of obesity-related metabolic disease are leading to a dramatic increase in HCC cases in former low-incidence areas such as the United States and Canada [6, 9, 12].

1.1.2 Pathogenesis of HCC

In HCC, the malignant transformation progresses through a multi-step process as summarized in Figure 1.1. Liver diseases of different etiologies cause hepatocyte damage and therefore induce infinite cycles of cell injury and regeneration, eventually leading to chronic liver disease and ultimately to liver cirrhosis. Cirrhosis is marked by a growth arrest (senescence) of hepatocytes, abnormal liver nodules and

liver scarring. In the further process, hyperplastic nodules progress to dysplastic nodules and finally to HCC and thereby increasingly harbor abnormal cytological features (e.g. nuclear crowding) and genomic instability [2]. Altogether, this malignant transformation process can take 30 years or more [13, 14].

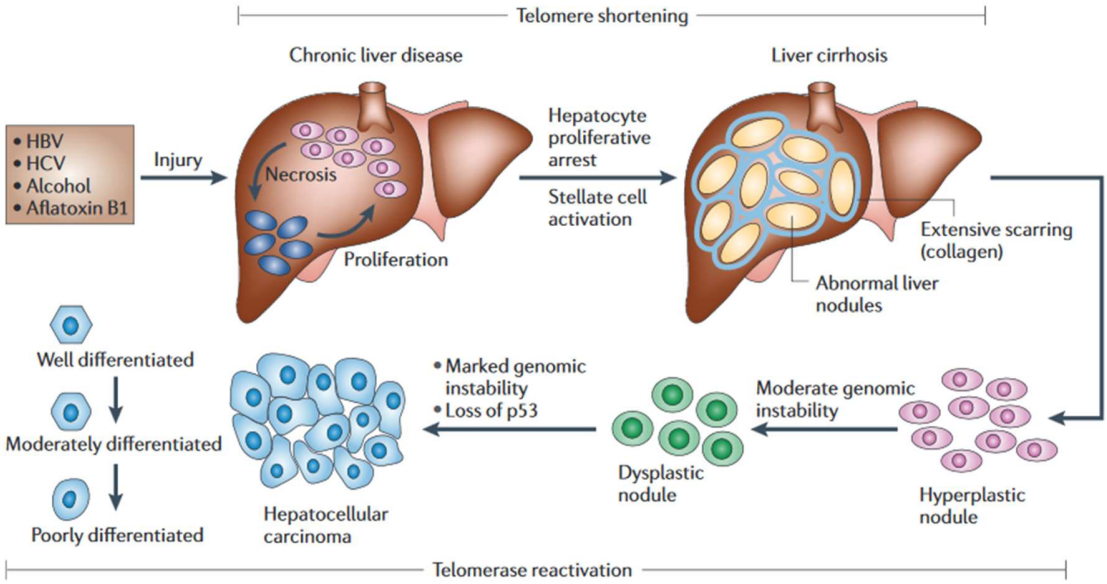

Figure 1.1: Schematic depiction of the multi-step process of hepatocarcinogenesis. Liver diseases of different etiologies cause necrosis, which further fosters hepatocyte proliferation. This process gives rise to chronic liver disease and eventually to liver cirrhosis. Abnormal liver nodules develop and progress to hyperplasic and dysplastic nodules and finally to HCC. Reprinted with permission from [2].

Complementary to the multi-step model of liver carcinogenesis, the stem cell model suggests that HCC cells originate from progenitor cells or de-differentiated transformed cells, paralleling the behavior of embryonic stem cells and cancer stem cells [15].

1.1.3 Molecular alteration in HCC

The hallmarks of cancer, first postulated by Hanahan and Weinberg in 2000, summarize six complementary mechanisms that drive carcinogenesis and tumor progression. Originally, these hallmarks comprised the abilities of tumor cells to sustain unlimited proliferation, evade the action of tumor suppressors, resist apoptosis, induce angiogenesis, harbor replicative immortality and are capable of invasion and metastasis [16]. Revising these hallmarks, Hanahan and Weinberg later complemented the described mechanisms by the so-called emerging hallmarks [17]. Therefore, the next generation of the hallmark of cancer includes reprogramming of the cellular energy metabolism and evasion of the immune system by cancer cells [17]. Taken together, these pro-tumorigenic mechanisms are most prominently enabled by the development of genomic instability in malignant cells, generating mutations and chromosomal aberrations [17]. In the

course of molecular hepatocarcinogenesis, genomic aberrations start to occur randomly in pre-malignant lesions and further increase extensively in dysplastic nodules and HCCs [13]. Somatic mutations in cancer cell genomes include point mutations, insertions or deletions of DNA segments and chromosomal translocations, as well as copy number alterations. In case of viral infections exogenous DNA can be integrated in the genome, adding an additional mode how viruses such as HBV can contribute to carcinogenesis [18]. Molecular screenings of human HCCs showed mutations of different (driver) oncogenes and tumor suppressor genes such as *TP53*, *c-MYC, CTNNB1* (β-catenin), *TERT* and *COX2* (cyclooxygenase 2) [2, 13, 19].

The p53 tumor suppressor is a main coordinator of extra- and intracellular stress signals including DNA damage and induces a variety of cellular responses such as DNA damage repair, cell cycle arrest, senescence and apoptosis [20–22]. Following activation, p53 acts as transcription factor, thus trans-activating or -repressing hundreds of different target genes or interacts with other proteins to modulate cellular signaling cascades and thereby mainly activates apoptosis, senescence or, if the damage is reversible, cell-cycle arrest [20, 23–25]. Over 50% of human malignancies acquire mutations in the *TP53* gene or in genes that encode for proteins interfering with the p53 network, which highlights its outstanding significance in tumor biology [22, 26, 27]. The vast majority of cancer-related *TP53* mutations affect the p53 DNA binding domain and therefore p53's function as transcriptional activator [22]. Moreover, mutations in the *TP53* locus are usually either accompanied by loss of heterozygosity in the course of tumor progression or the mutated proteins exert a dominant-negative behavior over the left wildtype allele [28–30]. Additionally, the p53 pathway can be inactivated via amplification and subsequently over-activation of p53-inhibitors (e.g. MDM2, MDMX) or binding to viral proteins. Controversially, gain-of-function mutations can transform p53 into a potent oncogene [20–22, 26, 31]. In conclusion, loss of p53 wild-type function is beneficial for (hepato-)carcinogenesis and tumor progression, enabling tumor cells to inactivate multiple tumor-suppressive responses by inactivation of one key protein. Next to mutations in p53, WNT/β-catenin signaling is among the most frequently altered pathways in HCC [32]. This pathway is usually involved in embryogenesis and tightly regulated during fetal liver development [5, 32]. Induction of the canonical WNT pathway triggers enrichment of β-catenin in the cytoplasm followed by translocation into the nucleus where β-catenin can act as transcription factor for genes involved in differentiation, proliferation and tumor initiation [32]. As WNT/β-catenin signaling is involved in embryonic development, activation of this pathway in HCC supports the above-mentioned stem cell model of hepatocarcinogenesis.

Additional to these somatic mutations, shortening of telomeres in combination with chronic liver disease and turnover of hepatocytes has been described to trigger genomic instability which further promotes HCC initiation. On the contrary, a strong increase in *TERT* expression and therefore reactivation of telomerase is a characteristic of HCC progression and was found in nearly all human HCCs [2, 19]. Next to molecular alterations, epigenetic changes, i.e. variations in the methylation of chromatin residues that subsequently alter gene expression, have been observed in different stages of hepatocarcinogenesis [18][2]. Altogether, HCCs show a broad heterogeneity in genomic alterations which ultimately affect multiple signaling pathways [13].

1.1.4 Surveillance, diagnosis and treatment options

Since HCC is often diagnosed in late stages due to the lack of clinical symptoms, the European Association for the Study of the Liver (EASL-EORTC) and the American Association for the Study of Liver Diseases (AASLD) guidelines recommend surveillance of high risk patients by ultrasonography every six months [33–35]. However, surveillance programs are controversially discussed due to their dependency on the ultrasonography operator, the question whether prognostic markers (e.g. α-fetoprotein) are suitable for early detection of HCC and the inconsistent results of different surveillance program meta-analyses [36].

As surveillance, diagnosis is usually done using different imaging techniques and, if results are inconclusive, by additional biopsy analyses [36]. Tumor staging is pivotal for the choice of the appropriate treatment regime. Several different staging systems exist with the Barcelona Clinic Liver Cancer (BCLC) classification being the most effective for prognosis and selection of therapy [33, 37]. Depending on the stage of HCC at the point of diagnosis, different treatment options are implemented. Curative therapies include tumor resection, liver transplantation and local ablation (radiofrequency or ethanol injection), while transcatheter arterial chemoembolization (TRACE) and systemic therapies are applied in patients with intermediate and advanced HCCs [33, 38]. Far advanced HCC is untreatable and usually lethal within 3-6 months. In this stage, patients only receive palliative care [33, 36].

The high mortality is partially due to resistance to established anti-cancer drugs, a lack of reliable biomarkers and the causal liver disease which limits chemotherapeutical treatment options [2]. Sorafenib is the first-line therapy for patients with advanced HCC and increases the average survival of patients from 7.9 to 10.7 months with manageable side-effects [33, 39]. Sorafenib is an oral multi-kinase inhibitor that disables the Ras-Raf-MAP2K-MAPK pathway, thereby blocking angiogenesis, proliferation and migration and ultimately the resistance to apoptosis [40]. So far, Sorafenib, which was approved in 2008, has been the only systemic treatment for advanced HCC. In a recent study, Regorafenib, an oral multi-kinase

inhibitor used for the treatment of colorectal and gastrointestinal cancer, showed a further survival benefit in HCC patients that progressed under Sorafenib treatment and was approved as second-line therapy [41, 42]. Other promising drug candidates tested in different studies as first-line treatments either did not improve overall survival or showed an adverse toxicity profile compared to Sorafenib [42].

Intra-tumor heterogeneity, cell plasticity and resistance mechanisms put a limit on highly selective therapeutic approaches in HCC. Combined systemic treatments are often accompanied by high liver toxicity which is unfavorable in combination with the underlying chronic liver disease [38]. A deeper understanding of the molecular mechanisms that shape the malignant phenotype of HCC cells is critical to identify novel drug targets and will provide the basis for improved therapeutic approaches [43].

1.2 The nuclear transport system

1.2.1 Nuclear import and export mechanisms

The eukaryotic nucleus is separated from the cytoplasm by the nuclear envelope, thereby not only uncoupling transcription and translation, but also adding an additional mode of protein activity regulation [44–46]. To enable controlled transport in and out of the nucleus, protein channels, the nuclear pore complexes (NPC), are enclosed in the nuclear membrane. An average NPC is composed of roughly 30 different proteins, most of them so-called nucleoporins (Nups, Figure 1.2), and has a molecular mass of approximately 125 MDa [44–47].

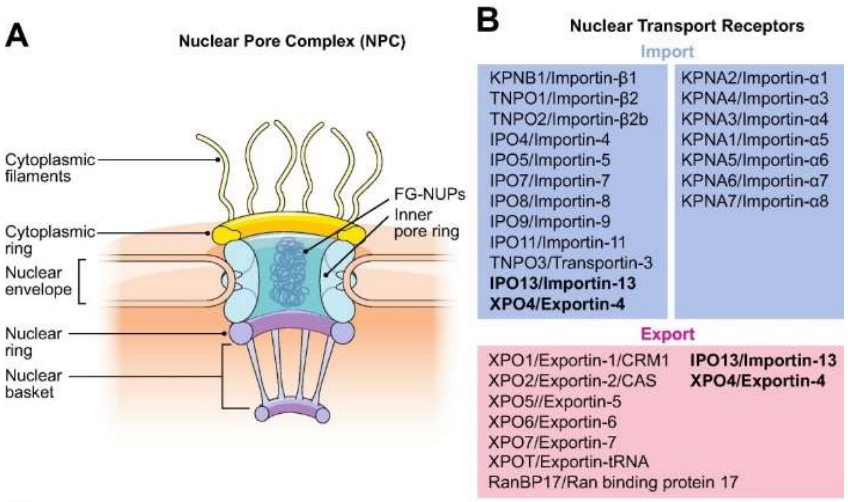

Figure 1.2: Components of the nuclear transport system. Structure of the NPC and its sub-complexes. **(B)** List of nuclear import and export receptors (bold: bi-directional shuttling receptors). Reprinted and modified with permission from [48].

Molecules smaller than 40 kDa (e.g. ATP) can diffuse freely through the NPCs, however, the transport of larger molecules (e.g. proteins, RNAs, ribosomal subunits) relies on an active transport system [46, 47, 49–51]. The canonical nucleocytoplasmic transport of proteins is facilitated by interactions between the cargo molecule, nuclear transport receptors (NTRs; e.g. importins, exportins, karyopherins) and the small GTPase Ran [44, 46]. In order to be imported, proteins have to contain a specific sequence, the nuclear localization signal (NLS), whereas proteins for export are labeled by a nuclear export signal (NES) [44, 46]. Protein shuttling across the nuclear envelope requires the following steps: recognition of the cargo protein (i.e. the import or export signal) by a receptor, binding of the protein-receptor complex to the NPC, transition of the transport channel and eventually the recycling of the transport receptors [52]. Thereby, the transport rate is controlled by the RanGTPase and its regulators [46].

Most proteins rely on nuclear transport receptors, mostly of the karyopherin superfamily, for their transport in and out of the nucleus. The mammalian karyopherin superfamily includes over 20 members, the so-called importins and exportins [46, 50], which have similar conformations although only having partial sequence identity [49]. There are two subclasses of importins: importin-α (karyopherin-α), an adaptor molecule that binds the cargo-NLS, and importin-β (karyopherin-β), which binds to the importin-α-cargo-complex and leads the trimeric complex through the transport channel. After binding of RanGTP to importin-β, the transport complex dissociates and the cargo is released into the nucleoplasm. Eventually, both karyopherins are translocated back to the cytoplasm: importin-α binds to its export receptor CAS (cellular apoptosis susceptibility) and RanGTP, while the RanGTP-importin-β dimer passes the NPC independently (Figure 1.3 A) [46, 50].

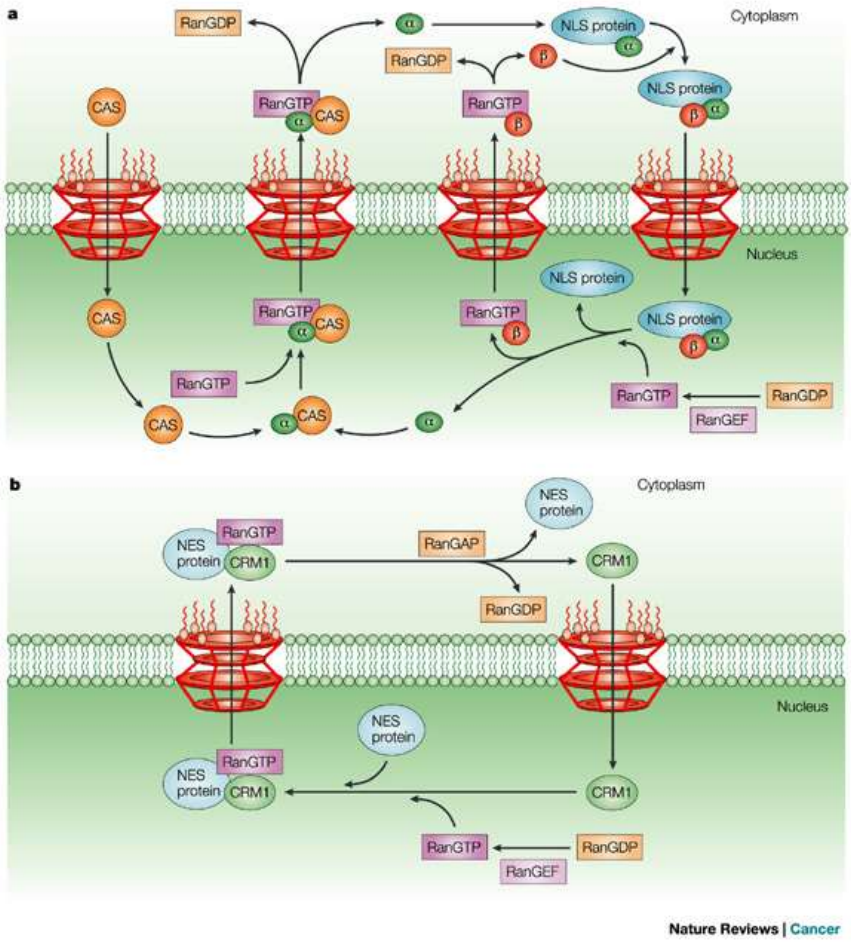

Figure 1.3: Nuclear import and export cycle. (A) Nuclear import: The adaptor protein importin-α (α, green) binds to the nuclear localization signal on the cargo protein (NLS protein, blue) and forms a trimer with importin-β (β, red). The complex passes the nuclear pore complex and enters the nucleus. After binding of RanGTP (purple) to importin-β, the complex dissociates, the cargo is released and the transport receptors are recycled to the cytoplasm [46, 50]. **(B)** Nuclear export: Proteins labeled with a nuclear export signal-specific sequence (NES protein, blue) are recognized by CRM1 (green). The protein-CRM1 complex binds to RanGTP (purple) via CRM1 and passes the NPC. In the cytoplasm, RanGTP is hydrolyzed to RanGDP (orange), the cargo is released and CRM1 is recycled to the nucleus. Reprinted with permission from [46].

Cargo proteins that have to be exported from the nucleus to the cytoplasm and contain a NES are recognized by a member of the karyopherin-β family, the export receptor CRM1 (chromosomal maintenance 1 or exportin-1). After binding of the cargo, CRM1 complexes with RanGTP and transits the nuclear pore. In the cytoplasm, RanGTP is hydrolyzed to RanGDP by RanGAP (RanGTPase-activating protein) and the export complex dissociates (Figure 1.3 B) [46].

Nuclear transport can be regulated either by modifications of the cargo, expression (rate) of the transport receptors or the number of the NPCs embedded in the nuclear envelope [46]. Karyopherin cargo proteins are involved in a wide range of cellular processes and adequate nuclear-cytoplasmic localization is pivotal for the execution of normal cell functions [51]. In cancer, the intracellular location of tumor suppressor and oncogenes shows a subcellular maldistribution promoting unrestricted cell growth [46].

1.2.2 Karyopherin-α2

The karyopherin-α family comprises seven known members, one of them being karyopherin-α2 (KPNA2, importin-α subunit 1). KPNA2 is a 58 kDa protein containing an N-terminal karyopherin-β binding domain and a central region of ten armadillo repeats that mediates binding of the NLS as well as of CAS [50]. However, karyopherin-α can also bind to cargo proteins independently of karyopherin-β [46].

KPNA2 mediates the nuclear import of various different cargo proteins involved in a broad range of cellular processes [49, 53]. Tumor-associated KPNA2 transport substrates include BRCA1, NBS1, E2F1 and the MRN complex which is crucial for DNA double-strand break repair [49, 54–57]. In addition to the nuclear import of cancer-related factors, several studies proved the overexpression of KPNA2 itself in tumor tissue (e.g. breast, bladder, liver and ovarian cancer) [58–62]. However, its functional role particularly in HCC remains incompletely understood.

1.3 Microtubule dynamics

1.4.1 Structure and function of microtubules

Microtubules (MTs) are α-/β-tubulin heterodimers that are part of all eukaryotic cells and spatially structure the cytoplasm in non-dividing cells and thereby constitute the cytoskeleton. Besides their role in cell structure, MTs form the mitotic spindle apparatus during the process of mitosis, allowing chromosome segregation and orientation of the cleavage plane [63]. MTs polymerize by adding GTP-tubulin dimers to the MT end which is further stabilized by a GTP-tubulin enriched cap. MT growth and shrinkage is determined by MT polymerases and depolymerases as well as kinesins located at their ends. Loss of the cap induces rapid shrinkage (depolymerization), the so-called MT catastrophe [64]. MTs are polymerizing and depolymerizing constantly in a highly dynamic process that enables rapid reorganization of the cytoplasm [63] and is pivotal for tumor cell growth, migration and invasion [65].

1.4.2 Stathmin

MT-interacting proteins act on the dynamic MT-turnover either by MT-stabilization or -destabilization [64]. Stathmin (*STMN1*; also oncoprotein 18, Op18) is a soluble, cytosolic phosphoprotein that destabilizes MTs during mitosis. In humans, it is encoded by the *STMN1* gene [66]. Next to stathmin, the family comprises

three other members (stathmin 2-4) which are all involved in the regulation of MT stability [67]. Stathmin regulates MT dynamics by sequestering α/β-tubulin-dimers, thereby preventing the polymerization of MTs. Additionally, stathmin binds to MTs directly to promote their catastrophe. If stathmin gets phosphorylated, it is inactivated and mitotic spindles can assemble [68].

In normal tissue, stathmin is ubiquitously expressed, with the lowest levels found in the liver [69]. It was shown that stathmin is predominantly present in proliferating cells with a peak in S- and G2/M-phases [70]. Consequently, stathmin depletion promotes cell cycle arrest and apoptosis [71]. In human tumors (e.g. breast, lung, ovarian cancer and HCC) stathmin is frequently overexpressed and associated with metastasis and poor survival suggesting an involvement in cancer progression and dissemination [65, 66, 72, 73]. Furthermore, experimental data demonstrate that RNA*i*-mediated protein silencing inhibits clonogenicity and migration and promotes apoptosis in different tumor entities *in vitro*, making stathmin a potential candidate for targeted therapy [65, 73, 74].

2 OBJECTIVES

A deeper understanding of the molecular mechanisms that shape the malignant phenotype of HCC cells is critical to identify novel drug targets and will provide the basis for improved therapeutic approaches [43]. It was previously reported that members of the nuclear transport machinery are involved in protumorigenic processes in different tumor entities, however, several NTS-related mechanisms in (liver-) tumor biology remain poorly understood. Regulating the nuclear import of oncogenes and/or tumor suppressors, nuclear transport factors are pivotal mediators of (aberrant) gene expression in cancer [48, 51, 75]. Based on a previous report describing deregulation of nuclear transport factors in HCC [61], the nuclear import receptor KPNA2 was chosen for further investigation.

Therefore, within this doctoral thesis, I aimed to:

- Identify KPNA2 downstream targets in an unbiased approach using LC-MS/MS
- Characterize the functional significance of KPNA2 in HCC
- Characterize the functional implications of the identified KPNA2 downstream target stathmin
- Elucidate the mechanisms by which KPNA2 regulates stathmin
- Correlate the results obtained *in vitro* with the *in vivo* situation by analyzing data derived from HCC patient cohorts

3 MATERIALS

3.1 Cell culture

3.1.1 Cell lines

The used cell lines are summarized in Table 3.1.

Table 3.1: Cell lines: origin and cultivation media.

Cell line	Origin	Cultivation medium	Supplier
Hep3B	HCC	MEM	ATCC, LGC Standards, Wesel, Germany
HepG2	hepatoblastoma	RPMI	ATCC, LGC Standards, Wesel, Germany
HLE	HCC	DMEM	JCRB, Tokyo, Japan
HLF	HCC	DMEM	JCRB, Tokyo, Japan
HuH1	HCC	DMEM	JCRB, Tokyo, Japan
HuH6	hepatoblastoma	DMEM	JCRB, Tokyo, Japan
HuH7	HCC	DMEM	JCRB, Tokyo, Japan
PLC/PRF/5	HCC	DMEM	ATCC, LGC Standards, Wesel, Germany
Snu182	HCC	RPMI	ATCC, LGC Standards, Wesel, Germany
Sk-Hep1	liver endothelial cells	DMEM	ATCC, LGC Standards, Wesel, Germany
THLE-2	hepatocytes (SV40 transformed)	BEBM	ATCC, LGC Standards, Wesel, Germany

3.1.2 Cell culture media and reagents

All media, reagents and supplements used for cell cultivation and treatment are summarized in Table 3.2.

Table 3.2: Cell culture media and reagents.

Reagent	Order number	Supplier
Media and supplements		
Bronchial Epithelial Cell Growth Basal Medium (BEBM)	CC-3171	Lonza, Cologne, Germany
Dulbecco's Modified Eagle Medium (DMEM)	D5796	Sigma-Aldrich, Taufkirchen, Germany
Dulbecco's Phosphate Buffered Saline (DPBS)	D8537	Sigma-Aldrich, Taufkirchen, Germany
Fetal Bovine Serum (qualified, heat inactivated)	10500064	Thermo Fisher Scientific, Waltham, USA
Opti-MEM® I Reduced Serum Medium	31985047	Thermo Fisher Scientific, Waltham, USA
Penicillin-Streptomycin Solution (10,000 units each)	15140130	Thermo Fisher Scientific, Waltham, USA
Roswell Park Memorial Institute 1640 (RPMI 1640)	R8758	Sigma-Aldrich, Taufkirchen, Germany
Trypsin-EDTA solution	T3924	Sigma-Aldrich, Taufkirchen, Germany
Reagents		
Doxycycline hyclate	D9891	Sigma-Aldrich, Taufkirchen, Germany
Fugene® HD Transfection Reagent	E2311	Promega, Mannheim, Germany
Hepatocyte growth factor (HGF)	294-HG	R&D, Minneapolis, USA
Hexadimethrine bromide (Polybrene)	H9268	Sigma-Aldrich, Taufkirchen, Germany
Mitomycin C	-	Pharmacy, University Hospital Heidelberg, Heidelberg, Germany
Nutlin-3a	N6287	Sigma-Aldrich, Taufkirchen, Germany
Oligofectamine™ Transfection Reagent	12252011	Thermo Fisher Scientific, Waltham, USA
Puromycin	P8833	Sigma-Aldrich, Taufkirchen, Germany

3.1.3 Small interfering RNAs

All small interfering RNAs (siRNAs) used for transient gene knockdown are summarized in Table 3.3.

Table 3.3: siRNAs used for protein depletion. Eurofins Genomics siRNAs were modified with a 3'-poly-T-tail.

siRNA	Sequence (5'-3')	Order number	Supplier
AllStars Neg. Control siRNA		1027280	QIAGEN, Hilden, Germany
c-JUN#1	AAG AAC GUG ACA GAU GAG CAG	SI00300580	QIAGEN, Hilden, Germany
c-JUN#2	CCC GAG CUG GAG CGC CUG AUA	SI03077599	QIAGEN, Hilden, Germany
E2F1#1	AAC UCC UCG CAG AUC GUC AUC	SI00300083	QIAGEN, Hilden, Germany
E2F1#2	CAG AUC UCC CUU AAG AGC AAA	SI03064775	QIAGEN, Hilden, Germany
FBP-1#1	(AUA CAG AUA GCU CCU GAC A)TT		Eurofins Genomics, Ebersberg, Germany
FBP-1#2	(GGC AGG AAC GGA UCC AAA U)TT		Eurofins Genomics, Ebersberg, Germany
FBP-2#1	(GAG AUC AAC CGG AGA GCA A)TT		Eurofins Genomics, Ebersberg, Germany
FBP-2#2	(CAG GAC GGA UCU CAG AAU A)TT		Eurofins Genomics, Ebersberg, Germany
KPNA2#1	(AAU CUU ACC UGG ACA CUU U)TT		Eurofins Genomics, Ebersberg, Germany
KPNA2#2	(UUC GUU AAG CUU AAU UGA GAA)TT		Eurofins Genomics, Ebersberg, Germany
p53#1	(UGU UCC GAG AGC UGA AUG A)TT		Eurofins Genomics, Ebersberg, Germany
p53#2	(AGA CCU AUG GAA ACU ACU U)TT		Eurofins Genomics, Ebersberg, Germany
STMN1#1	(AGG CAA UAG AAG AGA ACA A)TT		Eurofins Genomics, Ebersberg, Germany
STMN1#2	(AAG AGA AAC UGA CCC ACA A)TT		Eurofins Genomics, Ebersberg, Germany
TFDP1#1	CAG AAC CUU AGU CCC GGG AAA	SI00094654	QIAGEN, Hilden, Germany
TFDP1#2	CAC AUU UGA AAU CCA CGA UGA	SI03056858	QIAGEN, Hilden, Germany

3.2 Molecular cloning

3.2.1 Reagents for molecular techniques

All reagents used for methods of molecular biology (cloning, transformation etc.) are summarized in Table 3.4.

Table 3.4: List of reagents used for molecular biological techniques.

Reagent	Order number	Supplier
Agarose	2267.4	Carl Roth, Karlsruhe, Germany
Ampicillin Sodium Salt	A9518	Sigma-Aldrich, Taufkirchen, Germany
Dimethyl sulfoxide (DMSO)	D8418	Sigma-Aldrich, Taufkirchen, Germany
DNA Gel Loading Dye 6x	R0611	Thermo Fisher Scientific, Waltham, USA
DPN I (10 U/µL)	ER1701	Thermo Fisher Scientific, Waltham, USA
GelRed Nucleid Acid Gel Stain	41003	Biotium, Hayward, USA
GeneRuler 1 kb DNA Ladder	SM0314	Thermo Fisher Scientific, Waltham, USA
Kanamycin sulphate	T832.2	Carl Roth, Karlsruhe, Germany
Phusion GC Buffer 5x	F-519	Thermo Fisher Scientific, Waltham, USA
Phusion DNA polymerase (2 U/µL)	F-530L	Thermo Fisher Scientific, Waltham, USA
Proteinase K	59895	Thermo Fisher Scientific, Waltham, USA
Tango Buffer 10x	BY5	Thermo Fisher Scientific, Waltham, USA
Ultra Pure™ Distilled Water	10977-035	Thermo Fisher Scientific, Waltham, USA

3.2.2 Primers for molecular cloning

Primers used for cloning of KPNA2 and STMN1 Gateway vectors are summarized in Table 3.5. Cloning primers were obtained from Apara Bioscience (HPLC purified; Denzlingen, Germany).

Table 3.5: Primers for Gateway cloning. Green: *att*B1/*attB*2 site; red: Kozak sequence.

Name	NCBI Accession numbers	Sequences (5'-3')
KPNA2	NM_001320611.1 NM_002266.3	For: GGGGACAAGTTTGTACAAAAAAGCAGGCTCCACCATGTCCACCAACGAGA ATG Rev: GGGGACCACTTTGTACAAGAAAGCTGGGTTCTAAAAGTTAAAGGTCCCAG

3.2.3 Vectors for molecular cloning

All vectors used for molecular cloning are summarized in Table 3.6.

Table 3.6: Vectors for cloning. Vector backbones, entry and expression vectors.

Vector	Technology	Comment
Vector backbones		
pDonor201	Gateway entry vector	Kindly provided by Dr. Stefan Pusch
pDest26-N-FLAG	Gateway destination vector	Kindly provided by Dr. Stefan Pusch
pDest26-N-HA	Gateway destination vector	Kindly provided by Dr. Stefan Pusch
pcDNA3		
Entry clones		
pDONR201-E2F1	Gateway cloning	+/- stop codon; kindly provided by Dr. Stefan Pusch
pDonor201-KPNA2	Gateway cloning	Silent mutation
pDonor255-TFDP1	Gateway cloning	Addgene (#70627); kindly provided by Dr. Dominic Esposito
Expression vectors		
pCMVTNT-T7-KPNA2		Addgene (#26678); kindly provided by Dr. Bryce Paschal
pDest26-N-FLAG-E2F1	Gateway cloning	
pDest26-N-HA-E2F1	Gateway cloning	
pDest26-N-HA-KPNA2	Gateway cloning	
pDest26-N-FLAG-TFDP1	Gateway cloning	
pDest26-N-HA-TFDP1	Gateway cloning	

3.2.4 Bacterial strains

Bacteria used for transformation and vector production are summarized in Table 3.7.

Table 3.7: Bacteria for vector production.

Bacterial strain	Supplier
One Shot™ Mach1™ T1 Phage-Resistant Chemically Competent *E. coli*	Thermo Fisher Scientific, Waltham, USA
One Shot™ ccdB Survival™ 2 T1R Competent Cells	Thermo Fisher Scientific, Waltham, USA

3.2.5 Sanger sequencing

Primers for sanger sequencing are summarized in Table 3.8.

Table 3.8: Primers used for sanger sequencing.

Name	Application	Sequence (5'-3')
pDONR for	pDonor forward primer	TAACGCTAGCATGGATCTC
pDONR rev	pDonor reverse primer	GCAATGTAACATCAGAGAT
CMV for	pDest forward primer	CGCAAATGGGCGGTAGGCGTG
T7	pDest reverse primer	TAATACGACTCACTATAGG

3.3 Primers for semi-quantitative real-time PCR

All primers used for semi-quantitative real-time PCR were obtained from Thermo Fisher Scientific (Waltham, USA) or Apara Bioscience (Denzlingen, Germany) and are summarized in Table 3.9.

Table 3.9: List of primers used for semi-quantitative real-time PCR.

Name	NCBI Accession number(s)	Sequences (5'-3')
Human genes		
E2F1	NM_005225	For: GCCAAGAAGTCCAAGAACCAC Rev: CGCAGCTGCGTAGTACAGATATTC
KPNA2	NM_001320611 NM_002266	For: AGGAAAACCGCAACAACCAG Rev: ACCAGCCCGGATTATGTTGT
RPL32	NM_000994 NM_001007073 NM_001007074	For: TTCCGGTCCACAACGTCAAG Rev: TGTGAGCGATCTCGGCAC
STMN1	NM_001145454 NM_005563 NM_203399 NM_203401	For: TGCAGAATACACTGCCTGTC Rev: AGGCACGCTTCTCCAGTTCT
TFDP1	NM_007111	For: GTAGGAAGCCCACACACCCCCA Rev: GAAATGCCGTAGGCCCTTGCCA
Murine genes		
Actb	NM_007393	For: GCTTCTTTGCAGCTCCTTCGT Rev: ACCAGCGCAGCGATATCG
Gapdh	NM_008084	For: TGTCCGTCGTGGATCTGAC Rev: CCTGCTTCACCACCTTCTTG
Hprt	NM_013556	For: TCCTCCTCAGACCGCTTTT Rev: CCTGGTTCATCATCGCTAATC
Ppia	NM_008907	For: GCATACAGGTCCTGGCATCT Rev: AGCTGTCCACAGTCGGAAAT
Tbp	NM_013684	For: TTGTCTGCCATGTTCTCCTG Rev: CAGGGTGATTTCAGTGCAGA
Stmn1	NM_019641	For: GACCTTTCCCTGGAGGAAATCC Rev: GAAGTTGTTGTTCTCCTCGATGGC

Primers used for quantification of precipitated DNA following chromatin immunoprecipitation (ChIP) were obtained from Thermo Fisher Scientific (Waltham, USA) and are summarized in Table 10.

Table 3.10: List of primers used for quantification of precipitated DNA. BS: binding site.

Name	Sequence (5'-3')
***STMN1* Promoter Negative Control BS**	For: CACAACCCAGGAGGGAAACAG Rev: CACCCTGTTCTGACTTGGATGC
CDC2-*STMN1* Promoter BS	For: CGCCCTTTCCTCTTTCTTTC Rev: ATCGGGTAGCCCGTAGACTT
E2F1-*STMN1* Promoter BS1	For: ACCCACCTGCTCAGTCCG Rev: CGGGTCTGTTGGTGCTCAGAG
E2F1-*STMN1* Promoter BS2	For: CTCCCCGCGCCTTTTCGAATC Rev: GGCTCCGGGGTGTTGAGTTC

3.4 Antibodies

All antibodies used for western blot, immunoprecipitation and immunohistochemistry are summarized in Table 3.11.

Table 3.11: List of used antibodies. WB: western blot; ChIP: chromatin immunoprecipitation; CoIP: co-immunoprecipitation; IHC: immunohistochemistry.

Antibody Primary antibodies	Species	Dilution	Order number	Supplier
Actin (Clone C4)	mouse	1:10,000 (WB)	69100	MP Biomedicals, Heidelberg, Germany
ATF-2 (N-96)	rabbit	1:200 (WB)	sc-6233	Santa Cruz Biotechnology, Heidelberg, Germany
β-tubulin	mouse	1:1000 (WB)	556321	Becton, Dickinson and Company, Franklin Lakes, USA
E2F-1 (ChIP Ab+)	mouse	3 µg (ChIP)	17-10061	Millipore, Burlington, USA
E2F-1 (C-20)	rabbit	1:300 (WB)	sc-193	Santa Cruz Biotechnology, Heidelberg, Germany
GFP	rabbit	1:2000 (WB)	G1544	Sigma-Aldrich, Taufkirchen, Germany
IgG1	mouse	IP control	sc-2025	Santa Cruz Biotechnology, Heidelberg, Germany
KPNA2	rabbit	1:2000 (WB), 1:50 (IHC)	ab84440	Abcam, Cambridge, UK

Antibody Primary antibodies	Species	Dilution	Order number	Supplier
KPNA2	mouse	2 µg (CoIP)	610485	Becton, Dickinson and Company, Franklin Lakes, USA
PARP	rabbit	1:500 (WB)	9542	Cell Signaling Technology, Frankfurt am Main, Germany
p53	mouse	1:5000 (WB)	554293	Becton, Dickinson and Company, Franklin Lakes, USA
Phospho-Stathmin (Ser38; D19H10)	rabbit	1:1000 (WB)	4191	Cell Signaling Technology, Frankfurt am Main, Germany
Stathmin 1 (EP1573Y)	rabbit	1:2000 (WB), 1:50 (IHC)	ab52630	Abcam, Cambridge, UK
TFDP1	mouse	1:200 (WB)	AM00404AF-N	Acris, Herford, Germany
TFDP1	rabbit	1:500 (WB)	ab186831	Abcam, Cambridge, UK
Vinculin	mouse	1:5000 (WB)	V9131	Sigma-Aldrich, Taufkirchen, Germany
Secondary antibodies				
IRDye 680LT anti-mouse	donkey IgG	1:10,000 (WB)	926-68022	LI-COR Bioscience, Bad Homburg, Germany
IRDye 680LT anti-rabbit	donkey IgG	1:10,000 (WB)	926-68023	LI-COR Bioscience, Bad Homburg, Germany
IRDye 800CW anti-mouse	donkey IgG	1:10,000 (WB)	926-32212	LI-COR Bioscience, Bad Homburg, Germany
IRDye 800CW anti-rabbit	donkey IgG	1:10,000 (WB)	926-32213	LI-COR Bioscience, Bad Homburg, Germany

3.5 Chemicals and reagents

All used chemicals and reagents are summarized in Table 3.12.

Table 3.12: Chemicals and reagents.

Chemical/reagent	Order number	Supplier
Agarose	2267.4	Carl Roth, Karlsruhe, Germany
Albumin Bovine, DNase/RNase-Free (BSA)	11967.09	SERVA, Heidelberg, Germany
Ammonium persulfate (APS)	1610700	Bio-Rad, Munich, Germany
Boric acid (≥ 99.8%)	6943.1	Carl Roth, Karlsruhe, Germany
Cell Lysis Buffer 10x	9803	Cell Signaling Technology, Frankfurt am Main, Germany
Cristal violet	C-3886	Sigma-Aldrich, Taufkirchen, Germany

Chemical/reagent	Order number	Supplier
Dimethyl sulfoxide (DMSO)	D8418	Sigma-Aldrich, Taufkirchen, Germany
dNTP Mix (10 mM each)	R0192	Thermo Fisher Scientific, Waltham, USA
Dynabeads Protein G	10004D	Thermo Fisher Scientific, Waltham, USA
Ethanol	32205	Sigma-Aldrich, Taufkirchen, Germany
Fisher's EZ-Run™ Pre-Stained *Rec* Protein Ladder	BP3603-506	Thermo Fisher Scientific, Waltham, USA
Glycine	LC-4522.2	Labochem, Heidelberg, Germany
Guava® Cell Cycle Reagent	4500-0220	Merck, Darmstadt, Germany
Isopropanol	190764	Sigma-Aldrich, Taufkirchen, Germany
Milk powder	T145.2	Carl Roth, Karlsruhe, Germany
Phenylmethanesulfonylfluoride (PMSF)	P7626	Sigma-Aldrich, Taufkirchen, Germany
PhosSTOP 10x	4906845001	Roche, Mannheim, Germany
Protease-Inhibitor Mix G 1000x	39101	SERVA, Heidelberg, Germany
Protein Assay Dye Reagent Concentrate (Bradford reagent)	500-0006	Bio-Rad, Munich, Germany
PrimaQUANT qPCR-CYBR-Green-MasterMix-high-ROX	SL-9912	Steinbrenner, Heidelberg, Germany
Random Hexamer Primer	SO142	Thermo Fisher Scientific, Waltham, USA
Salmon sperm DNA solution	10605543	Thermo Fisher Scientific, Waltham, USA
SOC Outgrowth Medium	B9035	New England Biolabs, Frankfurt, Germany
TEMED	2367.3	Carl Roth, Karlsruhe, Germany
Tris(hydroxymethyl)-aminomethane (TRIS)	4855.2	Carl Roth, Karlsruhe, Germany
Tween 20	9127.1	Carl Roth, Karlsruhe, Germany
Ultra Pure™ Distilled Water	10977-035	Thermo Fisher Scientific, Waltham, USA

3.6 Buffers

All prepared buffers and solutions are summarized in Table 3.13.

Table 3.13: Buffers and solutions.

Name	Formula
Borate buffer (pH 8.8; blotting buffer)	20 mM Boric acid, 1.27 mM EDTA
Crystal violet staining solution	1% Crystal violet, 25% Methanol
Glycine solution (pH 2.8)	50 mM Glycine
IP wash buffer	100 mM Tris pH 8.5, 500 mM LiCl, 1% Igepal CA 630, 1% Na-Deoxycholate
Laemmli Buffer (4x)	250 mM Tris-HCl pH 6.8, 8% SDS, 40% Glycerol, 0.04% Bromophenol blue, 100 mM DTT
LB agar	1.5% Agar in LB medium
LB medium (pH 7)	1% Tryptone, 0.5% yeast extract, 1% NaCl
Lysis buffer (pH 7.4; CoIP)	50 mM Tris HCl pH 7.4, 0.25% Sodium deoxycholate, 150 mM NaCl, 1 mM EDTA, 1% NP-40
Phosphate buffered saline (PBS)	140 mM NaCl, 2.7 mM KCl, 10 mM Na2HPO4x2H2O, 1.8 mM KH2PO4
PBST	0.02% Tween-20 in PBS
Running buffer (SDS-PAGE)	25 mM Tris, 192 mM Glycine, 0.1% SDS
TAE buffer (pH 8.0)	40 mM Tris-Acetate, 1 mM EDTA
Talianidis buffer (ChIP elution)	70 mM Tris pH 8, 1 mM EDTA, 1.5% SDS
TE buffer	70 mM Tris pH 8, 1 mM EDTA
Tris buffered saline (pH 7.6; TBS)	20 mM Tris-HCl, 140 mM NaCl
TBST	0.1% Tween-20 in TBS

3.7 Kits

All kits used for mycoplasma tests, cellular fractionation, RNA isolation and molecular biology assays are summarized in Table 3.14.

Table 3.14: List of used kits.

Kit	Order number	Supplier
MycoAlert™ Plus Mycoplasma Detection Kit	LT07	Lonza, Cologne, Germany
NE-PER Nuclear and Cytoplasmic Extraction Reagents	78833	Thermo Scientific, Rockford, USA
NucleoBond® Xtra Maxi EF	740424	Macherey-Nagel, Dueren, Germany
NucleoSpin® Gel and PCR Clean-up	740609	Macherey-Nagel, Dueren, Germany
NucleoSpin® Plasmid	740588	Macherey-Nagel, Dueren, Germany
NucleoSpin® RNA	740955	Macherey-Nagel, Dueren, Germany
PureYield™ Plasmid Midiprep System	A2495	Promega, Mannheim, Germany
Quick Western Kit – IRDye® 680 RD	926-68100	LI-COR Bioscience, Bad Homburg, Germany

3.8 Equipment and devices

All used equipment and devices are summarized in Table 3.15.

Table 3.15: List of used equipment and devices.

Equipment	Supplier
General equipment	
12-Tube magnet	QIAGEN, Hilden, Germany
Amersham Protran nitrocellulose membrane, 0.45 µM	GE Healthcare, Buckinghamshire, UK
Mini PROTEAN Multi casting chamber	Bio-Rad, Munich, Germany
Mini PROTEAN 3 Cell SDS-gel electrophoresis system	Bio-Rad, Munich, Germany
Mini Trans-Blot Cell	Bio-Rad, Munich, Germany
Mr. Frosty™ Freezing Container	Thermo Fisher Scientific, Waltham, USA
Neubauer Counting Chamber (improved)	Brand, Frankfurt, Germany
Electric devices	
AlphaImager™ MultiImage Light Cabinet	Biozym, Hessisch Oldendorf, Germany
BIOWIZARD Silver Line safety cabinet	Ewald, Bad Nenndorf, Germany
Compact Shaker KS 15 control and Incubator Hood TH 15	Edmund Bühler GmbH, Hechingen, Germany
FLUOstar Omega microplate reader	BMG Labtech, Ortenberg, Germany
Guava easyCyte flow cytometer	EMD Millipore, Darmstadt, Germany
INCOmed CO_2 incubator	Memmert, Schwabach, Germany
Incubator (Bacteria)	Memmert, Schwabach, Germany
Labnet Spectrafuge Mini centrifuge	Sigma-Aldrich, Taufkirchen, Germany
Megafuge 16R centrifuge	Thermo Fisher Scientific, Waltham, USA
Mikro 200R centrifuge	Hettich, Tuttlingen, Germany
NanoDrop ND-1000	Thermo Fisher Scientific, Waltham, USA
Odyssey Sa Infrared Imaging System	LI-COR Bioscience, Bad Homburg, Germany
Orbital shaker DOS-10L	neoLab, Heidelberg, Germany
Overhead rotator RM-2M	neoLab, Heidelberg, Germany
pH meter Microprocessor pH 210	Hanna Instruments, Voehringen, Germany
Photometer	Eppendorf, Hamburg, Germany
Power supply EV231	Consort, Turnhout, Belgium
PTC-200 PCR Cycler	Bio-Rad, Munich, Germany
S-4000 Sonicator	Qsonica, Newton, USA
Secuflow fume hood	Waldner, Wangen, Germany
Scale	Kern, Balingen-Frommern, Germany
StepOnePlus™ Real-Time PCR	Applied Biosystems, Darmstadt, Germany
Thermomixer compact	Eppendorf, Hamburg, Germany
Tube roller CAT RM5	neoLab, Heidelberg, Germany
Universal 32R centrifuge	Hettich, Tuttlingen, Germany
Vortexer	neoLab, Heidelberg, Germany
Microscopes	
Axiovert 25	Zeiss, Oberkochen, Germany
CKX31 (inverted microscope)	Olympus, Hamburg, Germany
CKX41 (inverted microscope)	Olympus, Hamburg, Germany
ORCA-R2 Camera controller	Hamamatsu, Hersching, Germany

3.9 Software

All used software is summarized in Table 3.16.

Table 3.16: List of used software.

Software	Provider
ApE v2.0.47	www.biologylabs.utah.edu/jorgensen/wayned/ape
CellSens Dimension	Olympus, Hamburg, Germany
Fiji	www.fiji.sc
GraphPad Prism 6	GraphPad Software, San Diego, USA
IBM SPSS Statistics 24.0	IBM, Ehningen, Germany
Image Studio v3.1.4	LI-COR Bioscience, Bad Homburg, Germany
InCyte™ FACS Software	EMD Millipore, Darmstadt, Germany
StepOne v2.3	Applied Biosystems, Darmstadt, Germany
ZEN 2012 v8.0	Zeiss, Oberkochen, Germany

4 METHODS

4.1 Cell culture methods

4.1.1 Cell cultivation

Cells were cultured in the media described in table 3.1 supplemented with 10% fetal calf serum (FCS) and 1% penicillin/streptomycin in an incubator at 37°C in an atmosphere containing 5% CO_2. Cells were maintained on 10 cm cell culture dishes and split twice a week in a ratio according to their growth behavior. Cell culture supernatants were tested twice a year for mycoplasma contamination.

4.1.2 Cryoconservation of cell lines

For long-time storage, cells were trypsinized from sub-confluent 10 cm dishes, centrifuged to remove trypsin-EDTA (110 x g, 5 min) and resuspended in cryomedium containing 10% DMSO, 20% FCS and 70% of the respective growth medium. For freezing of cryogenic vials, a Mr.Frosty™ freezing container was used to freeze cells with a cooling rate of -1°C/min. For long term storage, cryoconserved cells were stored in a liquid nitrogen tank. To thaw cryo-conserved cells, warm growth medium was added to the cryogenic vials and the cell/cryomedium mixture was resuspended in growth medium. Cells were centrifuged as described above to remove DMSO and plated on a 10 cm dish.

4.1.3 Seeding of cell lines

Cells were seeded one day prior to the start of experiments. Cells were trypsinized, centrifuged to remove trypsin-EDTA (110 x g, 5 min), resuspended in growth medium and counted using an improved Neubauer chamber. Different cell number were seeded depending on the cell line, cell size, growth rate and type of experiment. The used cell numbers are summarized in Table 4.1.

Table 4.1: Cell numbers seeded for different experiments.

Cell line	12-well plate	6-well plate	6 cm dish	10 cm dish
HepG2	-	250,000	-	-
HLE	35,000	40,000	25,000 (KPNA2 siRNA treatment)	70,000 (KPNA2 siRNA treatment)
HLF	-	30,000	-	-
HuH6	-	300,000	-	-
HuH7	150,000	-	-	-
PLC	-	250,000	-	-
Snu182	-	60,000 (96 h) 70,000 (48 h)	80,000 (KPNA2 siRNA treatment)	-
Sk-Hep1	-	150,000	-	-

4.1.4 Transient protein depletion using small interfering RNAs

For small interfering RNA (siRNA)-mediated gene knockdown cells were seeded onto 12-well or 6-well plates or 6 cm dishes the day prior to transfection. The day of transfection, cells were washed once and covered with 800 µL (6-well plates) or 1.6 mL (6 cm dishes) Opti-MEM. All siRNAs are summarized in Table 3.3 and used at a final concentration of 50 nM with the exception of siRNAs directed against FBP-1 and FBP-2 (20 nM). For replication of experiments in the cell line Snu182, two siRNAs targeting the same gene were pooled (25 nM/siRNA). The QIAGEN AllStars Duplex served as control. Oligofectamine was used as transfection reagent. The transfection protocol is summarized in Table 4.2. Solution A and B were incubated at ambient temperature for 10 min, combined and incubated for another 10 min before they were added dropwise to the wells/dishes.

Table 4.2: Protocol for siRNA transfection.

Reagent	12-well plates	6-well plates	6 cm dishes
Solution A			
Opti-MEM	90 µL	180 µL	360 µL
siRNA/AllStars (20 µM)	1.25 µL	2.5 µL	5 µL
Solution B			
Opti-MEM	7.5 µL	15 µL	30 µL
Oligofectamine	1.5 µL	3 µL	6 µL

Four hours after siRNA-treatment 0.5 mL (12-well plates), 1 mL (6-well plates) or 2 mL (6 cm dishes) of growth medium was added, 24 h after transfection the medium was completely exchanged. Cells were harvested 48-96 h after transfection for protein or RNA isolation.

4.1.5 Transient protein overexpression

For transient overexpression of proteins 0.5 or 1 µg of the respective plasmid DNA were mixed in a ratio of 1:3 with Fugene HD Reagent, added to Opti-MEM and incubated for 15 min at ambient temperature. Following incubation, the DNA/Fugene/Opti-MEM mixture was added dropwise to the cells. The vector backbone served as a control. If not mentioned otherwise, cells were harvested 24 h after transfection.

4.1.6 Treatment with Nutlin-3a

Nutlin-3a was used to induce p53 in liver cancer cell lines harboring wildtype p53. Nutlin-3a was resolved in DMSO to concentrations of 20 mM, respectively. Therefore, DMSO served as control in the subsequent experiments. For cell treatment, Nutlin-3a was diluted in growth medium to a final concentration of 10 µM.

4.2 Molecular biological methods

4.2.1 Gateway cloning

To clone vectors for KPNA2 and stathmin overexpression, the Gateway Cloning System was used. *att*B-flanked primers (Table 3.5) for the respective inserts and Gateway recombination were used to amplify the CDS sequences of the two genes from cDNAs obtained from HLE whole cell lysates. PCR was performed according to the manufacturer's protocol using a gradient PCR with annealing temperatures around the primer melt temperatures. The used master mix is summarized in Table 4.3.

Table 4.3: Master mix for Gateway gradient PCR.

Reagent	Volume
cDNA	15 ng
dNTP Mix (10 mM)	1 µL
Forward primer (10 µM)	2.5 µL
Reverse primer (10 µM)	2.5 µL
5x Phusion GC Buffer	10 µL
Phusion DNA Polymerase	1 µL
dH_2O	ad 50 µL

The conditions used for Gateway gradient PCR are summarized in Table 4.4.

Table 4.4: PCR program for Gateway gradient PCR.

PCR step	Temperature	Time	Cycles
Initial denaturation	98°C	30 sec	1
Denaturation	98°C	30 sec	30
Annealing	Primer dependent gradient	30 sec	
Elongation	72°C	30 sec/kb template DNA	
Final elongation	72°C	10 min	1
Hold step	4°C	∞	1

PCR products were separated by agarose gel electrophoresis. Therefore, 1.5% agarose was dissolved in TAE buffer and GelRed Nucleid Acid Gel Stain was added for UV light-based DNA detection. The PCR products were mixed with loading dye and pipetted into the wells of the solidified gel next to the GeneRuler 1 kb DNA ladder. Electrophoresis was performed for 1-2 h at 65-120 V. DNA was visualized using the AlphaImager gel documentation system and fragments consistent with the expected insert size were isolated from the gel. DNA was purified using the NucleoSpin® Gel and PCR Clean-up Kit as described in the manufacturer's protocol.

In a next step, the respective PCR products were sub-cloned into pDONR201, which was used as entry vector, by BP reaction. Therefore, 75 ng of PCR product were mixed with 150 ng pDONR201 plasmid and 1 µL BP Clonase II enzyme mix and adjusted to a final volume of 5 µL with TE buffer. The BP reaction was performed at 25°C for 2 h until the reaction was stopped by addition of 0.5 µL Proteinase K and incubation at 37°C for 10 min. For recombination of the insert from the pDONR201 entry clone into the destination vector, LR reaction was performed. In brief, 75 ng of the entry clone were mixed with 150 ng of the respective destination vector (i.e. pDest26, see Table 3.6) and 1 µL LR Clonase II enzyme mix and adjusted to a final volume of 5 µL with TE buffer. The LR reaction was incubated at 25°C overnight and inactivated using Proteinase K as described above.

4.2.2 Bacterial transformation and plasmid isolation

For the following transformation 50 µL of One Shot™ Mach1™ T1 Phage-Resistant Chemically Competent *E. coli* were carefully mixed with 5 µL of the plasmid obtained from BP or LR reactions and incubated on ice for 30 min. After a heat shock for 1 min at 42°C was performed, bacteria were incubated for 2 min on ice and 150 µL SOC Outgrowth Medium was added. Transformed bacteria were incubated for 1 h at 37°C while shaking and plated to selective agar plates depending on their respective resistance gene (Ampicillin or Kanamycin, 50 µg/mL). Plates were incubated overnight at 37°C. For transformation of vector backbones One Shot™ ccdB Survival™ 2 T1R Competent Cells were used to enable bacterial survival in presence of the ccdB site integrated into the plasmid.

For expansion, single colonies were picked, resuspended in antibiotics-containing LB medium (50 mg/mL) and shaken overnight at 37°C. Depending on the used LB medium volume, the NucleoSpin® Plasmid, the PureYield™ Plasmid Midiprep or the NucleoBond® Xtra Maxi EF kit was used for plasmid isolation according to the manufacturer's protocol. For long-term storage, 30% glycerol was added to bacterial suspensions and bacteria were snap-frozen and stored at -80°C.

4.2.3 Sequencing

To verify the sequence of cloned vectors, sanger sequencing was carried out by Microsynth SeqLab (Goettingen, Germany) and results were compared to CDS and vector backbone sequences using the software ApE.

4.2.4 Isolation of total RNA and cDNA synthesis

The NucleoSpin RNA kit was used for isolation of total RNA. Cells were scraped in buffer RA1 supplemented with 1% β-mercaptoethanol and RNA was isolated according to the manufacturer's protocol. The

concentration of isolated RNA per samples was quantified using a spectrophotometer and 1 µg of RNA was used for cDNA synthesis. The master mix for cDNA synthesis is summarized in Table 4.5.

Table 4.5: Master mix for cDNA synthesis.

Reagent	Volume
RNA	1 µg
dH_2O	Ad 12 µL
dNTP Mix (10 mM)	2 µL
Random Hexamer Primer (100 µM)	1 µL
Addition after initial denaturation	
Buffer RT 5x	4 µL
ReverseAid H Minus RT	1 µL

The PCR settings used for cDNA synthesis are summarized in Table 4.6. After the initial denaturation, the PCR program was paused and 5x Buffer RT was added. 5 min later, the program was put on hold a second time for ReverseAid H Minus RT addition.

Table 4.6: PCR program for cDNA synthesis.

PCR step	Temperature	Time
Initial denaturation	75°C	5 min
RevertAid activation	25°C	15 min
dNTP annealing	42°C	1 h
RevertAid inactivation	70°C	10 min
Hold step	4°C	∞

Readily synthesized cDNA was diluted 1:80 to a final concentration of 0.625 ng/µL and stored at -20°C until further use.

4.2.5 Semi-quantitative real-time PCR

Semi-quantitative real-time PCR (qPCR) was performed to quantify mRNA expression levels using SYBR Green technology. The used primers are summarized in table 3.9. Forward and reverse primers were diluted in dH_2O to a concentration of 10 µM per primer and used as a primer mix. Samples were analyzed in technical duplicates. The qPCR master mix is listed in Table 4.7.

Table 4.7: Master mix for qPCR.

Reagent	Volume
cDNA	1.25 ng
Primer mix (10 µM/primer)	0.8 µL
CYBR-Green-MasterMix-high-ROX	5 µL
dH_2O	ad 10 µL

The qPCR settings are summarized in Table 4.8. Following signal quantification, the melt curve was measured to ensure the quality of the method. qPCR was performed using a StepOnePlus™ Real-Time PCR device.

Table 4.8: qPCR program and melt curve.

PCR step	Temperature	Time	Cycles
qPCR			
Initial denaturation	95°C	15 min	1
Denaturation	95°C	15 sec	40
Annealing/elongation/ fluorescence detection	60°C	1 min	
Melt curve			
Denaturation	95°C	15 sec	1
Annealing	60°C	30 sec	
Dissociation	60-95°C	0.5°C/5 sec	
Denaturation	95°C	15 sec	

To increase comparability of experiments, the threshold for ct-values was manually adjusted to 0.4 in all analyses. If not mentioned otherwise, *RPL32* was used as reference gene. For analysis of murine tissue samples, five reference genes were measured and normalized using the GENORM algorithm. mRNA expression was calculated relative to the control sample using the comparative ΔΔCt method as described by Livak et al. [76].

4.2.6 Chromatin immunoprecipitation

Chromatin immunoprecipitation (ChIP) assay was performed to study binding of proteins to regulatory DNA regions. To study binding of E2F1 to the *STMN1* promoter, cells were seeded onto 15 cm dishes. The next day, protein and DNA were crosslinked by incubation of cells with 1% formaldehyde/PBS for 15 min followed by a quenching step with 125 mM glycine for 5 min and two washing steps with cold PBS. Subsequently, cells were harvested in 1 mL RIPA buffer (supplemented with protease inhibitor) and sonicated (2x 30 sec, power level 1.5, amplitude 15) to fragment genomic DNA to a size of 200-300 bp. Cell lysates were then centrifuged (18,000 x g, 4°C) for 15 min to remove cell debris. The protein concentration

of the supernatant was quantified using Bradford assay and adjusted to 1 mg/mL with RIPA buffer. For preclearing, 30 µL of pre-washed Dynabeads Protein G were added to every sample and rotated for 1.5 h at 4°C. Simultaneously, 50 µL pre-washed Dynabeads Protein G were blocked in salmon sperm DNA/BSA while rotating for 1.5 h at 4°C. Following preclearing, the Dynabeads were removed from the samples using a magnetic rack. The blocked Dynabeads were washed with RIPA buffer and added to the precleared samples together with 2 µg of the respective IP-antibody (control: IgG; see table 3.11). Samples were incubated overnight while rotating at 4°C. The next day, samples were washed as follows:

- 2x with 500 µL RIPA buffer (while rotating, 5 min, 4°C)
- 4x with 500 µL IP wash buffer (while rotating, 5 min, 4°C)
- 2x with 500 µL RIPA buffer (while rotating, 5 min, 4°C)
- 2x with 500 µL TE buffer

Subsequently, Dynabeads were resuspended in 100 µL TE buffer and binding of the protein-DNA complexes to the Dynabeads was reversed by addition of 200 µL Talianidis elution buffer and incubation for 10 min at 65°C. In a next step, the supernatant was removed from the Dynabeads and the protein-DNA crosslink was reversed by addition of 13 µL of 4 M NaCl and incubation for 5 h at 65°C. DNA was purified using the NucleoSpin® Gel and PCR Clean-up Kit according to the manufacturer's protocol.

ChIP primers (table 3.10) were designed according to sequences obtained from publicly available ChIP-Seq datasets following E2F1 precipitation. As a negative control, a random sequence upstream of the predicted binding sequence was additionally quantified. Precipitated DNA was quantified using qPCR relative to the respective IgG control IP.

4.3 Protein analytical methods

4.3.1 Isolation of total protein

For total protein isolation cells were washed twice with cold PBS and scraped in 30-100 µL 1x cell lysis buffer supplemented with protease and phosphatase inhibitors. Tubes containing the lysates were snap-frozen in liquid nitrogen to enhance cell membrane disruption. Protein lysates were then centrifuged at 18,000 x g for 10 min at 4 °C to pellet cell debris and the supernatant was used for further analyses.

Bradford reagent was used for quantification of total protein concentrations. In a photometer cuvette, 625 µL 1x Bradford reagent was added to 11.25 µL dH_2O and 1.25 µL sample. After 5 min of incubation at ambient temperature, the optical density was measured at 595 nm using a photometer. Protein

concentration was calculated using a formerly established BSA standard curve. Protein samples were stored at -20°C until further usage.

4.3.2 SDS-polyacrylamide gel electrophoresis and western blotting

For semi-quantitative protein analysis, samples were separated using SDS-polyacrylamide gel electrophoresis (SDS-PAGE). Gels were prepared as described in Table 4.9.

Table 4.9: SDS-PAGE gel preparation protocol. Volumes equal one gel (10 mL).

Reagent	5% Stacking gel	8% Separating gel	12% Separating gel
dH_2O	6.8 mL	4.6 mL	3.3 mL
30 % Acrylamide/Bis Solution (29:1)	1.7 mL	2.7 mL	4 mL
1.5 M Tris-HCL (pH 8.8)	-	2.5 mL	2.5 mL
1 M Tris-HCL (pH 6.8)	1.25 mL	-	-
10% SDS	100 µL	100 µL	100 µL
10% APS	100 µL	100 µL	100 µL
TEMED	10 µL	6 µL	4 µL

Protein lysates were adjusted to a protein concentration of 30 µg and 4x Laemmli buffer was added. Samples were denatured for 5 min at 95°C and subsequently loaded on polyacrylamide gels next to a protein size marker. The gels were placed into a blotting chamber together with running buffer and electrophoresis was performed for 1.5-2 h at 85-150 V.

For immunoblotting, a stack of Whatman filter papers, the separating gel and a nitrocellulose membrane were placed into a blotting chamber together with borate transfer buffer and blotting was performed for 1.5 h at 90 V. Blotted membranes were blocked in 5% milk or BSA in TBST for 1 h and incubated with the respective primary antibodies (see Table 3.11) at 4°C on a shaker overnight. If not mentioned otherwise, β-actin served as loading control. The following day, membranes were washed 3x with TBST for 15 min and incubated with IRDye secondary antibodies (see Table 3.11) for 1 h at ambient temperature. After another washing step, fluorescence signals were detected using an Odyssey Sa Infrared Imaging System.

4.3.3 Nuclear cytoplasmic fractionation

NE-PER Nuclear and Cytoplasmic Extraction Reagents were used as described in the manufacturer's instructions. An additional washing step was performed after isolation of the cytoplasmic fraction to increase purity of the nuclear fraction. Fractionated samples were immunoblotted as described above. PARP and β-tubulin served as loading controls for the nuclear and cytoplasmic fractions.

4.3.4 Co-immunoprecipitation

Co-immunoprecipitation (CoIP) was used to study protein-protein interactions. Cells were seeded onto 15 cm cell culture dishes and transfected with 1 µg of the KPNA2 (pDest-N-HA-KPNA2) and E2F1 or TFDP1 (pDest-N-FLAG-E2F1 or pDest-N-FLAG-TFDP1) expression vectors using the Fugene HD Reagent the following day. CoIP assay was started 24 h after transfection.

For each sample, 50 µL Dynabeads Protein G were incubated in Glycine (pH 2.8) for 5 min at ambient temperature followed by 4 h of incubation with 2 µg antibody/PBST (see table 3.11) at 4°C on an overhead rotator. IgG was used as a negative control. Plasmid-transfected cells were washed twice and scraped in a non-denaturing CoIP lysis buffer supplemented with DTT, PMSF and protease inhibitor. Lysates were incubated for 15 min while rotating at 4°C and centrifuged for 15 min (18,000 x g) to remove cell debris. The protein concentration was measured using Bradford reagent and adjusted to 1 mg/mL. 20 µL of every sample was removed as input control for immunoblotting. After antibody incubation, Dynabeads Protein G were washed twice using DPBS and 1 mL cell lysate was added. The Dynabeads/lysate mixture was incubated overnight at 4°C while rotating. The following day, the Dynabeads were washed three times using DPBS and resuspended in 1x Laemmli buffer. After 20 min of shaking (500 rpm) at ambient temperature samples were denatured for 8 min at 95°C and western blot was performed as described above. To avoid artefacts of the heavy chains of antibodies or IgG, the Quick Western Kit – IRDye® 680RD was used for antibody incubation according to the manufacturer's instructions.

4.3.5 Quantitative proteomics.

To asses differential protein expression upon KPNA2 depletion, HLE cells were treated with a siRNA targeting KPNA2 (KPNA2#1) or the AllStars negative control. Liquid chromatography-tandem mass spectrometry was carried out at the European Molecular Biology Laboratory (EMBL, Heidelberg, Germany) in collaboration with the Beck group as previously described [61].

In brief, cells were harvested using an urea and Rapigest containing lysis buffer followed by sonication, reduction of solubilized proteins by addition of DTT and alkylation of cystein using idoacetaminde. In a next step, proteins were digested using LysC and trypsin. TFA was added to acidify the samples before they were further cleaved by heat-induced Rapigest activation. Afterwards, samples were centrifuged and the supernatants were desalted using C18 spin columns. Peptides were analyzed using a nano-Acquity UPLC (Ultra performance liquid chromatography) system connected to a LTQ-Orbitrap Velos Pro instrument. Quantitative label-free data analysis was performed using MaxQuant v1.2.2.5. MS/MS spectra were matched with human SwissProt entries. Results were analyzed using R v2.14.2 by the Beck Laboratory.

4.4 Functional assays

4.4.1 Colony formation assay

Colony formation assays were performed to analyze clonogenic capacity in presence or absence of KPNA2 and stathmin. Two days after siRNA-mediated knockdown of KPNA2 or stathmin, cells were re-seeded in a very low density (HLE: 500 cells/well; Snu182: 1000 cells/well) into a 6-well plate. 14 days after siRNA-treatment colonies were stained for 35 min using a 1% crystal violet solution. The number of colonies was counted and evaluated compared to the All-Stars negative control.

4.4.2 Migration assay

Migration of HLE and Snu182 cells upon KPNA2 or stathmin depletion was analyzed using a "scratch" assay. Cells were seeded into 12-well-plates and treated with siRNAs targeting KPNA2 or stathmin. 48 h after protein knockdown, cells were treated with mitomycin C (5 µg/µL) in serum-free medium for 3 h to repress proliferation. After removal of mitomycin C, the cell monolayer was scratched using a 200 µL pipette tip and hepatocyte growth factor (HGF, 10 ng/mL) was added to enhance cell migration. Migration was monitored using an inverse microscope (Olympus CKX41) with connected camera by taking four pictures per scratch 0 h and 18 h after scratching. The cell free area was quantified using the software Fiji.

4.4.3 Cell cycle assay

To study the influence of KPNA2 on cell cycle kinetics, cells were treated with siRNAs targeting the respective gene in duplicates. Cells were fixed and cellular DNA was stained using the Guava® Cell Cycle Reagent 72 h after treatment according to the manufacturer's protocol. The percentage of cells in the different cell cycle phases was analyzed using a Guava easyCyte flow cytometer (10,000 cells/sample). For data analysis, peaks were annotated to the respective cell cycle phase according to the measured DNA content.

4.5 Analysis of murine and human HCC samples

4.5.1 Tissue microarray

The HCC tissue microarray (TMA) was kindly provided by the Tissue Bank of the National Center for Tumor Diseases (NCT) Heidelberg and approved by the local Ethics Committee. The TMA contained 95 formalin-fixed paraffin-embedded human HCC samples with following tumor grades: 14x G1; 52x G2; 27x G3; 2x G4. Grading was conducted by an experienced pathologist. Immunohistochemical staining (i.e. H&E, KPNA2 and stathmin staining) was carried out at the Institute of Pathology Greifswald (University Medicine Greifswald, Germany). For scoring, only tumor cells were assessed according to the scheme shown in Table 4.10.

Table 4.10: TMA scoring protocol.

Score	Quantity of stained cells	Intensity of staining
0	0%	Negative (no staining)
1	< 1%	Low
2	1-10%	Moderate
3	11-50%	High
4	> 50%	-

Staining of nucleus and cytoplasm were scored individually and independently by two researchers. The final IHC score was calculated by multiplication of quantity and intensity values per patient (dot on the array).

4.5.2 Immunohistochemical staining of murine liver tissues

Formalin-fixed paraffin embedded (FFPE) tissue samples originated from E2F1-driven murine HCCs (n=11; male; 9-15 months) were engineered and characterized by the Thorgeirsson Laboratory (Maryland, USA) [77] and kindly provided by Dr. Diego Calvisi. Immunohistochemical staining (i.e. H&E and stathmin staining) of full FFPE sections was carried out at the Institute of Pathology Greifswald (University Medicine Greifswald, Germany) and analyzed by an experienced pathologist.

4.5.3 Expression and survival analysis of human HCCs

To analyze expression of KPNA2, stathmin, E2F1 and TFDP1 in human HCC and adjacent tissue a published Affymetrix U133A2.0 gene expression data set (Gene Expression Omnibus accession number GSE14520) originating from 256 HCC patients (247 tumor and 239 adjacent non-neoplastic samples) was used. The majority of patients developed HCC on the background of HBV infections. All patients underwent total tumor resection. For 242 patients survival data existed [78]. Complementary, a second published HCC patient cohort, the TCGA LIHC cohort (the cancer genome atlas, liver hepatocellular carcinoma, accessible via: http://cancergenome.nih.gov) was analyzed. The TCGA LIHC cohort contains HCC samples of 371 patients of mixed sex and etiologies and Caucasian and Asian background.

4.6 Statistical analyses

Data are presented as means ± standard deviation. Expression differences between two different test conditions were compared by non-parametric two-tailed Mann-Whitney U tests using SPSS Statistics24. For statistical analysis of correlations, the Spearman's rank correlation coefficient was calculated with SPSS Statistics24 or GraphPad Prism 6. Overall survival was assessed by Kaplan-Mayer analysis using GraphPad

Prism 6. p-values < 0.05 were considered significant with the following gradation: * $p<0.05$; ** $p<0.01$ and *** $p<0.001$.

5 RESULTS

5.1 Members of the nuclear transport machinery are deregulated in HCC

A deeper understanding of the molecular mechanisms shaping the malignant phenotype of HCC is crucial to identify novel drug targets and to enable development of new therapeutic approaches [43]. Substantial deregulation of members of the nuclear transport machinery was previously described in different cancers [48, 49, 51, 61, 79]. Winkler et al. analyzed a published DNA microarray dataset (GEO: GSE50579) of 40 human tumor and seven non-tumorous liver samples and thereby identified a subset of overall 37 nuclear transport-related genes to be differentially expressed in HCC [61, 80]. The most prominently overexpressed genes included exportin-1 and -2 (XPO1, also CRM1; and XPO2, also CAS) and the karyopherins-α1 and 2 (KPNA1 and KPNA2) [61]. The authors could further demonstrate prosurvival properties of the CAS/KPNA2 transport cycle in HCC, being repressed by p53 [61]. However, several functional and mechanistic aspects of KPNA2 in HCC remain to be defined.

To follow up on the above-mentioned data and prior to further functional and mechanistic studies, the protein expression of KPNA2 was evaluated in different liver derived cancer cells lines and the immortalized hepatocyte cell line THLE-2.

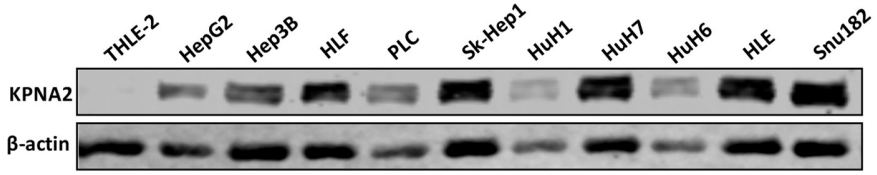

Figure 5.1: KPNA2 expression in liver cancer cell lines. Western blot analysis of KPNA2 expression in the immortalized hepatocyte cell line THLE-2 and different liver cancer cell lines. Samples were immunoblotted using the indicated antibodies.

As depicted in Figure 5.1, THLE-2 cells showed the lowest KPNA2 expression compared all analyzed cancer cell lines, supporting the reported overexpression of KPNA2 in human HCC patient samples [61]. Based on the strong protein expression and their favorable cell culture behavior, HLE cells were chosen as standard cell line for further experiments.

5.2 Quantitative proteomics reveals regulation of microtubule-related proteins by KPNA2

A proteomics approach was used to identify downstream targets of KPNA2 and to further elucidate its functional role in HCC. Therefore, KPNA2 was depleted in HLE cells by siRNA-treatment (siRNA KPNA2#1) and changes in total protein abundance were analyzed 72 h later by quantitative mass spectrometry (n=3; Figure 5.2 A). Using a label-free technique, where control and treatment conditions are measured individually, sample preparation included protein isolation, reduction, alkylation and finally digestion into peptides [81]. Subsequently, samples were separated by UPLC and analyzed using tandem mass spectrometry (LC-MS/MS), which allows collection of detailed information of the analyzed peptides compared to conventional LC-MS techniques [81, 82]. Peptides and proteins were then identified by database comparison (human SwissProt) and expression differences between the control siRNA and KPNA2 siRNA treated groups were quantified.

1759 proteins were measured in total. Table 5.1 shows a subset of the most deregulated proteins upon KPNA2 knockdown relative to the control samples. The 35 most up- and downregulated hits are summarized in Supplementary tables S1 and S2.

Table 5.1: Selected proteins differentially expressed upon KPNA2 depletion. HLE cells were treated with a siRNA directed against KPNA2 (KPNA2#1) or a control siRNA and changes in global protein abundance were analyzed by LC-MS/MS. TPX2: Targeting protein for *Xenopus* kinesin-like protein 2; GSTF1: Gametocyte-specific factor 1; HMOX1: Heme oxygenase 1.

Protein	Fold change (log_2)	p-value
KPNA2	-4.07	$2.22*10^{-8}$
TPX2	0.80	$7.14*10^{-5}$
Syntenin-1	-1.39	0.0002
Vinculin	-0.64	0.0005
Stathmin	-0.92	0.0034
GTSF1	-1.47	0.0043
HMOX1	0.44	0.0075

As demonstrated by the volcano plot (Figure 5.2 B), data analysis revealed differential regulation of the MT-associated proteins stathmin (gene: *STMN1*) and targeting protein for *Xenopus* kinesin-like protein 2 (TPX2) following KPNA2 depletion. Total protein abundance of stathmin was reduced by 50% while other members of the stathmin family were not identified in the dataset. For TPX2 a 1.75-fold

increase in protein expression was found upon KPNA2 knockdown. Consistent with this finding, it was previously shown that TPX2 is inactivated by binding to KPNA2 and that sequestration of KPNA2 by the Golgi matrix protein GM130 is required for TPX2-mediated microtubule nucleation during mitosis [83]. Due to this already reported link to KPNA2, TPX2 was not subjected to further analysis. However, stathmin with its well documented oncogenic role in (liver-) cancer [65, 66, 72, 74, 84] and no found published link to KPNA2 stathmin was considered a promising candidate for further validation.

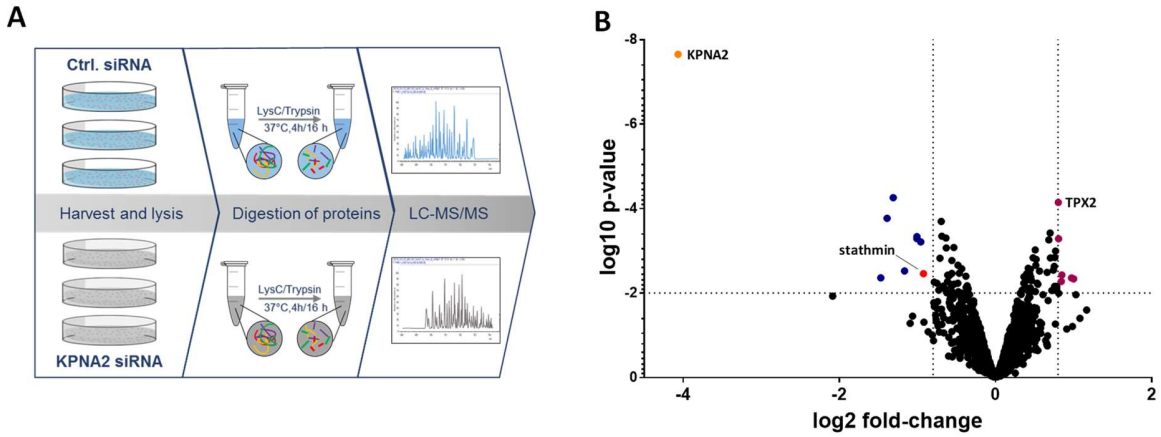

Figure 5.2: Stathmin is downregulated following KPNA2 depletion. (A) Workflow of quantitative mass spectrometry: HLE cells were treated with a siRNA directed against KPNA2 or a control siRNA and cells were harvested and lysed 72 h later. Following protein digestion, samples were analyzed using a nano-Acquity UPLC system connected to a LTQ-Orbitrap Velos Pro instrument (LC-MS/MS, n=3). Quantitative label-free data analysis was performed using MaxQuant and MS/MS spectra were matched with human SwissProt entries. **(B)** HLE cells were treated as described in (A) and changes in global protein abundance were analyzed by LC-MS/MS. Volcano plot shows the resulting changes in global protein abundances (log_2 fold changes) relative to the control and the corresponding p-values (log_{10}). Horizontal dotted line: p=0.01; vertical dotted lines: log_2 fold change +/-0.8.

5.3 KPNA2 is required for full expression of *STMN1*

Immunoblotting was used to validate the reduction of stathmin protein upon KPNA2 depletion as indicated by the proteomic approach. Indeed, also by including two additional siRNAs all tree KPNA2 knockdown conditions caused a reduction in stathmin protein abundance as indicated by western blot analysis (Figure 5.3 A). Since siRNAs KPNA2#1 and KPNA2#2 showed similar effect sizes, these siRNAs were used in further experiments. Also, other factors suggested to be deregulated based on the proteomic data set were tested by immunoblotting: gametocyte-specific factors 1 (GSF1), home oxygenase 1 (HMOX1) and Syntenin-1. As depicted in Figure 5.3 B (left panel), downregulation of GSF1, a protein predominately expressed in male germ cells and involved in spermatogenesis, and

upregulation of HMOX1, which is reportedly associated in inflammatory processes within the liver [85–87], could be validated with both siRNAs. Inconclusive results were obtained for Syntenin-1 (melanoma differentiation-associated gene 9, MDM9), a highly conserved protein related to cancer invasion in different tumor entities [88, 89], for which siRNAs KPNA2#1 and #2 showed opposing effects (Figure 5.3 B, right panel).

The effect of KPNA2 depletion on stathmin protein was observed not only in HLE, but also in the HCC cell lines HLF and Snu182 (Figure 5.3 C). Snu182 cells, which also showed strong KPNA2 expression in the liver derived cancer cell line screening (figure 5.1), were chosen as second cell line for further studies to ensure cell line independence of the results. For further experiments in Snu182 cells, siRNAs KPNA2#1 and #2 were pooled. Interestingly, exogenous (over)expression of KPNA2 does not further increase stathmin protein abundance (Figure 5.3 D). This observation is possibly due to the already high KPNA2 expression reflecting a saturated system. Additionally, qRT-PCR analyses showed that reduced stathmin protein levels upon KPNA2 knockdown were paralleled by a significant decrease in mRNA expression levels (Figure 5.3 E), suggesting a transcriptional level of regulation.

In conclusion, the above presented LC-MS/MS dataset revealed a connection between the nuclear import receptor KPNA2 and the MT-interacting protein stathmin which could be further validated by western blot. Reduced *STMN1* mRNA levels following KPNA2 depletion suggest a regulation at the transcript level. In a next step, functional significance of KPNA2 related to stathmin was evaluated.

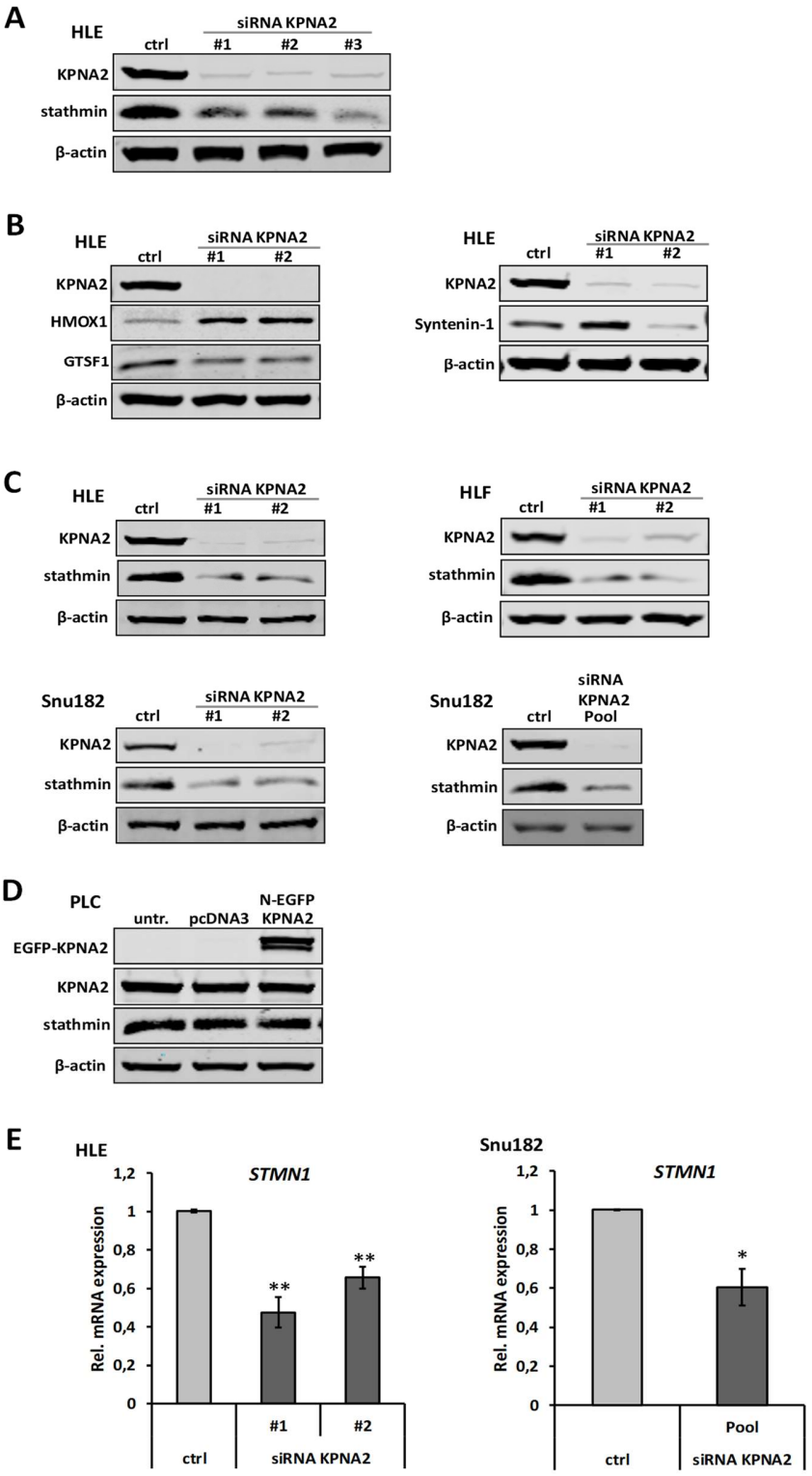

Figure 5.3: KPNA2 depletion induces downregulation of stathmin. HLE cells were treated with siRNAs targeting KPNA2 or a control siRNA (ctrl). Changes in protein abundance were analyzed 72 h later by immunoblotting using the indicated antibodies. **(B)** HLE cells were treated as described in (A) and changes

in protein abundance were analyzed 72 h later by immunoblotting using the indicated antibodies. **(C)** HLE, HLF and Snu182 cells were treated as described in (A). Changes in protein abundance were analyzed 72 h later by immunoblotting using the indicated antibodies. **(D)** PLC cells were either left untreated (untr.) or transfected with a control plasmid (pcDNA3) or a plasmid encoding KPNA2 (N-EGFP KPNA2) and protein expression was analyzed 24 h later by immunoblotting using the indicated antibodies. **(E)** HLE and Snu182 cells were treated as described in (A) and *STMN1* mRNA expression was analyzed by qRT-PCR (HLE: n=5, SD ctrl: +/- 0.007; **p<0.01; Snu182: n=4; SD ctrl: +/- 0.001; *p<0.05). qRT-PCR data were normalized to the respective control siRNA.
(B)

5.4 Functional properties of KPNA2 and stathmin in HCC

5.4.1 KPNA2 and stathmin are required for full clonogenic capacity of HCC cells

The function of stathmin in cell cycle and mitosis, as well as in tumor invasion and metastases is well reported [70, 71, 73]. Therefore, it was hypothesized that KPNA2 depletion and the associated decrease of stathmin expression leads to a reduction in clonogenic potential, cell cycle arrest and/or decreased migratory capacity of HCC cells. Prior to further experiments, two different stathmin siRNAs were tested in HLE cells and displayed substantial knockdown of stathmin as indicated by western blot analysis (Figure 5.4).

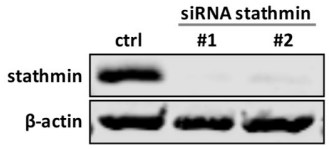

Figure 5.4: Testing of stathmin siRNAs. HLE cells were treated with siRNAs targeting stathmin or a control siRNA (ctrl). Changes in protein abundance were analyzed 72 h later by immunoblotting using the indicated antibodies.

To address the above-mentioned hypothesis, HLE and Snu182 cells were seeded in a very low density following siRNA-mediated KPNA2 depletion and colony formation was assayed 14 days after knockdown by crystal violet staining. In line with the proposed theory, significantly less colonies formed upon KPNA2 ablation compared to the control siRNA (Figure 5.5 A and B). Direct stathmin knockdown let to led to a similar or, in case of siRNA#1, more pronounced reduction of colony formation by 50-90% compared to the control condition, largely phenocopying the effect observed upon KPNA2 depletion (Figure 5.5 C and D).

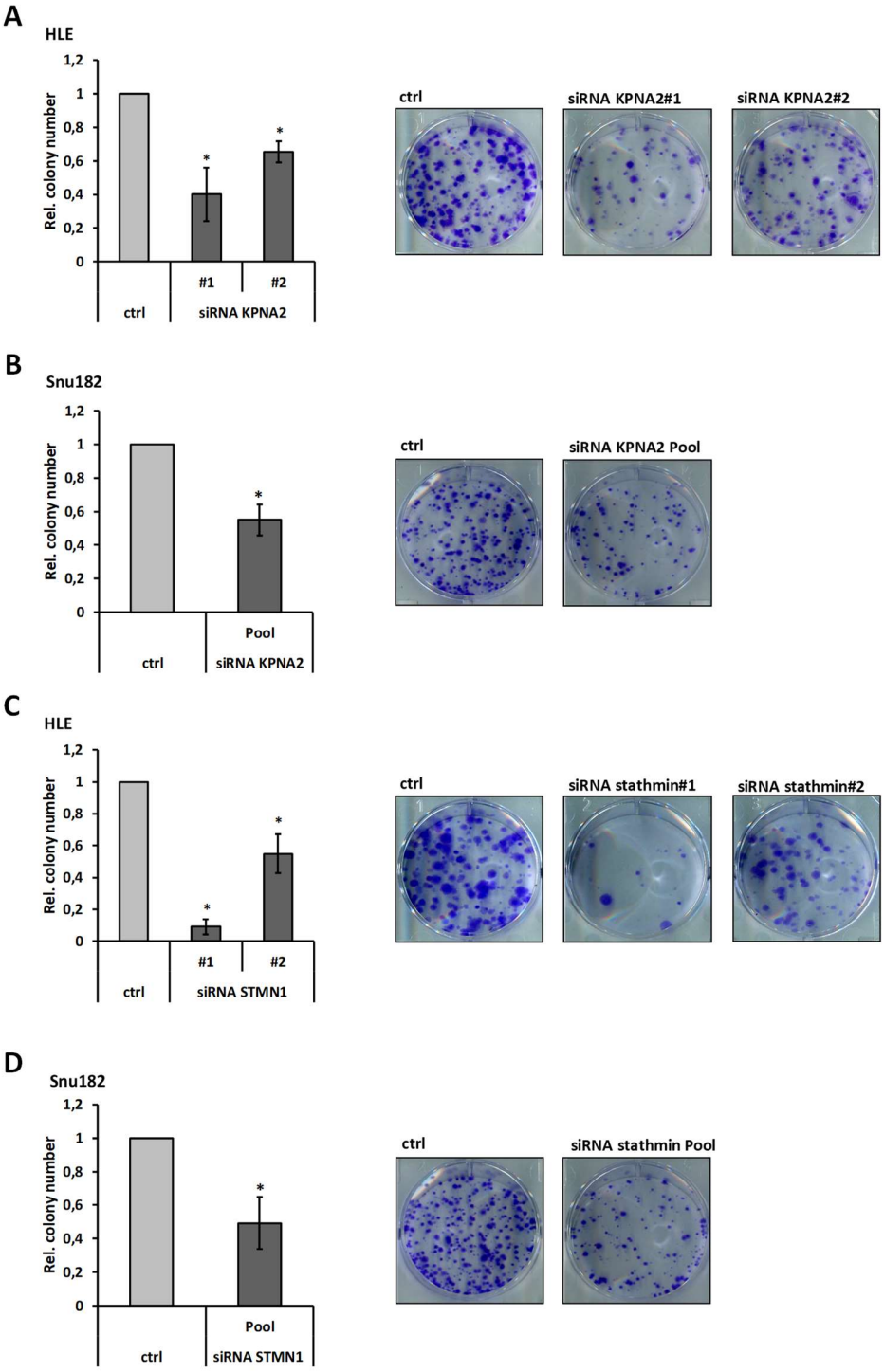

Figure 5.5: Reduction of colony formation upon KPNA2 knockdown is phenocopied by stathmin depletion. **(A)** HLE cells were treated with siRNAs directed against KPNA2 or a control siRNA (ctrl) and colony formation was analyzed 14 days later by crystal violet staining (n=4; *p<0.05). **(B)** Snu182 cells were treated with an siRNA pool (KPNA2#1/2) directed against KPNA2 or a control siRNA (ctrl) and colony formation was analyzed 14 days later by crystal violet staining (n=4; *p<0.05). **(C)** HLE cells were treated with siRNAs directed against stathmin or a control siRNA (ctrl) and colony formation was analyzed 14 days later by crystal violet staining

(n=4; *p<0.05). **(D)** Snu182 cells were treated with an siRNA pool (stathmin#1/2) directed against stathmin or a control siRNA (ctrl) and colony formation was analyzed 14 days later by crystal violet staining (n=4; *p<0.05). All quantifications are shown relative to the respective control condition.

5.4.2 KPNA2 is potentially involved in cell cycle progression

Cell cycle dependent regulation of stathmin was extensively reported [90, 91]. It is well documented that stathmin is inactivated by phosphorylation at four serine residues as a cell enters mitosis and that stathmin depletion causes cell cycle arrest in the G2/M phase of mitosis [90, 92–94]. For the involvement of KPNA2 in cell cycle control and progression, controversial results were reported so far. Huang et al. found evidence that KPNA2 depletion leads to G1 phase arrest via modulation of Akt and FOXO3a phosphorylation in epithelial ovarian carcinoma [95]. In contrast, two studies carried out in NSCLC and esophageal squamous cell carcinoma cell lines showed that KPNA2 knockdown results in G2/M phase arrest [49, 96]. Therefore, the role of KPNA2 in cell cycle in HCC was studied by siRNA-mediated KPNA2 depletion in HLE cells. Subsequently, the distribution of cells to G1, S and G2 phase was assessed according to the DNA copy number of single cells using propidium iodide staining in combination with flow cytometry. Preliminary results indicate a reduced percentage of HLE cells in G2 phase by roughly 10% following KPNA2 knockdown (Figure 5.6). Noteworthy, a larger fraction off cells did not appear to distributed to G1, S or G2 phase following KPNA2 depletion than in the control conditions. Limiting the explanatory power of cell cycle analysis, this technique does not allow to distinguish between viable and apoptotic cells. However, to draw firm conclusions about the function of KPNA2 in cell cycle progression in HCC cells further analysis is required.

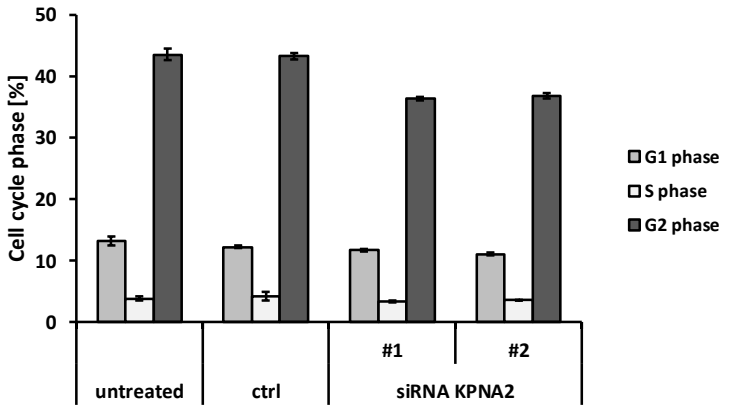

Figure 5.6: KPNA2 expression is involved in cell cycle progression. HLE cells were treated with siRNAs targeting KPNA2 or a control siRNA (ctrl) and distribution of cells to different cell cycle phases was analyzed 48 h later using flow cytometry (n=1).

5.4.3 KPNA2 and stathmin are required for full migratory capacity of HCC cells

To assess the involvement of the KPNA2-stathmin-axis in migration in HCC, two-dimensional scratch assays following KPNA2 and stathmin knockdown were performed. HLE cells were plated in high density and 48 h after siRNA treatment tumor cell proliferation was suppressed by Mitomycin C and migration stimulated by hepatocyte growth factor (HGF) treatment. As shown in Figure 5.7 A, HLE cells showed a significant reduction in migration following KPNA2 depletion compared to the control condition 18 h after the scratch was performed. An even more pronounced effect was observed upon stathmin knockdown indicated by an up to 70% reduction in gap closure compared to the control treatment (Figure 5.7 B).

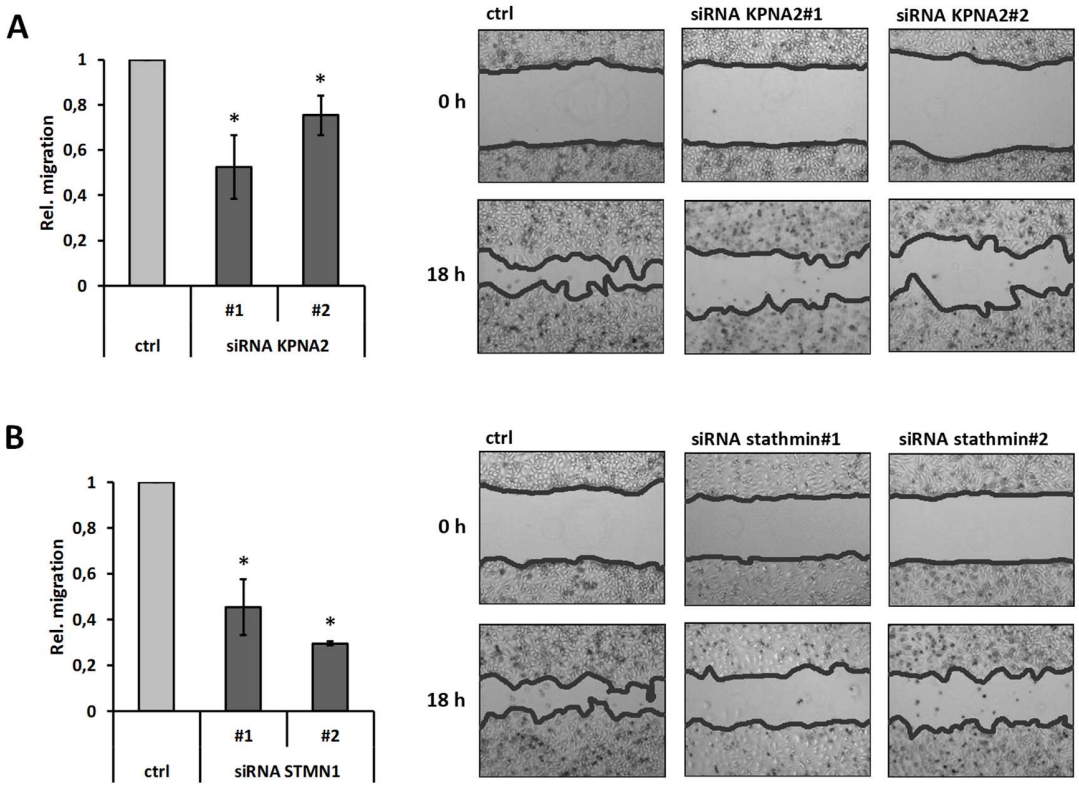

Figure 5.7: Reduction of migration capacity upon KPNA2 knockdown is phenocopied by stathmin depletion. (A) HLE cells were treated with siRNAs directed against KPNA2 or a control siRNA (ctrl) and two-dimensional scratch assay was performed 48 h later. Cell free areas were analyzed 0 h and 18 h after scratching (n=4; *p<0.05). **(B)** HLE cells were treated siRNAs directed against stathmin or a control siRNA (ctrl) and two-dimensional scratch assay was performed 48 h later. Cell free areas were analyzed 0 h and 18 h after scratching (n=4; *p<0.05). All quantifications are shown relative to the respective control condition.

These data suggest that KPNA2 is required for the full clonogenic and migratory capacity of HCC cells by maintaining stathmin expression. Thus, the mechanism by which KPNA2 regulates stathmin expression was assessed as a next step of this study.

5.5 KPNA2 regulates *STMN1* expression by nuclear import of its transcription factors E2F1 and TFDP1

5.5.1 KPNA2 depletion does not modulate phosphorylation of stathmin

It was first tested whether KPNA2 modulates stathmin phosphorylation as a critical determinant in stathmin activity. Phosphorylation of stathmin was previously observed not only during mitosis but also in response to activation of different intracellular signaling pathways (e.g. MAPK, CDK, PKA and STAT3 signaling) [66, 97]. Besides inactivation, phosphorylation was also reported to cause partially protein degradation [98]. To exclude phosphorylation and subsequent inactivation/degradation of stathmin by KPNA2 knockdown western blot analysis of stathmin phosphorylation (P-stathmin S38) was performed. As shown in Figure 5.8, phosphorylation status of stathmin did not change following KPNA2 depletion in HLE cells.

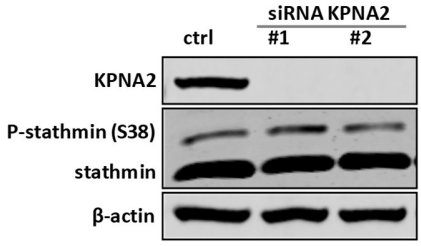

Figure 5.8: KPNA2 knockdown does not modulate stathmin phosphorylation. HLE cells were treated with siRNAs directed against KPNA2 or a control siRNA (ctrl) and stathmin phosphorylation was analyzed 72 h later by immunoblotting using the indicated antibodies.

5.5.2 Screening for *STMN1* transcription factors

Since no evidence for an association between KPNA2 depletion and stathmin phosphorylation was found and *STMN1* transcript levels were decreased upon KPNA2 knockdown it was hypothesized that KPNA2 regulates stathmin by import of its transcription factors. By evaluation of the *STMN1* promoter region and its binding sites using online databases (PROMO3.0, accessible via http://alggen.lsi.upc.es/cgi-bin/promo_v3/promo/promoinit.cgi?dirDB=TF_8.3; TFBIND, accessible via http://tfbind.hgc.jp/) numerous possible transcription factors were identified (e.g. FoxM1, members of the MAPK family). Based on the initial hits, literature research was performed to narrow down the number of possible transcription factors to the most promising candidates (Table 5.2).

Table 5.2: *STMN1* transcription factor candidates. Online database and literature research were combined to identify the most promising candidates that could act as *STMN1* transcription factors. FBP-1/2: fuse binding protein 1/2.

Candidate	Entity	Reference
FBP-1/2	NSCLC	[73, 99]
c-JUN	Rat-1a (rat fibroblasts)	[100]
E2F1	HCC	[101]
TFDP1	HCC	[101, 102]

Subsequently, nuclear and cytoplasmic fractionation assays and CoIP were used to analyze the nuclear import of and direct binding to the above-mentioned transcription factors by KPNA2. Direct protein knockdown of the candidates was performed to assay the downregulation of *STMN1* following depletion of the predicted transcription factors.

5.5.3 FBP-1/2 and c-JUN are not involved in KPNA2-mediated *STMN1* regulation

According to the hypothesis that KPNA2 acts as nuclear import receptor for *STMN1* transcription factors, depletion of KPNA2 would result in retention of the respective candidate protein in the cytoplasm. Therefore, HLE cells were treated with siRNAs directed against KPNA2 or a control siRNA and the nuclear-cytoplasmic distribution of FBP-1, FBP-2 and c-JUN was analyzed 72 h later using nuclear and cytoplasmic fractionation assay. As depicted in Figure 5.9 A, FBP-1 and FBP-2 showed no difference in their subcellular distribution following KPNA2 depletion while c-JUN protein abundance was increased in the cytoplasmic and decreased in the nuclear fraction as detected by immunoblotting. To further confirm the direct physical interaction of KPNA2 and c-JUN, CoIP was performed. Thus, KPNA2 was immunoprecipitated and co-binding of c-JUN was assessed using western blot. In line with the hypothesis and the findings of the fractionation assay, the direct interaction of KPNA2 and c-JUN was confirmed in HLE and Snu182 cells (Figure 5.9 B).

Acting as *STMN1* transcription factors, direct depletion of the candidates should result in decrease in *STMN1* transcription and subsequently in *STMN1* mRNA levels. Thus, HLE cells were treated with siRNAs targeting FBP-1, FBP-2 and c-JUN and *STMN1* expression was analyzed 72 h later using qRT-PCR. Data showed that FBP-1 strongly regulates *STMN1* as its depletion leads to a striking downregulation of mRNA expression (Figure 5.9 C). On the contrary, knockdown of FBP-2 and c-JUN caused a moderate or no reduction in *STMN1* mRNA levels (Figures 5.9 D and E).

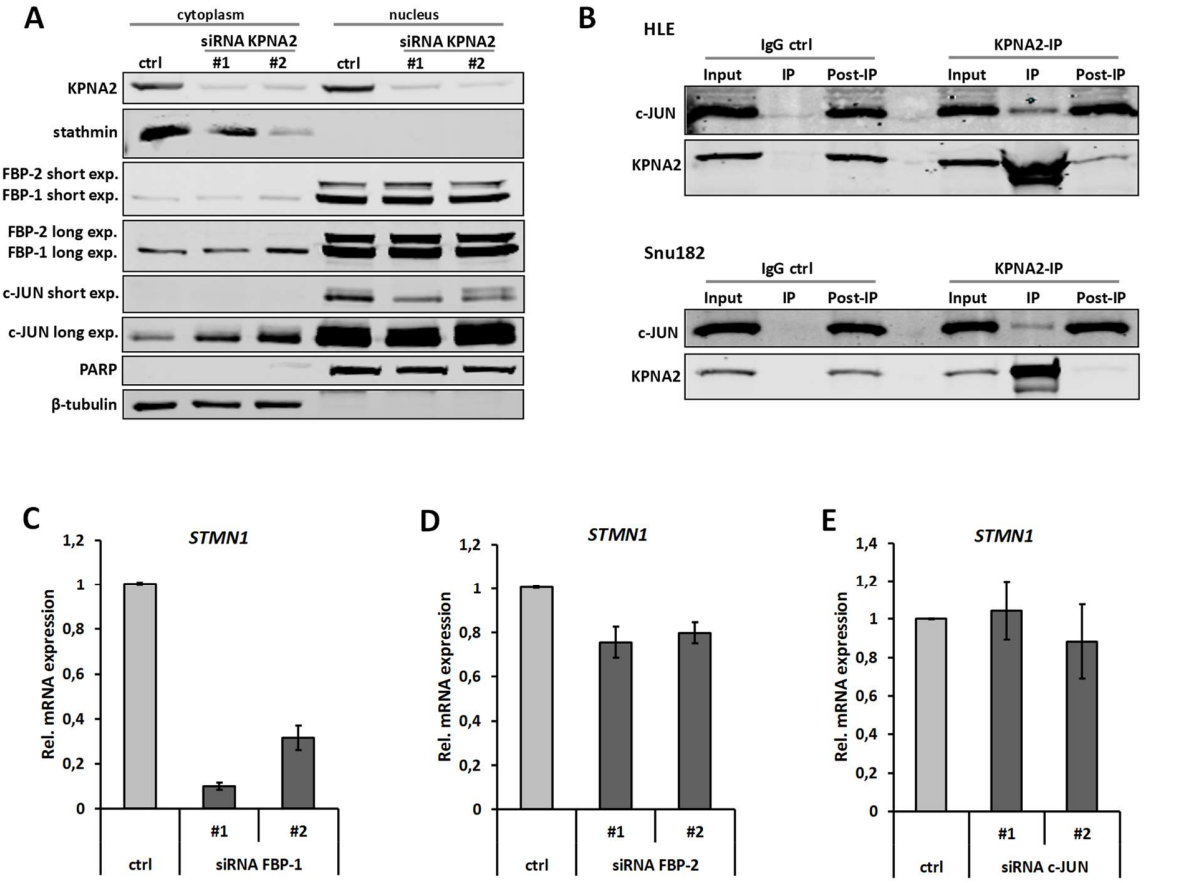

Figure 5.9: Interaction of FBP-1, FBP-2 and c-JUN with KPNA2 and their regulation of STMN1 expression. **(A)** HLE cells were treated with siRNAs directed against KPNA2 or a control siRNA (ctrl) and nuclear and cytoplasmic fractionation assay was performed 72 h later. Samples were immunoblotted using the indicated antibodies. β-tubulin (cytoplasmic fraction) and PARP (nuclear fraction) served as loading controls. **(B)** Endogenous KPNA2 was immunoprecipitated in HLE and Snu182 cells and binding of KPNA2 and c-JUN was analyzed by immunoblot. IgG served as an IP control. **(C, D, E)** HLE cells were treated with siRNAs directed against FBP-1, FBP-2 or c-JUN or a control siRNA (ctrl) and *STMN1* expression was analyzed 72 h later using qRT-PCR (n=2; FBP-1 knockdown: SD ctrl: +/- 0.007; FBP-2 knockdown: SD ctrl: +/- < 0.001; c-JUN knockdown: SD ctrl: +/- < 0.001). qRT-PCR data were normalized to the respective control siRNA.

Consequently, FBP-1, FBP-2 and c-JUN were excluded as relevant players involved in KPNA2 dependent regulation of *STMN1* transcription. c-JUN seemed to be a promising candidate due to its strong interaction with KPNA2, however, its depletion did not lead to a reduction in *STMN1* mRNA expression. FBP-1 and FBP-2 could not be identified as transport substrates of KPNA2 in HCC cells. Therefore, other candidates were tested as follows.

5.5.4 KPNA2 facilitates the import of the *STMN1* transcription factors E2F1 and TFDP1

Consistent with the approach used for the above-mentioned candidates, it was tested whether E2F1 and TFDP1 are KPNA2 nuclear import substrates and if they are *STMN1* transcription factors. Thus, HLE cells were treated with siRNAs directed against KPNA2 and nuclear-cytoplasmic fractionation assay was performed 72 h later.

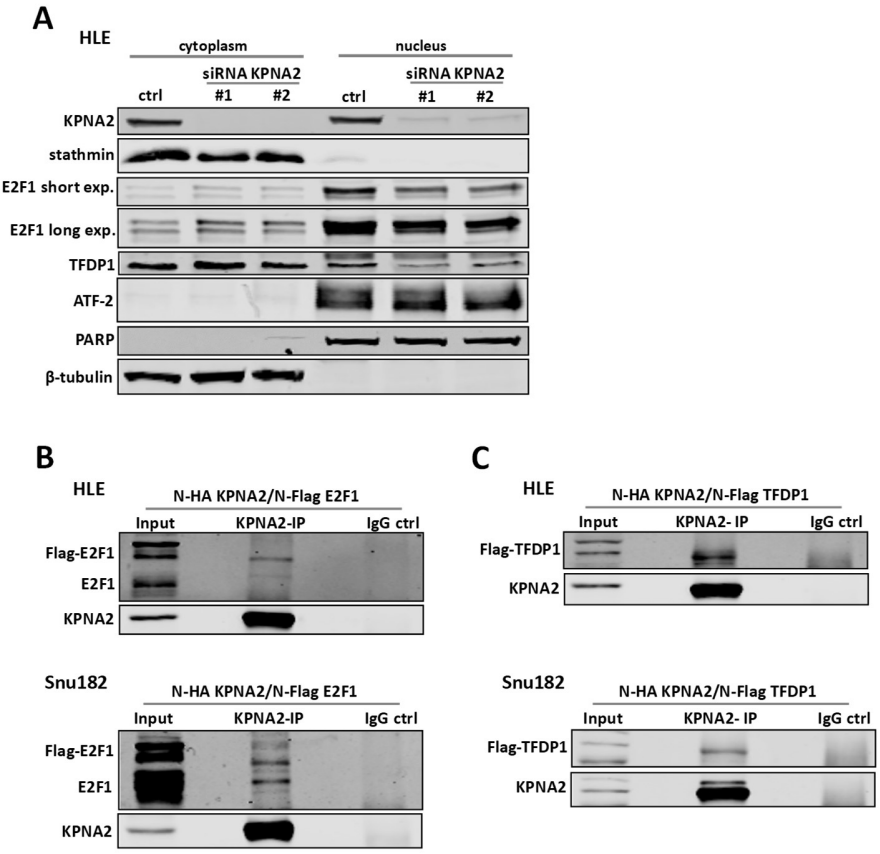

Figure 5.10: KPNA2 mediates the nuclear import of E2F1 and TFDP1. (A) HLE cells were treated with siRNAs directed against KPNA2 or a control siRNA (ctrl) and nuclear and cytoplasmic fractionation assay was performed 72 h later. Samples were immunoblotted using the indicated antibodies. β-tubulin (cytoplasmic fraction) and PARP (nuclear fraction) served as loading controls. **(B)** KPNA2 (N-HA KPNA2) was overexpressed in HLE and Snu182 cells in combination with E2F1 (N-Flag E2F1) and KPNA2 was immunoprecipitated 24 h later. Binding of KPNA2 and E2F1 was analyzed by immunoblot. IgG served as an IP control. **(C)** KPNA2 (N-HA KPNA2) was overexpressed in HLE and Snu182 cells in combination with TFDP1 (N-Flag TFDP1) and KPNA2 was immunoprecipitated 24 h later. Binding of KPNA2 and TFDP1 was analyzed by immunoblot. IgG served as an IP control.

As depicted in Figure 5.10 A, immunoblot analysis showed a retention of E2F1 and TFDP1 in the cytoplasmic fraction and subsequently a decrease in the nuclear fraction. The transcription factor ATF-2 served as a negative control to exclude a general import defect. As a next step, CoIP was performed to

confirm direct interaction between KPNA2 and E2F1/TFDP1. Therefore, KPNA2 (N-HA KPNA2) was overexpressed in combination with E2F1 (N-Flag E2F1) or TFDP1 (N-Flag TFDP1) in HLE and Snu182 cells and CoIP assays were carried out 24 h later. Following immunoprecipitation of KPNA2, E2F1 (Figure 5.10 B) and TFDP1 (Figure 5.10 C) could be detected as KPNA2 binding partners by immunoblotting, confirming KPNA2 as nuclear import receptor for both proteins.

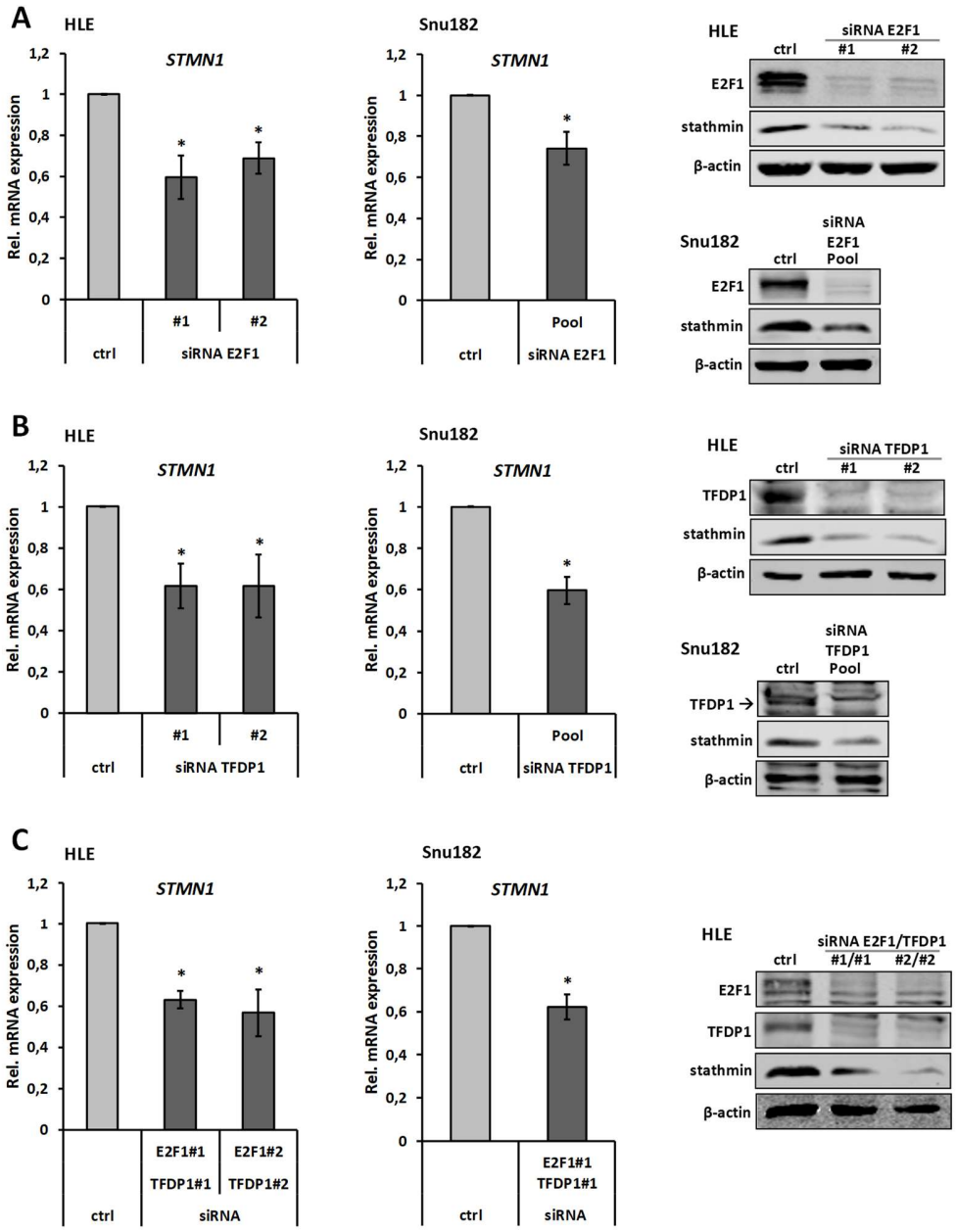

Figure 5.11: E2F1 and TFDP1 are required for full expression of *STMN1*. (A) HLE and Snu182 cells were treated with siRNAs directed against E2F1 or a control siRNA (ctrl) and *STMN1* expression was analyzed 48 h later using qRT-PCR (n=4; *p<0.05; HLE SD ctrl: +/- 0.001; Snu182 SD ctrl: +/- < 0.001) or 96 h later by western

blot using the indicated antibodies. **(B)** HLE and Snu182 cells were treated with a siRNAs directed against TFDP1 or a control siRNA (ctrl) and *STMN1* expression was analyzed 48 h later using qRT-PCR (n=4; *p<0.05; HLE SD ctrl: +/- < 0.001; Snu182 SD ctrl: +/- 0.002) or 96 h later by western blot using the indicated antibodies. **(C)** HLE and Snu182 cells were treated with a combination of siRNAs directed against E2F1 and TFDP1 or a control siRNA (ctrl) and *STMN1* expression was analyzed 48 h later using qRT-PCR (n=4; *p<0.05; HLE SD ctrl: +/- 0.002; Snu182 SD ctrl: +/- < 0.001) or 96 h later by western blot using the indicated antibodies. qRT-PCR data were normalized to the respective control siRNA.

Subsequently, direct siRNA-mediated knockdown of E2F1 and TFDP1 was performed. In line with the hypothesis, results showed significantly reduced *STMN1* expression on protein and mRNA level as demonstrated by immunoblot and qRT-PCR analysis in HLE and Snu182 cells (Figures 5.11 A and B). Interestingly, combined depletion of E2F1 and TFDP1 did not further increase the effect on *STMN1* transcript or protein abundance compared to the individual knockdowns (Figure 5.11 C). In conclusion, the obtained data indicate that KPNA2 regulates *STMN1* by nuclear import of its transcription factors E2F1 and TFDP1. Most likely due to the fact that the two proteins bind to DNA as heterodimers [103], combined depletion of both transcription factors does not increase the effect size on the *STMN1* transcription.

5.5.5 E2F1 binds to the promoter region of *STMN1*

To ascertain direct binding of E2F1 to the promoter region of *STMN1* ChIP assays were performed. In a first step binding sites for E2F1 within the regulatory region of *STMN1* were searched for using a publicly available ChIP-Seq database (accessible via https://www.encodeproject.org/). Indeed, three ChIP-Seq datasets for E2F1 IP in the cell lines HeLa-S3, K562 and MCF-7 were found (see Appendix). Each dataset showed two peaks indicating strong protein-DNA binding within the *STMN1* promoter region. The respective DNA sequences were aligned resulting in two roughly 250 bp long consensus sequences. Subsequently, primers were designed to amplify sequences within the predicted binding sites. The E2F1 binding sites within the *STMN1* promoter are depicted in Figure 5.12 A. The promoter region of *CDC2* served as a positive control due to its reported interaction with E2F1 [104]. Following E2F1 IP, a 5-20-fold larger amount of DNA was precipitated at the predicted *STMN1* promoter binding sites compared to the IgG control IP, while no significant amount of DNA was obtained of the negative control region (Figure 5.12 B). Therefore, the data indicated direct binding of E2F1 to the regulatory region of *STMN1*.

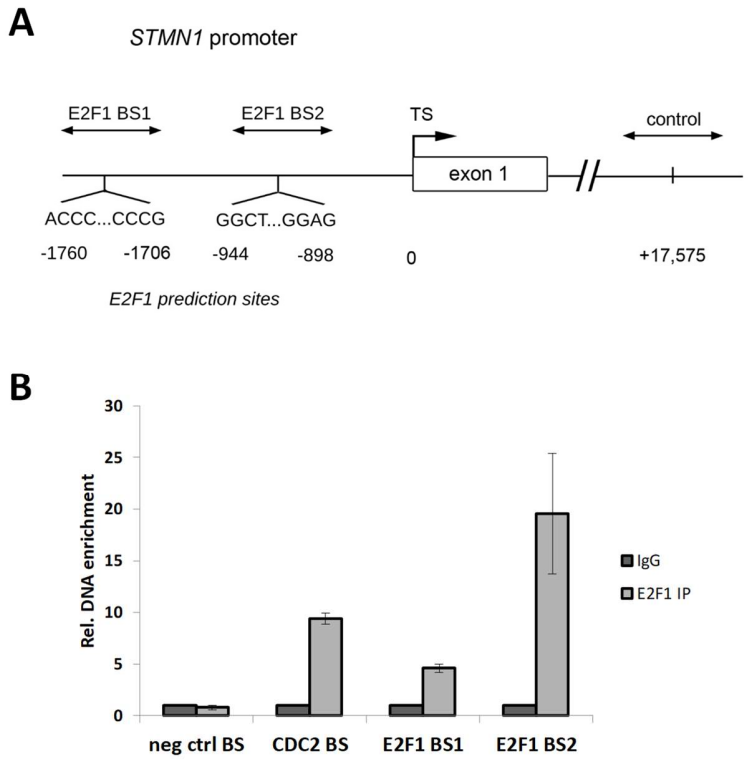

Figure 5.12: E2F1 binds to the promoter region of *STMN1*. (A) Scheme of the predicted E2F1 binding sites within the *STMN1* promoter and the negative control region as predicted by encodeproject.org. **(B)** E2F1 was immunoprecipitated in HLE cells, ChIP assay was performed and precipitated DNA of the predicted *STMN1* bindings sites was quantified using qPCR. DNA enrichment was quantified relative to the IgG control IP. One representative experiment is shown (n=2). BS: binding site; TS: transcription start site.

5.6 Regulation of *KPNA2* expression in HCC

5.6.1 E2F1 and TFDP1 are not involved in the regulation of KPNA2 in HCC

As shown in Figure 5.10, KPNA2 facilitates the nuclear import of E2F1 and TFDP1 in HCC. In addition, it was reported that E2F1 and TFDP1 act as *KPNA2* transcription factors and thereby drive its overexpression in cancer [105, 106]. These data suggest a positive feedback loop in which KPNA2 translocates its own transcription factors to the nucleus. Therefore, E2F1 and TFDP1 were depleted in HLE cells and *KPNA2* mRNA expression was analyzed 48 h later by qRT-PCR. As depicted in Figure 5.13 A, measurement of two biological replicates showed inconsistent results for the two used siRNAs. Data analysis following TFDP1 knockdown showed no decrease of *KPNA2* mRNA levels (Figure 5.13 B). In summary, no convincing evidence was found for the regulation of *KPNA2* by E2F1/TFDP1 in HCC cells.

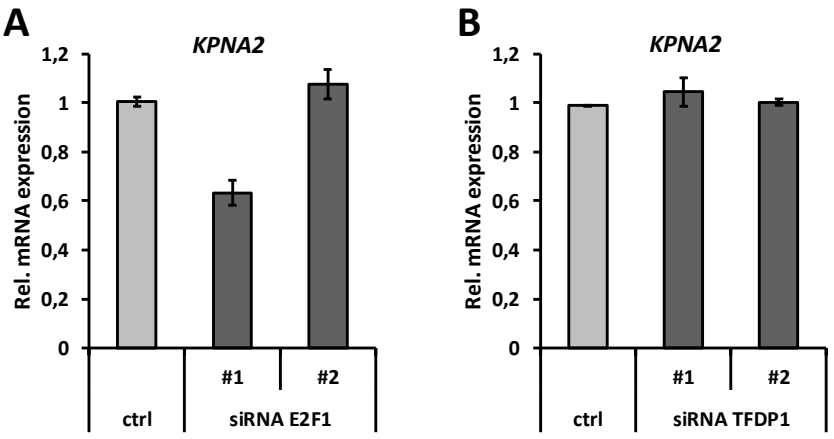

Figure 5.13: Regulation of *KPNA2* expression by E2F1 and TFDP1. (A) HLE cells were treated with siRNAs directed against E2F1 or a control siRNA (ctrl) and KPNA2 mRNA expression was analyzed 48 h later by qRT-PCR (n=2; SD ctrl: +/- 0.019). **(B)** HLE cells were treated with siRNAs directed against TFDP1 or a control siRNA (ctrl) and KPNA2 mRNA expression was analyzed 48 h later by qRT-PCR (n=2; SD ctrl: +/- < 0.001). Data were normalized to the respective control siRNA.

5.6.2 KPNA2 is a p53 repression target in liver cancer

The significance of mutations in the *TP53* locus and alterations of the p53 pathway in tumor development, maintenance and progression is indisputable [22, 107, 108]. Winkler et al. previously reported repression of KPNA2 by p53 [61]. Following up on these findings, Sk-Hep1 and HuH6 cells were treated with Nutlin-3a or DMSO as a control for 24 h and 48 h and protein and mRNA expression were analyzed using immunoblotting and qRT-PCR. Recapitulating the results of the above-mentioned study, repression of KPNA2 by p53 could be confirmed in Sk-Hep1 cells (Figure 5.14 A) and further validated in HuH6 cells (Figure 5.14 B). Since p53 is frequently mutated in HCC and p53 gain-of-function mutations were demonstrated to drive overexpression of different (onco-)genes in cancer it was hypothesized that mutant p53 is involved in the strong expression of KPNA2 in liver cancer cell lines [108–111]. Therefore, p53 was depleted in the HCC cell lines HLE and Snu182 which harbor different p53 aberrations (HLE: 249 R→S; Snu182: 215: S→I [112, 113]) . However, knockdown of mutant p53 did not change KPNA2 protein abundance (Figure 5.14 C). In summary, a strong negative regulation of KPNA2 by wildtype p53 induction could be confirmed by western blot and qRT-PCR in liver cancer *in vitro*.

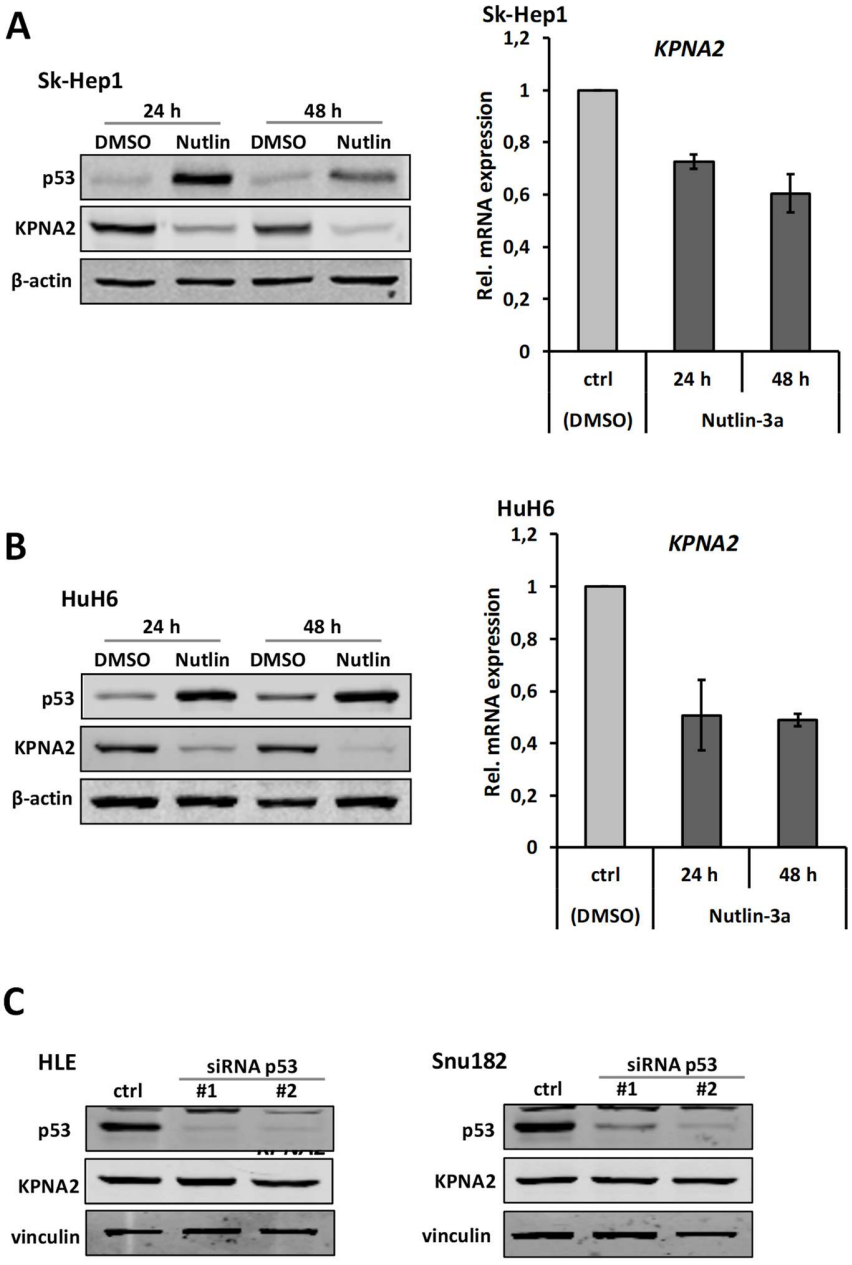

Figure 5.14: KPNA2 is a repression target of p53. (A) Sk-Hep1 cells were treated with Nutlin-3a for 24 h and 48 h or DMSO as a control (ctrl) and analyzed by immunoblotting using the indicated antibodies and by qRT-PCR (n=2; SD ctrl: +/- < 0.001). **(B)** HuH6 cells were treated as described in (A) and analyzed by immunoblotting using the indicated antibodies and by qRT-PCR (n=2; SD ctrl: +/- < 0.001). **(C)** HLE and Snu182 were treated with siRNAs targeting p53 or a control siRNA (ctrl) and KPNA2 expression was analyzed 72 h later by immunoblotting using the indicated antibodies. Vinculin served as loading control. qRT-PCR data were normalized to the respective control siRNA.

5.7 The Kpna2-E2f1/Tfdp1-Stathmin axis in murine HCC models

5.7.1 Stathmin is overexpressed in murine HCC models with different genetic alterations

To overcome the limitations of *in vitro* experiments, different strategies exist for induction of HCC in mouse models. Murine liver cancer models combine overexpression of oncogenes with depletion of tumor suppressor genes that were demonstrated to be aberrantly expressed in human HCC [114]. To follow up on the regulation of KPNA2 by p53, a collection of murine HCC samples was analyzed where HCCs developed in Black 6 mice with a *p19^{ARF}* and/or *Trp53* deleted background in combination with transposon-based expression of mutated N-ras (*N-ras^{G12V}*), c-myc (*Myc^{OE}*) and/or Akt-1 in murine livers following hydrodynamic tail-vein injection (samples kindly provided by Dr. Daniel Dauch) [115].

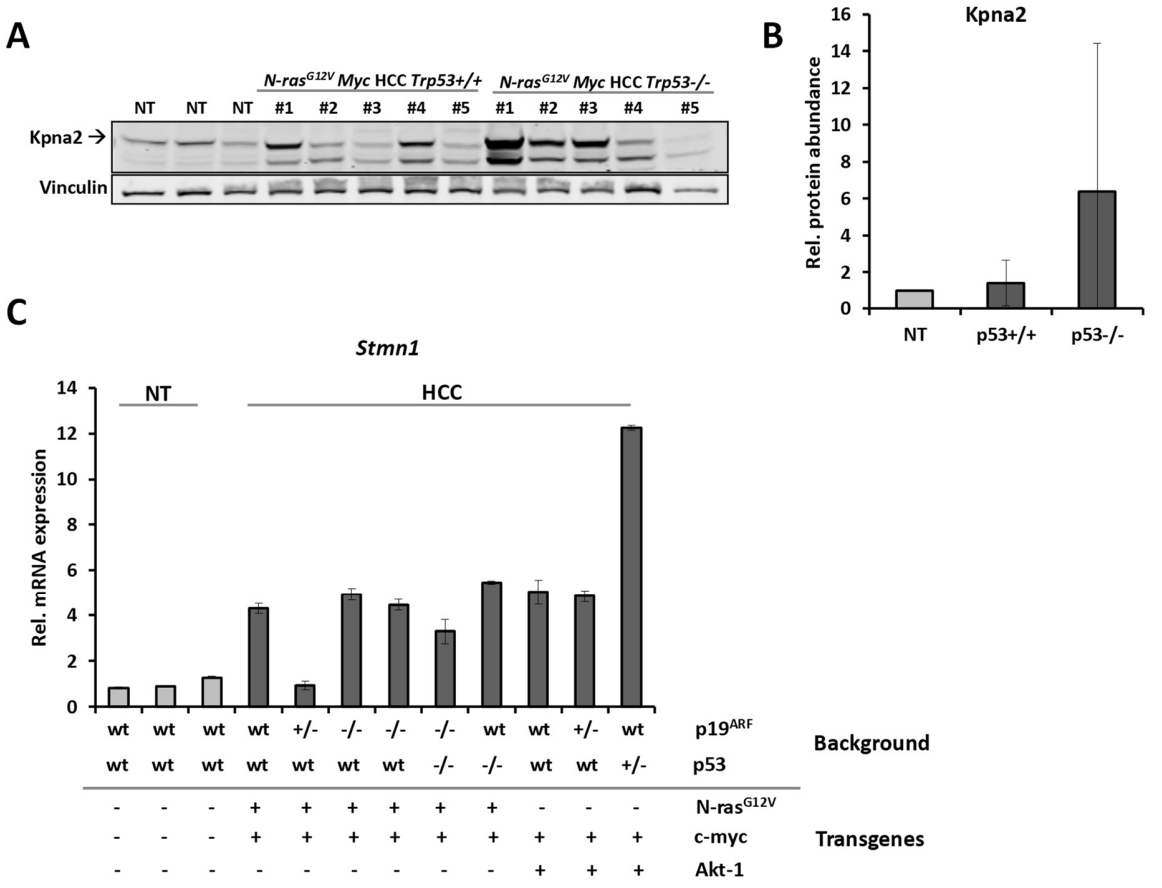

Figure 5.15: Stathmin is overexpressed in murine liver tumors with different genetic alterations. **(A)** Western blot analysis of KPNA2 expression in three Black 6 liver and 10 HCC tissue samples of mice harboring p53 wildtype or p53-/- background. Transgenes (N-ras^{G12V} and Myc) were delivered using hydrodynamic tail-vein injection. Vinculin served as loading control (wt: wildtype; NT: non-tumorous liver tissue). **(B)** Densitometric analysis of the antibody signal intensities of the western blot depicted in (A). **(C)** Analysis of *Stmn1* mRNA expression in three Black 6 liver and 11 HCC tissue samples of different genetic background. Transgenes (N-ras^{G12V}, Myc and Akt-1) were delivered using hydrodynamic tail-vein injection.

mRNA expression was normalized to five different reference genes using GENORM. Results were normalized to the mean of the three non-tumorous samples.

As depicted in Figure 5.15 A, western blot analysis of *Trp53* wildtype versus depleted samples revealed a moderate to strong expression of Kpna2 compared to non-tumorous tissue (NT) in roughly 50% of the tested murine HCCs. In line with the previously indicated negative regulation of KPNA2 by p53, higher Kpna2 protein levels were observed in tumor samples obtained from *Trp53-/-* mice (Figure 5.15 B). Analysis of *Stmn1* mRNA in the same mouse model showed a 4- to 12-fold increased expression in 10 out of 11 tested murine HCCs (Figure 5.15 C). Based on the genetic alterations of the mice, a specific pattern driving the overexpression of *STMN1* could not be identified. Next to the negative regulation of KPNA2 by p53, these data suggest an overexpression of Kpna2 and Stathmin in murine tumor compared to normal liver tissue.

5.7.2 Stathmin is overexpressed in an E2f1-driven murine HCC model

An E2f1-driven HCC mouse model was used to analyze E2F1-dependent Stathmin expression in a setting closer to the human *in vivo* situation. Therefore, Conner et al. generated transgenic mice which express E2f1 under the control of an albumin-promoter and therefore in a liver specific manner [77]. Additionally, the authors experimentally validated binding of E2f1 to Tfdp1 by CoIP, ensuring that the two proteins can form heterodimers and subsequently act as potent transcriptional activators in this model [77]. To analyze Stathmin expression, full FFPE sections of murine livers containing non-tumorous tissue, precursor lesions and HCC were H&E stained and by using immunohistochemistry (IHC) with a Stathmin antibody. As shown in Figure 5.16 A, already the precursor lesions (right column) showed a high Stathmin immunoreactivity compared to the adjacent liver tissue that became even more striking in the full-blown tumors (left column). All tumors found per mouse were evaluated individually. As depicted in Figure 5.16 B, a positivity for Stathmin was detected in all tumors found in the 11 tested transgenic mice with predominantly moderate to high staining intensity.

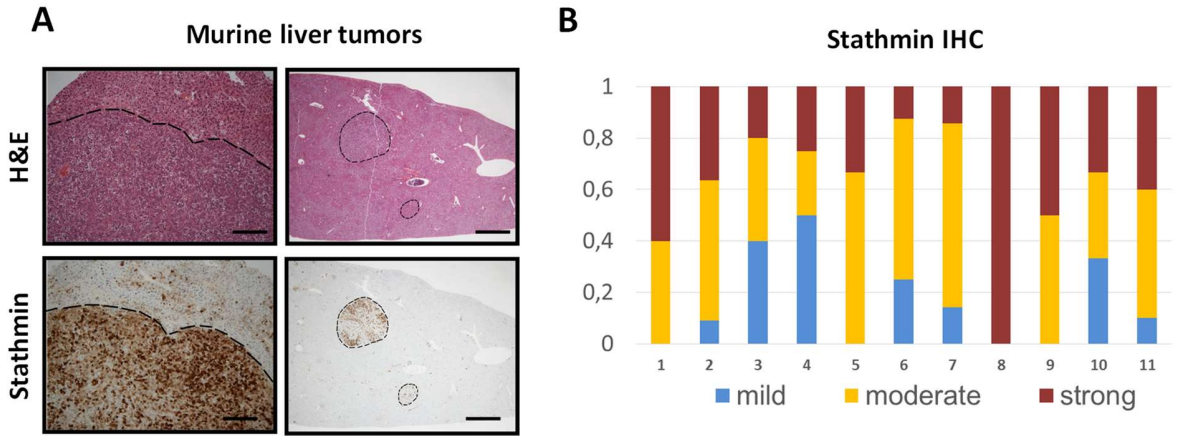

Figure 5.16: Stathmin is overexpressed in E2f1-driven murine liver tumors. (A) Representative H&E (upper row) and stathmin staining (lower row) of transgenic E2f1-driven murine liver tumors (left column) and precursor lesions (right column). Full FFPE sections; scale bars: 100 µM (left column), 1 mm (right column); dotted lines indicate tumor boarder. **(B)** The bar diagram shows Stathmin protein expression of liver tumors in the individual transgenic mice as percentage of total liver tumors per mouse showing mild, moderate or strong Stathmin immunoreactivity (n=11; IHC: immunohistochemistry).

5.8 The KPNA2-E2F1/TFDP1-stathmin axis in human HCC cohorts

5.8.1 *KPNA2* and *STMN1* expression are correlated in human HCC tissue

To correlate the obtained data to the human *in vivo* situation, KPNA2 and stathmin expression was investigated in human HCCs by using immunohistochemical staining of a tissue microarray (TMA) containing 95 HCC FFPE samples. Supporting the previous findings, a strong and highly significant correlation ($r=0.73$; $p<0.0001$) between the IHC scores of KPNA2 and stathmin was found (Figure 5.17 A). Immunoreactivity was additionally evaluated according to the respective tumor grades of the HCCs. As depicted in Figure 5.17 B a significant positive correlation between protein abundance and tumor grading was identified (KPNA2: $r=0.48$; $p<0.0001$; stathmin: $r=0.39$; $p<0.0001$).

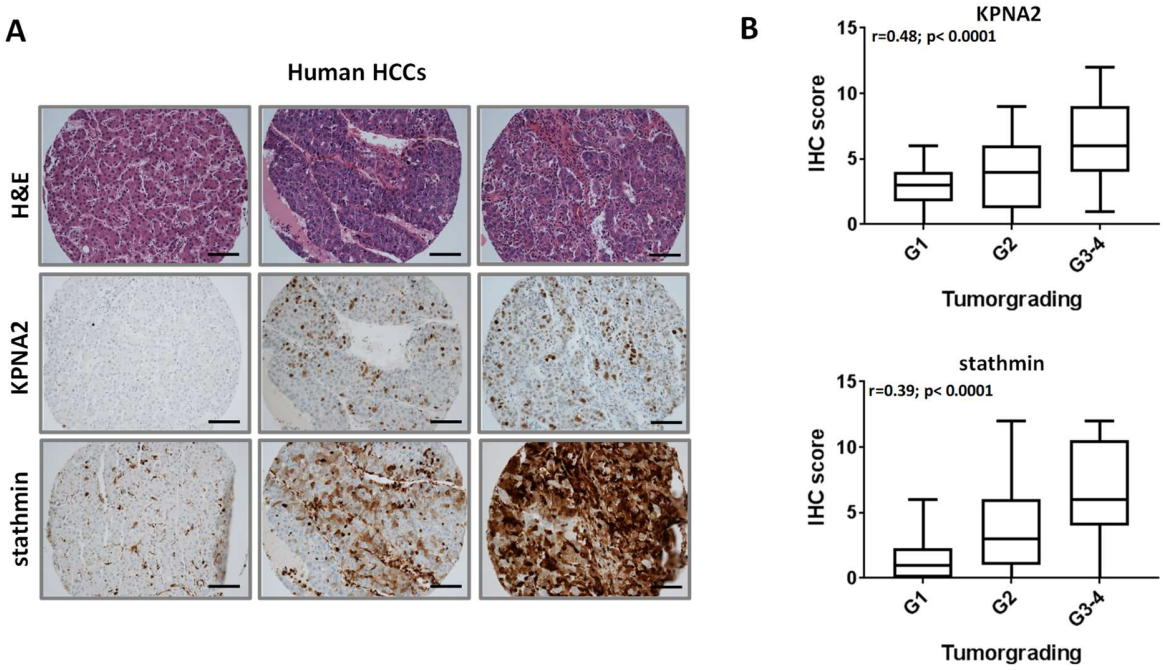

Figure 5.17: KPNA2 and stathmin expression are correlated in human HCC. (A) A tissue microarray (TMA) containing 95 human HCC FFPE samples was either H&E stained (upper row) or immunoassayed with KPNA2 (middle row) or stathmin (lower row) antibodies (r=0.73; p<0.0001; scale bar: 100 µm). **(B)** The whisker plots illustrate IHC scores of KPNA2 (upper panel) and stathmin (lower panel) dependent on tumor dedifferentiation (G1: well differentiated, n=14; G2: moderately, n=52; G3-4: poorly differentiated, n=29).

In vivo expression of KPNA2 and stathmin was further evaluated analyzing transcriptomic data from a larger cohort of 247 HCC patients (Roessler cohort) [78]. Samples within this cohort predominantly origin from patients with a HBV infections and Chinese ethnicity [78]. Analysis of *KPNA2* and *STMN1* RNA levels in tumor and adjacent non-tumorous liver tissue showed a significant overexpression of both proteins in HCC (Figure 5.18 A). Besides overexpression in HCC tissue, the correlation between KPNA2 and stathmin expression demonstrated in TMA samples was recapitulated on mRNA level (r=0.61; p<0.0001; Figure 5.18 B). Based on the observed KPNA2/stathmin-dependent effects on the clonogenic and migratory capacity, it was assumed that high levels of both factors correlate with a more aggressive phenotype as indicated by poor patient outcome. Thus, Kaplan-Meier analyses using survival data of the Roessler cohort was performed. In line with the above-mentioned assumption, patients with high expression of *KPNA2* and/or *STMN1* (cut-off: median) in tumor samples showed a poorer overall outcome (Figure 5.18 C).

To validate results obtained by evaluation of the Roessler cohort, transcriptomic expression data from a second independent cohort were analyzed. The TCGA LIHC cohort (the cancer genome atlas, liver

hepatocellular carcinoma, accessible via: http://cancergenome.nih.gov) contains HCC samples of 371 patients of mixed sex and etiologies and Caucasian and Asian background. Paralleling previous findings, the TCGA LIHC cohort revealed significantly higher expression levels of *KPNA2* and *STMN1* RNA in HCC compared to non-tumorous samples (Figure 5.18 D). Furthermore, a significant positive correlation between the expression levels of both factors was confirmed ($r=0.63$; $p<0.0001$; Figure 5.18 E). Finally, Kaplan-Meier analyses confirmed poorer overall survival in patients showing high expression of both factors (cut-off: median; Figure 5.18 F). In summary, it was demonstrated that KPNA2 and stathmin are overexpressed and positively correlated in human HCCs as shown by analysis of a HCC TMA and two independent HCC cohorts. Furthermore, in line with the involvement of KPNA2 and stathmin in clonogenicity and migration *in vitro*, high expression of both genes/proteins was associated with poor patient outcome.

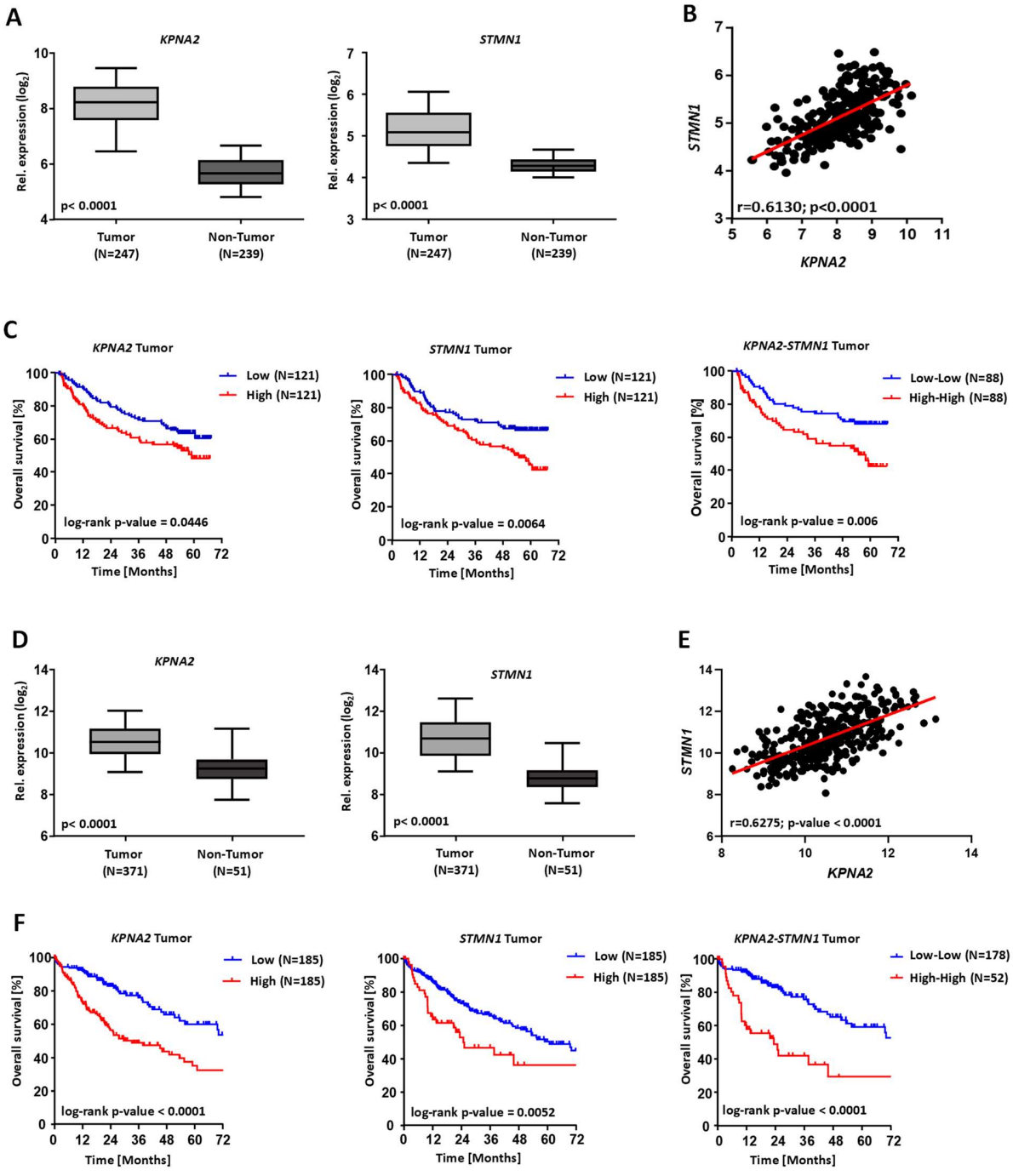

Figure 5.18: *KPNA2* and *STMN1* are overexpressed and related to poor survival in HCC patient samples. **(A)** Analysis of transcriptomic data of *KPNA2* and *STMN1* expression in human HCC and adjacent non-tumorous liver tissue of the Roessler cohort. **(B)** Spearman correlation between *KPNA2* and *STMN1* RNA expression in human HCC samples of the Roessler cohort. **(C)** Overall survival (Kaplan-Meier analysis) of patients of the Roessler cohort displaying a low and high expression of *KPNA2* and *STMN1* (cut-off: median). **(D)** Analysis of transcriptomic data of *KPNA2* and *STMN1* expression in human HCC and adjacent non-tumorous liver tissue of the TCGA LIHC cohort. **(E)** Spearman correlation between *KPNA2* and *STMN1* RNA expression in human HCC samples of the TCGA LIHC cohort. **(F)** Overall survival (Kaplan-Meier analysis) of

patients of the TCGA LIHC cohort displaying a low and high expression of *KPNA2* and *STMN1* (cut-off: median).

5.8.2 E2F1 is overexpressed in human HCC tissue

The expression of *E2F1* and *TFDP1* in human HCC was studied using data of the TCGA LIHC cohort described above. As depicted in Figure 5.19 A, analysis of *E2F1* and *TFDP1* RNA levels revealed a significant overexpression of *E2F1* in tumor compared to non-tumor tissue. However, for *TFDP1* no aberrant RNA expression was found within this cohort. Controversially, evaluation of the Roessler cohort showed no differential expression of *E2F1* in tumor and adjacent tissue (data not shown). Nevertheless, Kaplan-Meier analyses of overall survival of HCC patients exhibiting high and low expression of *E2F1* and *TFDP1* (cut-off: median) showed a significantly poorer outcome for patients highly expressing both genes (Figure 5.19 B). Thus, despite no difference in *TFDP1* RNA levels were found between tumor and non-tumor samples, heterogeneity within the tumor group allowed association of patients with higher *TFDP1* levels with a more aggressive phenotype.

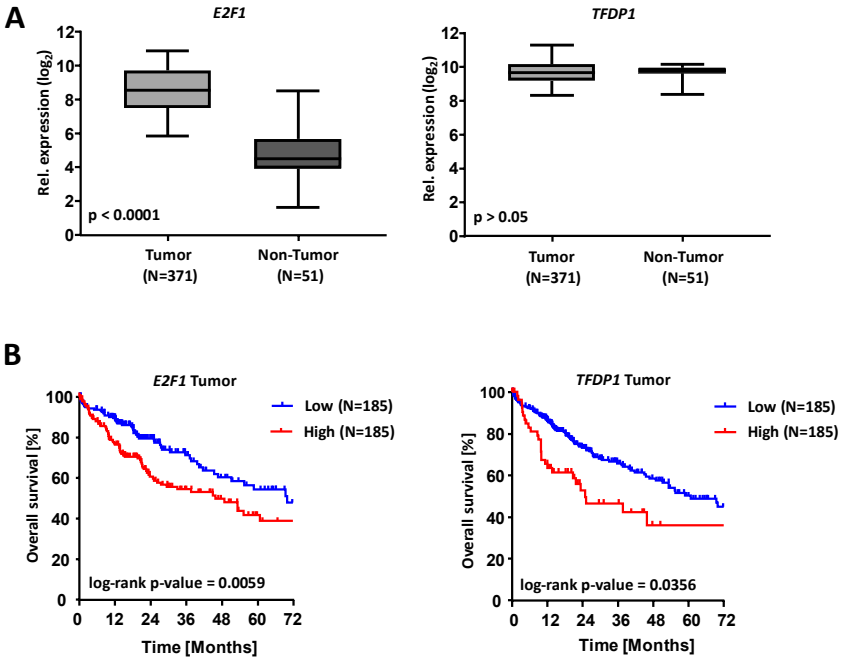

Figure 5.19: *E2F1* is overexpressed and related to poor survival in HCC patient samples. (A) Analysis of transcriptomic data of *E2F1* and *TFDP1* expression in human HCCs and adjacent non-tumorous liver tissue of the TCGA LIHC cohort. **(B)** Overall survival (Kaplan-Meier analysis) of patients of the TCGA LIHC cohort displaying a low and high expression of *E2F1* and *TFDP1* (cut-off: median).

Ultimately, to link the *in vitro* demonstrated regulation of *STMN1* by E2F1 and TFDP1, expression levels of the two transcription factors and *STMN1* were correlated using the transcriptomic data of the Roessler cohort. As shown in Figure 5.20, a positive correlation between *E2F1* and *STMN1* (r=0.400; p<0.0001) and *TFDP1* and *STMN1* (r=0.382; p<0.0001) was found. In summary, the data support the here demonstrated mechanism by which KPNA2 regulates oncogenic *STMN1* expression via the import of E2F1 and TFDP1 in HCC. As shown by patient data of the Roessler and TCGA LIHC cohorts, even in human HCCs which harbor manifold and complex genetic alterations overexpression of KPNA2 could be linked to stathmin and its transcription factors E2F1 and TFDP1.

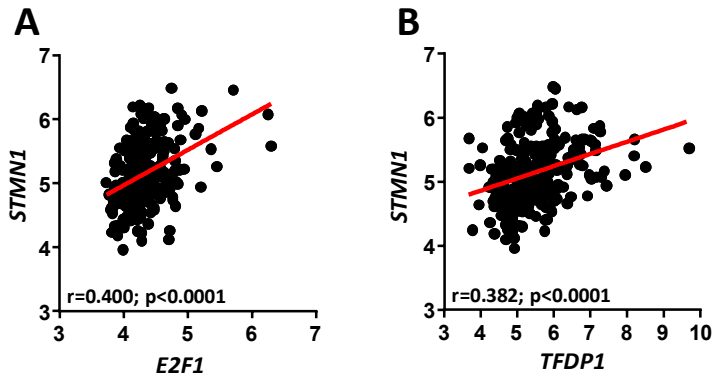

Figure 5.20: Expression of *STMN1* and its transcription factors *E2F1* and *TFDP1* are correlated in HCC patient samples. (A) Spearman correlation between *E2F1* and *STMN1* RNA expression in human HCC samples of the Roessler cohort (n=247). **(B)** Spearman correlation between *TFDP1* and *STMN1* RNA expression in human HCC samples of the Roessler cohort (n=247).

6 DISCUSSION

6.1 Protumorigenic expression of stathmin is mediated by KPNA2-dependent nuclear import of E2F1 and TFDP1 in liver cancer

Owing to its substantial role in nucleo-cytoplasmic translocation of oncogenes and tumor suppressors, the nuclear transport machinery is of outstanding importance in tumorigenesis [46, 51, 116]. Following up on previous data showing the aberrant expression of karyopherins in liver cancer [61], the functional and mechanistic role of KPNA2 was further elucidated. Here, a novel link between KPNA2 and the MT-associated protein stathmin was identified using a proteomic approach. It was demonstrated that KPNA2 expression correlates with clonogenic and migratory capacity of HCC cells suggesting a protumorigenic role in hepatocarcinogenesis. Furthermore, the decrease in clonogenicity and migration upon KPNA2 depletion was phenocopied upon stathmin knockdown. Elucidating the underlying mechanism by which KPNA2 regulates the expression of *STMN1*, the transcription factors E2F1 and TFDP1 were identified as nuclear import substrates of KPNA2 (Figure 6.1).

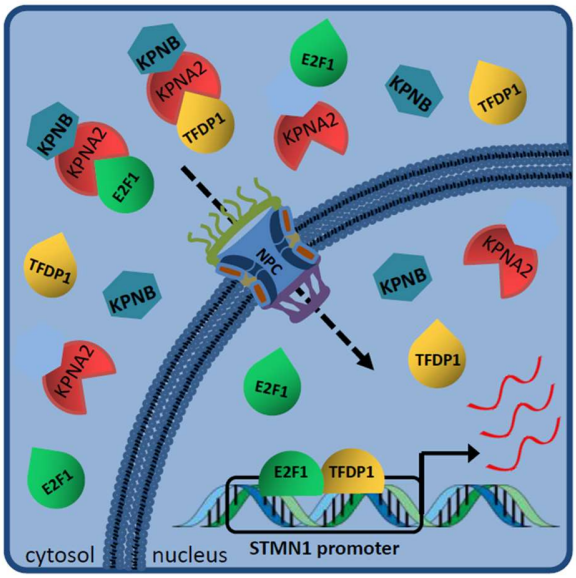

Figure 6.1: KPNA2 drives protumorigenic *STMN1* expression by nuclear import of E2F1 and TFDP1. KPNA2 binds to NLS of E2F1/TFDP1 and form a trimeric complex with KPNB. Upon translocated to nucleus through the NPC, the complex dissociates and E2F1 and TFDP1 can act as *STMN1* transcription factors.

Correlating these *in vitro* findings with data from murine and human HCC tissues, overexpression of KPNA2 and stathmin and a strong correlation to each other could be verified *in vivo*. In conclusion,

though extensively more research is needed, targeting KPNA2 could represent a promising therapeutic approach in treatment of HCC.

6.2 Differential expression of nuclear transport factors in cancer

Mediating nuclear import of oncogenes and/or tumor suppressors, nuclear transport factors are pivotal for regulation of (aberrant) gene expression in cancer [48, 51, 75]. Transcription factors of small molecular weight (i.e. < 40 kDa) such as β-catenin and SMADs 2-4 can enter the nucleus independently, however, the import of bigger molecules (e.g. STAT 1-3, p65) relies on nuclear transport receptors [46–48, 51]. In general, nuclear transport is regulated by modifications of the cargo protein (e.g. phosphorylation, methylation), the abundance of the transport receptors and the quantity of nuclear pores [46]. In cancer, deregulation of nuclear import can occur on different levels and mainly involves masking of the nuclear localization signal, aberrant upstream signaling or protein modifications [46]. Subsequent mislocalization of proteins can severely alter cellular processes and therefore drive tumorigenesis [46]. For instance, the normal function of the tumor suppressor p53 as transcription factor relies on its localization in the nucleus [24, 27]. It is well known that many, if not most, human tumors harbor mutations in the *TP53* locus [22, 26, 27]. However, sequestration of wild-type p53 in the cytoplasmic compartment can also cause functional inactivation and was shown in different tumor entities (e.g. colorectal and ovarian cancer) [117, 118].

With few exceptions, almost all members of the karyopherin family, including KPNA2, have been shown to be aberrantly expressed in human cancers [51, 61, 75, 116]. Within this thesis, it was shown that KPNA2 is not only strongly expressed in different liver cancer cell lines (Figure 5.1), but also in murine and human HCCs (Figures 5.17 and 5.18). Overexpression of KPNA2 could be caused by transcriptional as well as post-transcriptional mechanisms. Since KPNA2 was reported to be repressed by p53, one possible event could be de-repression resulting from inactivating mutations of wildtype p53 [49, 61]. Furthermore, the *KPNA2* gene is located in the 17q24.2 region in which gene amplifications have been previously described in HCC [119]. At the post-transcriptional level, it was shown that the KPNA2 mRNA is a target of miRNA26b, which is downregulated in HCC [120]. Moreover, since tumors are highly proliferative tissues, upregulation of KPNA2 could be advantageous for cancer cells to mediate transcriptional activation of genes involved in (unlimited) cell growth.

6.3 Quantitative proteomics reveals regulation of stathmin by KPNA2

Using quantitative proteomics, the MT-interacting protein stathmin was identified as "downstream target" of KPNA2 (Figure 5.2). Stathmin is an ubiquitously expressed cytosolic phosphoprotein which is essential for and tightly regulated during cell cycle and cell division based on its inhibitory effect on microtubules formation [70, 121]. Additionally, stathmin was previously reported to be involved in tumor development and progression [65, 72, 73, 84]. Since interaction of karyopherins and microtubule regulation was not described before, connecting KPNA2 and stathmin expression provides a novel link between nuclear import and the microtubule network. Interestingly, the proteomic dataset also indicated upregulation of TPX2 following KPNA2 depletion. TPX2 is a microtubule-associated protein involved in microtubule nucleation and spindle pole formation during mitosis and meiosis [122]. In line with the here presented data, it was previously shown that karyopherin alpha inhibits microtubule nucleation during M phase of mitosis by inactivation of TPX2 [123]. Besides other malignancies, TPX2 was reported to be overexpressed in human HCC patient samples and associated with poor overall survival [124]. Moreover, TPX2 knockdown was linked to reduced tumor cell migration and invasion *in vitro* in HCC [123, 124]. Thus, stathmin and TPX2 could act as player and counter player in the regulation of microtubule dynamics with TPX2 compensating for the functional deficits upon KPNA2 depletion.

Next to stathmin, the proteomic dataset proposed aberrant expression of different proteins following KPNA2 knockdown (Table 5.1). The strongest downregulation was found for serine and arginine rich splicing factor 6 (SRSF6) and GTSF1. SRSF6 is a splicing factor documented to be frequently amplified and overexpressed in colon and lung cancer [125]. Thus, deregulated expression of SRSF6 was shown to result in alternative splicing of oncogenes and tumor suppressor, thereby enhancing tumor formation [125]. GTSF1 is a protein mainly expressed in male germ cells and involved in spermatogenesis [85]. Downregulation of GTSF1 following KPNA2 depletion as recognized in the proteomics dataset was verified using a second siRNA by immunoblotting (Figure 5.3), suggesting KPNA2 as nuclear import receptor for GTSF1. Additionally, GTSF1 was recently shown to be overexpressed and related to clonogenicity and tumor size in liver cancer [85, 86]. Although validation of the decrease of protein abundance of Syntenin-1 following KPNA2 knockdown as shown by LC-MS/MS analysis led to controversial results (Figure 5.3), other studies could demonstrate the significance of Syntenin-1 in cancer [89, 126, 127]. Syntenin-1 is a tandem PDZ domain containing protein involved in multiple cell signaling events located at the plasma membrane (e.g. receptor trafficking, cell adhesion, immunoregulation) [89, 126, 128]. In a liver cancer context, Liu et al. reported overexpression of Syntenin-1 in hepatoma cell lines compared to immortalized hepatocytes

(i.e. THLE-3) and were able to correlate the high Syntenin-1 expression to enhanced clonogenic and proliferative properties *in vitro* [127].

Taken together, evaluation of the here presented LC-MS/MS dataset revealed differential regulation of multiple proteins involved in cancer biology. The connection of KPNA2 to factors involved in development, alternative splicing of tumor suppressors/oncogenes and regulation of the immune response underlines the central role of KPNA2 in nuclear import of proteins that mediate the malignant behavior of tumor cells. Focusing on the microtubule network, the proteomic data in combination with published studies point towards a complex functional and mechanistic involvement of KPNA2 in the regulation of microtubule associated proteins. Since stathmin and TPX2 are of fundamental significance for mitosis, their differential regulation in HCC is most likely required to maintain a highly proliferative phenotype.

6.4 KPNA2 and stathmin expression drive colony formation and tumor cell migration in HCC

The ability of cancer cells to sustain unlimited proliferation and to invade and metastasize are indisputable hallmarks of cancer [16]. Therefore, single tumor cells are capable of forming new colonies based on their unlimited proliferation capacity, which is also pivotal for invasion of surrounding tissues [16, 129]. In the here presented study it was demonstrated that the liver cancer cells show a significant reduction in clonogenic capacity following siRNA-mediated KPNA2 and stathmin depletion (Figure 5.5). In line with these findings, Noetzel et al. previously reported that the breast cancer cell line MCF-7 has a higher colony formation capacity than benign cells and that KPNA2 knockdown reduces the clonogenic potential of MCF-7 cells [130]. Similar results were found for shRNA-mediated KPNA2 knockdown in the liver cancer cell lines HepG2 and SMMC-7721 [131]. Additionally, impaired clonogenic capacity was also described after stathmin depletion in esophageal and oral squamous cell carcinoma, lung adenocarcinoma and pancreatic cancer [132–135].

Deregulation of migration pathways enables tumor cell migration and formation of metastases [136]. Thus, the significance of KPNA2 and stathmin expression for cancer progression in HCC was further underlined by the finding that depletion of both proteins results in a significant decrease in cell migration in HLE cells as indicated by two-dimensional scratch assays (Figure 5.7). Noteworthy, migration assay could not be performed in Snu182 cells due to high toxic effects following treatment. In order to inhibit proliferation and to secure measurement of migratory behavior itself cells were treated with Mitomycin C before scratching the cell monolayer [137]. Since a markedly higher cell

division rate was observed for Snu182 cells the loss in viability is most probably due to the higher sensitivity to Mitomycin C treatment. Paralleling the here shown data in HLE cells, it was previously demonstrated that KPNA2 knockdown decreases tumor cell migration in breast carcinoma and NSCLC cell lines [130, 138]. Consistent results were described after stathmin silencing in different entities including oral squamous cell carcinoma, NSCLC and most importantly in HCC [65, 73, 135]. As pivotal components of the cytoskeleton, microtubules and their regulatory proteins such as stathmin are crucial for cell migration and the therefore necessary re-orientation of the microtubules network [139]. Since stathmin has to be inactivate for mitosis, the fact that depletion of stathmin results in reduction of clonogenicity seems rather counter-intuitive. However, though extensively studied, not all mechanisms involved in cell cycle regulation are elucidated yet. Loss of stathmin could disbalance the complex signaling that tightly regulates mitosis. Since the functional decrease in colony formation and migration capacity following stathmin depletion exceeds the effect upon KPNA2 knockdown, the phenotype demonstrated after depletion of the latter could be due to the associated reduction in stathmin expression.

6.5 KPNA2 regulates *STMN1* by import of its transcription factors E2F1 and TFDP1

6.5.1 KPNA2 facilitates the nuclear import of E2F1 and TFDP1

Since KPNA2 is not known to act as transcription factor itself, regulation of stathmin expression was expected to rely on an indirect mechanism. Therefore, it was hypothesized that KPNA2 regulates stathmin by nuclear import of its transcription factors. It was previously demonstrated that siRNA mediated FBP-1 knockdown causes a decrease in stathmin expression in HCC and NSCLC [73, 99]. The FBP family member FBP-2 was assessed due to its reported co-regulation with stathmin, even though a transcriptional regulation could not be detected in the respective study [99]. However, respective cell fractionation experiments showed no accumulation of FBP-1 or -2 in the cytoplasm following KPNA2 depletion (Figure 5.9), indicating that KPNA2 does not act as nuclear import receptor for FBP-1/-2. Thus, FBP-1/-2 were not considered relevant for KPNA2-dependent stathmin regulation although direct knockdown of FBP-1 caused a strong downregulation of stathmin expression on transcript level. Since FBP-1 contains a NLS [140], it is most likely imported into the nucleus by another member of the karyopherin family. Using a proteomic approach, Fukumoto et al. identified KPNA1 as nuclear import receptor of FBP-1 in murine brain tissue [141]. Additionally, another proteomic study in murine embryotic fibroblasts indicates nuclear import of FBP-1 by KPNA6 [142]. Assessment of the AP-1 transcription factor c-JUN was conducted based on its regulation of stathmin in non-adherent Rat-1a cells (i.e. rat fibroblasts) as described by Kinoshita et al. [100]. Cell fractionation and CoIP experiments

confirmed nuclear import of c-JUN by KPNA2 (Figure 5.9). Controversially, Waldmann et al. reported that the nuclear import of c-JUN solely relies on karyopherin-beta and that the presence of karyopherin-alpha inhibits c-JUN translocation into the nucleus in HeLa cells [143]. In contrast, analysis of the control samples of the here shown fractionation experiment depicted the presence of c-JUN in the nucleus in the presence of KPNA2. However, subsequently direct knockdown of c-JUN showed no effect on stathmin expression levels. Thus, the here shown experiments indicate a nuclear import of c-JUN mediated by KPNA2 but no transcriptional regulation of stathmin by c-JUN.

Continuing the screening for stathmin transcription factors, nuclear import of E2F1 and TFDP1 by KPNA2 was analyzed. The E2F family comprises of several proteins that act either as transcriptional activators (E2F1-E2F3a) or repressors (E2F3b-E2F7) of genes involved in cell-cycle control [103, 104]. In order to exert its role as transcription factor and to bind to DNA, E2F1 has to heterodimerize with the dimerization partner family member TFDP1, thereby allowing cooperative binding to and activation of the respective promoter regions of target genes [144]. It was previously reported that exogenous overexpression of E2F1 alone or in combination with TFDP1, but not of TFDP1 alone, enhances *STMN1* expression on mRNA level in the liver cancer cell lines HuH7 and Hep3B [101]. The here performed cell fractionation and CoIP experiments revealed a sequestration of E2F1 and TFDP1 in the cytoplasm following KPNA2 depletion and direct binding of both transcription factors to KPNA2 (Figure 5.10), indicating a nuclear import of both proteins by KPNA2. Consistent with these results, co-localization and direct binding of KPNA2 and E2F1 was previously found in NSCLC cells [49]. Moreover, Mackmull et al. recently published an interactome dataset of nuclear transport receptors and their cargo proteins generated by coupling a proximity ligation approach with mass spectrometry analysis (BioID technique) [102]. Thereby the authors identified TFDP1 and the E2F family members E2F3 and E2F6 as KPNA2 transport cargo [102]. In contrast to the here presented data, E2F1 did not appear as KPNA2 interaction partner in this dataset which is mostly likely due to the use of HEK293 cells and their embryonic origin in the experimental setup, highlighting the importance of (liver) cancer specific interactome studies.

6.5.2 E2F1 and TFDP1 transcriptionally regulate *STMN1* expression

Transient silencing of E2F1 and TFDP1 showed a decrease in *STMN1* mRNA abundance following individual gene knockdown of roughly 40% which corresponds to the effect size observed upon KPNA2 depletion (Figure 5.11). Interestingly, combined knockdown of E2F1 and TFDP1 did not further enhance the observed effect. Since E2F1 and TFDP1 cooperate to induce target gene expression as heterodimer [104], it is most likely that absence of one dimerization partner is sufficient to cause reduced transcriptional activation. Surprisingly, interrogating the proteomics data obtained after KPNA2

knockdown in HLE cells no other known E2F1 targets (e.g. CDK1 MCM2-7, MYC) showed up in this dataset [145]. This result is probably due to the indirect regulation via nuclear import and the possible use of alternative import receptors of the karyopherin family. Additionally, using different large-scale techniques (e.g. microarrays, ChIP-Seq) hundreds of E2F1 target genes have been proposed [145], however, systematic overview of E2F1-responsive genes is hard to achieve. Since transcription of *STMN1* is only partially reduced following E2F1 and TFDP1 depletion the involvement of additional transcription factors is likely. As demonstrated in this thesis, FBP-1 is a potent *STMN1* transcription factor that is not imported into the nucleus by KPNA2. Therefore, despite the absence of E2F1/TFDP1 transcriptional activation of *STMN1* can still be exerted by binding of FBP-1 to its promoter region. Interestingly, Malz et al. reported that the FBP-interacting repressor (FIR), which is overexpressed in HCC cell lines and patient samples, triggers tumor cell proliferation and migration via E2F1 and TFDP1 dependent transcription of FBP-1 [146]. However, reduced abundance of FBP-1 was not detected analyzing the proteomic data generated following KPNA2 knockdown.

In order to verify direct binding of E2F1 to the *STMN1* promoter ChIP assays were performed. Analysis of three independent ChIP-Seq datasets upon E2F1 immunoprecipitation revealed two "binding hotspots" for E2F1 within the regulatory region of *STMN1*. Confirming the *STMN1* binding sites, ChIP assays revealed strong binding of E2F1 to both predicted binding sites (Figure 5.12). In line with the here presented data, Chen et al. previously reported that combined exogenous overexpression of E2F1 and TFDP1 enhances *STMN1* promoter activity in the HCC cell lines HuH7 and Hep3B [101]. However, the authors could not demonstrate the independent importance of TFDP1 in *STMN1* transcription. E2F1 and TFDP1 cooperatively bind to DNA as heterodimer [144], therefore they have to be able to bind to the same DNA sequence. Despite this fact, additional alignment of ChIP-Seq datasets generated upon E2F1 and TFDP1 pulldown showed the highest scores for protein-DNA binding in close proximity, but distinct regions of the *STMN1* promoter (data not shown). Thus, high affinity of one dimerization partner might be sufficient to enable promoter binding. To address this theory, additional ChIP experiments could be performed to analyze binding of E2F1 and TFDP1 to the *STMN1* promoter prediction site of the respective other dimerization partner.

6.6 Regulation of KPNA2 expression

Additional to the nuclear import of E2F1 and TFDP1 by KPNA2 it was previously reported that E2F1 acts as *KPNA2* transcription factor[105, 106], suggesting a possible positive feedback loop. However, the here performed experiments indicated no convincing transcriptional regulation of *KPNA2* by E2F1 or TFDP1 in HCC cells (Figure 5.13). Despite confirmed binding of E2F1 and TFDP1 to the *KPNA2* promoter

in lung and cervical cancer cells, van der Watt et al. did only demonstrate an effect of TFDP1, but not of E2F1 on KPNA2 protein expression in the above mentioned publication [105]. Noteworthy, Wang et al. showed KPNA2 downregulation on protein and mRNA level following combined depletion of E2F1 and TFDP1 in NSCLC without distinguishing between the regulatory impact of the single transcription factors [106]. Taken together, there is strong evidence for E2F1 and TFDP1 binding sites within the *KPNA2* promoter region, however, so far both cited publications lack individual knockdown of E2F1 and TFDP1 as well as appropriate control by the use of two individual siRNAs. Therefore, the transcriptional activation of *KPNA2* by E2F1 and TFDP1 remains to be further elucidated.

In normal cells p53 is usually inactivated by binding to its inhibitor MDM2 and located in the cytoplasm and translocates only into the nucleus upon cellular stress [147]. It was previously reported that p53 harbors three NLS which allow binding to members of the karyopherin-alpha family and that vice versa p53 inhibits KPNA2 expression [61, 148, 149]. Following up on the by Winkler et al. reported repression of KPNA2 by p53 in liver cancer [61], this finding could be confirmed in the here presented study (Figure 5.14). However, mRNA expression of *KPNA2* was affected to a lesser extent than protein abundance by p53 induction, suggesting the additional involvement of posttranslational regulation. Mutations of p53 not only cause functional inactivation of the resulting protein, they were also demonstrated to promote protumorigenic processes [108, 110]. Since the cell lines used in this study harbor mutations within the *TP53* locus, it was hypothesized that expression of mutated p53 could drive overexpression of KPNA2 in liver cancer. However, in line with previous findings [61], knockdown of mutated p53 (HLE: 249 R→S; Snu182: 215: S→I [112, 113]) did not cause the expected reduction in KPNA2 protein abundance. Therefore, overexpression of KPNA2 in HCC is most likely driven by inactivation of wildtype p53 signaling (e.g. by mutational and/or functional inactivation, cytoplasmic sequestration) in HCC. Furthermore, it has to be evaluated if other p53 mutations and especially gain-of-function mutations enhance KPNA2 expression. Therefore, further experiments are needed to study the impact of mutation, localization and functionality of p53 in a karyopherin-dependent context.

6.7 *In vivo* significance of the KPNA2-E2F1/TFDP1-stathmin axis

6.7.1 Kpna2 and Stathmin in murine HCC models

Samples of two different mouse models were used to evaluate the biological significance of Kpna2, E2f1/Tfdp1 and Stathmin *in vivo*. Analysis of HCC tissue samples of different genetic origin generated by Dauch et al. [115] revealed overexpression of Kpna2 on protein and of *Stmn1* on mRNA level in murine HCCs compared to non-tumorous liver tissue (Figure 5.15). Methodologically, comparison

between Kpna2 protein and *Stmn1* mRNA expression was chosen as suitable approach since data so far indicated regulation of *Stmn1* transcription by Kpna2-mediated nuclear import. Reflecting the human *in vivo* situation, Kpna2 expression was only enhanced in a subset of murine HCC samples of this model. Complementary, using an E2f1-driven HCC mouse model designed by Conner et al. [77], E2f1-dependent expression of Stathmin could be confirmed *in vivo* (Figure 5.16). The observed high Stathmin abundance especially in full-blown tumors indicates a steady rise in Stathmin expression in the course of HCC progression.

6.7.2 KPNA2 and stathmin expression are correlated and associated with poor survival in human HCCs

To ultimately correlate the here presented *in vitro* findings to patient data, tissue microarrays were immunoassayed for KPNA2 and stathmin expression, confirming a strong expression of KPNA2 and stathmin (Figure 5.17). Interestingly, when samples were grouped according to tumor dedifferentiation, a strong positive correlation between abundance of both proteins and tumor grade was found. These findings are in line with the in the E2f1-driven HCC mouse model observed stronger expression of Stathmin in full blown tumors compared to dysplastic nodules. Taken together, analysis of murine and human HCC tissues indicates a steady increase in KPNA2 and stathmin expression during cancer progression.

To confirm the observed data in a larger setup, two independent patient cohorts (Roessler and TCGA LIHC cohorts) that together comprise the transcriptomic data of more than 600 individuals were analyzed. Patient data of both cohorts revealed strong expression of *KPNA2* and *STMN1* in HCC compared to adjacent non-tumorous tissue and a significant positive correlation of the expression of the two proteins (Figure 5.18). Furthermore, high abundance of KPNA2 and *STMN1* was associated with poor patient outcome. Reflecting the controversially discussed role of E2F1 in HCC, analysis of *E2F1* expression showed no differential expression in the Roessler cohort (data not shown), but a significantly higher expression correlated with poor survival in tumor samples of the TCGA LIHC cohort (Figure 5.19). As previously mentioned, the vast majority of patients within the Roessler cohort developed HCC on the background of HBV infection. Interestingly, Choi et al. demonstrated that direct binding of E2F1 to HBx inhibits the HBx-mediated repression of p53 transcription, indicating a protective effect of high E2F1 expression in HBV driven hepatocarcinogenesis [150]. For *TFDP1*, both cohorts showed no alterations in RNA levels. However, within the tumor group of the TCGA LIHC cohort, high *TFDP1* expression was linked to low patient survival, underlining the molecular heterogeneity of tumors between individual patients. Overall, the congruent findings in the Roessler and TCGA LIHC

cohort substantiate the biological significance of KPNA2 and stathmin especially since the cohorts include patients with different tumor etiologies and ethnicities. In conclusion, the strong expression and correlation of KPNA2 and stathmin highlights the relevance of the KPNA2-E2F1/TFDP1-stathin axis at least in a significant fraction of human HCCs.

6.8 The KPNA2-E2F1/TFDP1-stathmin axis as potential therapeutic target

The overexpression of nuclear transport factors as shown here for KPNA2 along with the associated protumorigenic properties, the poor overall survival and the reported significance as prognostic markers make them valid candidates for targeted cancer therapies [116]. So far, the only available compounds are inhibitors of XPO1, karyopherin-beta 2 (KPNB2), karyopherin-beta 1 (KPNB1) and the KPNA/KPNB1 complex [51, 51, 116]. Although drugs exist that disrupt the KPNA/KPNB1 transport cycle (e.g. cSN50.1, Importazole), development never advanced to the stage of clinical trials [116]. A large proportion of research is done on so-called SINE (selective inhibitors of nuclear export) compounds targeting XPO1, with the most prominent of them being Selinexor (KPT-330) which is currently tested in clinical studies [151]. Zheng et al. studied the effect of Selinexor in HCC cell lines and reported reduction of viability and proliferation and PUMA-mediated induction of apoptosis following Selinexor treatment [152]. Using *in vivo* studies in mice, Selinexor was also proven to show potent anti-tumor effects after oral administration in pancreatic cancer by mediation of accumulation of the pro-apoptotic protein PAR-4 in the nucleus [153]. Similar results were for example found for Selinexor and other SINE compounds in triple-negative breast cancer via nuclear sequestration and inhibition of STAT3-mediated transcription of surviving and in NSCLC by induction of cell cycle arrest and pro-apoptotic factors [154, 155]. Currently, clinical trials (phase I and II) are ongoing for treatment of different hematologic and solid cancers [151]. As all KPNAs are translocated from the nucleus to the cytoplasm by XPO2 (KPNA-XPO2-RanGTP complex), which was previously shown to be highly expressed and of functional relevance in HCC [53, 61, 156], also inhibition of the KPNA-XPO2 interaction could be a promising therapeutic strategy. Using a chemo-proteomic approach, Tian et al. recently identified gambogic acid as potent inhibitor of XPO2 and demonstrated that gambogic acid treatment interrupts the XPO2/KPNA2 transport cycle by accumulation of both proteins in the nucleus [157]. However, due to the broad range of biological effects of gambogic acid (e.g. inhibition of topoisomerase IIa and Bcl-2, modulation of NFκB signaling) [157, 158], isolated investigation of the effects of KPNA2 inhibition on tumor treatment is challenging and needs further investigation.

The role of E2F1 in HCC is controversially discussed. As shown based on the TCGA LIHC data, E2F1 is overexpressed in HCC compared to adjacent non-tumorous tissue and high expression of E2F1 is related

to poor patient outcome. Moreover, E2F1 was shown to transcriptionally activate expression of genes involved in enhanced proliferation (e.g. *CDC2*) and it was previously demonstrated that depletion of E2F1 reduces liver cancer cell growth and survival [159]. Controversially, overexpression of E2F1 was also linked to pro-apoptotic features in HCC [159]. In the above-mentioned mouse model of Conner et al., authors showed that E2F1 signaling exerts proliferative and pro-apoptotic effects of E2F1 overexpression in different stages of hepatocarcinogenesis [77]. Conducting an *in vitro* study on Sorafenib in HCC Zhai et al. found that Sorafenib exerts its anti-cancer properties by inhibition of E2F1 [160]. However, due to the dual role of E2F1 in HCC downstream effectors/target genes of E2F1 could represent more eligible targets for future therapies. Thus, one option would be to target stathmin directly. Different studies showed that silencing of stathmin results, next to the here demonstrated inhibition of clonogenicity, in cell cycle arrest and apoptosis [71]. Based on their role in mitosis, microtubules are established targets in cancer therapy by treatment with destabilizing (vinca alkaloids, e.g. Vinblastin) or stabilizing (taxanes, e.g. Paclitaxel) compounds which ultimately induce apoptosis in dividing cells [161]. Like for many chemotherapeutic agents, also resistance of cancer cells to microtubule inhibitors have been reported [71]. Several studies demonstrated that overexpression of stathmin in solid tumors reduces sensitivity of cancer cells to treatment with taxanes while divergent reports exist for the interaction of stathmin and vinca alkaloids [162, 163]. In line with the reported inhibition of taxane activity by stathmin, Wang et al. demonstrated that stathmin depletion sensitizes osteosarcoma cells for taxane treatment [164]. Thus, development of a potent stathmin inhibitor could represent a viable candidate for combinational therapy.

Since KPNA2 exerts its function upstream of E2F1, stathmin and other oncogenic factors, targeting KPNA2 could have a substantial effect on tumor cells. So far, Sorafenib, and Regorafenib as second-line treatment, are the only available drugs for systemic treatment of advanced HCC, both extending overall survival only for roughly three months [41, 42]. Therefore, there is an urgent need for development of novel and more selective compounds for (targeted) therapy of HCC. Though extensively more research is needed, targeting KPNA2 and other karyopherins, which play a critical role in tumorigenesis by translocation of oncogenes and tumor suppressors [75], could provide a future perspective for selective treatment of liver cancer.

7 References

1. Laursen L. A preventable cancer. Nature. 2014:S2-S3. doi:10.1002/hep.27388.

2. Farazi PA, DePinho RA. Hepatocellular carcinoma pathogenesis: from genes to environment. Nat Rev Cancer. 2006;6:674–87. doi:10.1038/nrc1934.

3. Ferlay J, Soerjomataram I, Dikshit R, Eser S, Mathers C, Rebelo M, et al. Cancer incidence and mortality worldwide: sources, methods and major patterns in GLOBOCAN 2012. Int J Cancer. 2015;136:E359-86. doi:10.1002/ijc.29210.

4. El-Serag HB. Epidemiology of viral hepatitis and hepatocellular carcinoma. Gastroenterology. 2012;142:1264-1273.e1. doi:10.1053/j.gastro.2011.12.061.

5. El-Serag HB, Rudolph KL. Hepatocellular carcinoma: epidemiology and molecular carcinogenesis. Gastroenterology. 2007;132:2557–76. doi:10.1053/j.gastro.2007.04.061.

6. Massarweh NN, El-Serag HB. Epidemiology of Hepatocellular Carcinoma and Intrahepatic Cholangiocarcinoma. Cancer Control. 2017;24:1073274817729245. doi:10.1177/1073274817729245.

7. Scaglioni F, Ciccia S, Marino M, Bedogni G, Bellentani S. ASH and NASH. Dig Dis. 2011;29:202–10. doi:10.1159/000323886.

8. Balogh J, Victor D, Asham EH, Burroughs SG, Boktour M, Saharia A, et al. Hepatocellular carcinoma: a review. J Hepatocell Carcinoma. 2016;3:41–53. doi:10.2147/JHC.S61146.

9. Marengo A, Rosso C, Bugianesi E. Liver Cancer: Connections with Obesity, Fatty Liver, and Cirrhosis. Annu Rev Med. 2016;67:103–17. doi:10.1146/annurev-med-090514-013832.

10. Ladep NG, Lesi OA, Mark P, Lemoine M, Onyekwere C, Afihene M, et al. Problem of hepatocellular carcinoma in West Africa. World J Hepatol. 2014;6:783–92. doi:10.4254/wjh.v6.i11.783.

11. Meireles LC, Marinho RT, van Damme P. Three decades of hepatitis B control with vaccination. World J Hepatol. 2015;7:2127–32. doi:10.4254/wjh.v7.i18.2127.

12. Rahib L, Smith BD, Aizenberg R, Rosenzweig AB, Fleshman JM, Matrisian LM. Projecting cancer incidence and deaths to 2030: the unexpected burden of thyroid, liver, and pancreas cancers in the United States. Cancer Res. 2014;74:2913–21. doi:10.1158/0008-5472.CAN-14-0155.

13. Thorgeirsson SS, Grisham JW. Molecular pathogenesis of human hepatocellular carcinoma. Nat Genet. 2002;31:339–46. doi:10.1038/ng0802-339.

14. Kumar M, Zhao X, Wang XW. Molecular carcinogenesis of hepatocellular carcinoma and intrahepatic cholangiocarcinoma: one step closer to personalized medicine? Cell Biosci. 2011;1:5. doi:10.1186/2045-3701-1-5.

15. Yang X-R, Xu Y, Yu B, Zhou J, Qiu S-J, Shi G-M, et al. High expression levels of putative hepatic stem/progenitor cell biomarkers related to tumour angiogenesis and poor prognosis of hepatocellular carcinoma. Gut. 2010;59:953–62. doi:10.1136/gut.2008.176271.

16. Hanahan D, Weinberg RA. The Hallmarks of Cancer. Cell. 2000;100:57–70. doi:10.1016/S0092-8674(00)81683-9.

17. Hanahan D, Weinberg RA. Hallmarks of cancer: the next generation. Cell. 2011;144:646–74. doi:10.1016/j.cell.2011.02.013.

18. Stratton MR, Campbell PJ, Futreal PA. The cancer genome. Nature. 2009;458:719–24. doi:10.1038/nature07943.

19. Zucman-Rossi J, Villanueva A, Nault J-C, Llovet JM. Genetic Landscape and Biomarkers of Hepatocellular Carcinoma. Gastroenterology. 2015;149:1226-1239.e4. doi:10.1053/j.gastro.2015.05.061.

20. Vogelstein B, Lane D, Levine AJ. Surfing the p53 network. Nature. 2000;408:307–10. doi:10.1038/35042675.

21. Murray-Zmijewski F, Slee EA, Lu X. A complex barcode underlies the heterogeneous response of p53 to stress. Nat Rev Mol Cell Biol. 2008;9:702–12. doi:10.1038/nrm2451.

22. Bieging KT, Mello SS, Attardi LD. Unravelling mechanisms of p53-mediated tumour suppression. Nat Rev Cancer. 2014;14:359–70. doi:10.1038/nrc3711.

23. Riley T, Sontag E, Chen P, Levine A. Transcriptional control of human p53-regulated genes. Nat Rev Mol Cell Biol. 2008;9:402–12. doi:10.1038/nrm2395.

24. Pflaum J, Schlosser S, Müller M. p53 Family and Cellular Stress Responses in Cancer. Front Oncol. 2014;4:285. doi:10.3389/fonc.2014.00285.

25. Kastenhuber ER, Lowe SW. Putting p53 in Context. Cell. 2017;170:1062–78. doi:10.1016/j.cell.2017.08.028.

26. Soussi T. The p53 pathway and human cancer. Br J Surg. 2005;92:1331–2. doi:10.1002/bjs.5177.

27. Harris SL, Levine AJ. The p53 pathway: positive and negative feedback loops. Oncogene. 2005;24:2899–908. doi:10.1038/sj.onc.1208615.

28. Milner J, Medcalf EA, Cook AC. Tumor suppressor p53: analysis of wild-type and mutant p53 complexes. Mol. Cell. Biol. 1991;11:12–9. doi:10.1128/MCB.11.1.12.

29. Sigal A, Rotter V. Oncogenic mutations of the p53 tumor suppressor: the demons of the guardian of the genome. Cancer Res. 2000;60:6788–93.

30. Bullock AN, Fersht AR. Rescuing the function of mutant p53. Nat Rev Cancer. 2001;1:68–76. doi:10.1038/35094077.

31. Soussi T, Lozano G. p53 mutation heterogeneity in cancer. Biochem Biophys Res Commun. 2005;331:834–42. doi:10.1016/j.bbrc.2005.03.190.

32. Dhanasekaran R, Bandoh S, Roberts LR. Molecular pathogenesis of hepatocellular carcinoma and impact of therapeutic advances. F1000Res 2016. doi:10.12688/f1000research.6946.1.

33. European Association for the Study of the Liver, European Organisation for Research and Treatment of Cancer. EASL-EORTC clinical practice guidelines: management of hepatocellular carcinoma. J Hepatol. 2012;56:908–43. doi:10.1016/j.jhep.2011.12.001.

34. Heimbach JK, Kulik LM, Finn RS, Sirlin CB, Abecassis MM, Roberts LR, et al. AASLD guidelines for the treatment of hepatocellular carcinoma. Hepatology. 2018;67:358–80. doi:10.1002/hep.29086.

35. Sakamoto M. Early HCC: diagnosis and molecular markers. J Gastroenterol. 2009;44 Suppl 19:108–11. doi:10.1007/s00535-008-2245-y.

36. Bruix J, Reig M, Sherman M. Evidence-Based Diagnosis, Staging, and Treatment of Patients With Hepatocellular Carcinoma. Gastroenterology. 2016;150:835–53. doi:10.1053/j.gastro.2015.12.041.

37. Spangenberg H-C. Evolving therapies in the treatment of hepatocellular carcinoma. BTT. 2008;Volume 2:453–62. doi:10.2147/BTT.S3254.

38. Llovet JM, Villanueva A, Lachenmayer A, Finn RS. Advances in targeted therapies for hepatocellular carcinoma in the genomic era. Nat Rev Clin Oncol. 2015;12:408–24. doi:10.1038/nrclinonc.2015.103.

39. Llovet Josep M., Ricci Sergio, Mazzaferro Vincenzo, Hilgard Philip, Gane Edward, Blanc Jean-Frédéric, et al. Sorafenib in Advanced Hepatocellular Carcinoma.

40. Spangenberg HC, Thimme R, Blum HE. Targeted therapy for hepatocellular carcinoma. Nat Rev Gastroenterol Hepatol. 2009;6:423–32. doi:10.1038/nrgastro.2009.86.

41. Bruix J, Qin S, Merle P, Granito A, Huang Y-H, Bodoky G, et al. Regorafenib for patients with hepatocellular carcinoma who progressed on sorafenib treatment (RESORCE): a randomised, double-blind, placebo-controlled, phase 3 trial. The Lancet. 2017;389:56–66. doi:10.1016/S0140-6736(16)32453-9.

42. Reig M, da Fonseca LG, Faivre S. New trials and results in systemic treatment of HCC. J Hepatol. 2018;69:525–33. doi:10.1016/j.jhep.2018.03.028.

43. Cervello M, McCubrey JA, Cusimano A, Lampiasi N, Azzolina A, Montalto G. Targeted therapy for hepatocellular carcinoma: novel agents on the horizon. Oncotarget. 2012;3:236–60. doi:10.18632/oncotarget.466.

44. Kabachinski G, Schwartz TU. The nuclear pore complex - structure and function at a glance. Journal of Cell Science. 2015;128:423–9. doi:10.1242/jcs.083246.

45. Kohler A, Hurt E. Gene regulation by nucleoporins and links to cancer. Mol Cell. 2010;38:6–15. doi:10.1016/j.molcel.2010.01.040.

46. Kau TR, Way JC, Silver PA. Nuclear transport and cancer: from mechanism to intervention. Nat Rev Cancer. 2004;4:106–17. doi:10.1038/nrc1274.

47. Stewart M. Molecular mechanism of the nuclear protein import cycle. Nat Rev Mol Cell Biol. 2007;8:195–208. doi:10.1038/nrm2114.

48. Beck M, Schirmacher P, Singer S. Alterations of the nuclear transport system in hepatocellular carcinoma - New basis for therapeutic strategies. J Hepatol. 2017;67:1051–61. doi:10.1016/j.jhep.2017.06.021.

49. Wang C-I, Chien K-Y, Wang C-L, Liu H-P, Cheng C-C, Chang Y-S, et al. Quantitative proteomics reveals regulation of karyopherin subunit alpha-2 (KPNA2) and its potential novel cargo proteins in nonsmall cell lung cancer. Mol Cell Proteomics. 2012;11:1105–22. doi:10.1074/mcp.M111.016592.

50. Christiansen A, Dyrskjot L. The functional role of the novel biomarker karyopherin alpha 2 (KPNA2) in cancer. Cancer Lett. 2013;331:18–23. doi:10.1016/j.canlet.2012.12.013.

51. Çağatay T, Chook YM. Karyopherins in cancer. Current Opinion in Cell Biology. 2018;52:30–42. doi:10.1016/j.ceb.2018.01.006.

52. Fabbro M, Henderson BR. Regulation of tumor suppressors by nuclear-cytoplasmic shuttling. Experimental Cell Research. 2003;282:59–69. doi:10.1016/S0014-4827(02)00019-8.

53. Goldfarb DS, Corbett AH, Mason DA, Harreman MT, Adam SA. Importin alpha: a multipurpose nuclear-transport receptor. Trends Cell Biol. 2004;14:505–14. doi:10.1016/j.tcb.2004.07.016.

54. Clark SL, Rodriguez AM, Snyder RR, Hankins GDV, Boehning D. Structure-Function Of The Tumor Suppressor BRCA1. Comput Struct Biotechnol J 2012. doi:10.5936/csbj.201204005.

55. Tseng S-F, Chang C-Y, Wu K-J, Teng S-C. Importin KPNA2 is required for proper nuclear localization and multiple functions of NBS1. J Biol Chem. 2005;280:39594–600. doi:10.1074/jbc.M508425200.

56. Erben PB, Brunner K, Hecht M, Haderlein M, Büttner-Herold M, Agaimy A, et al. Low cytoplasmic and nuclear KPNA2 expression in radiotherapy-treated head and neck squamous cell cancer is associated with an adverse outcome. Int J Clin Exp Pathol. 2015;8:15814–24.

57. Teng S-C, Wu K-J, Tseng S-F, Wong C-W, Kao L. Importin KPNA2, NBS1, DNA repair and tumorigenesis. J Mol Histol. 2006;37:293–9. doi:10.1007/s10735-006-9032-y.

58. He L, Ding H, Wang J-H, Zhou Y, Li L, Yu Y-H, et al. Overexpression of karyopherin 2 in human ovarian malignant germ cell tumor correlates with poor prognosis. PLoS One. 2012;7:e42992. doi:10.1371/journal.pone.0042992.

59. Jensen JB, Munksgaard PP, Sorensen CM, Fristrup N, Birkenkamp-Demtroder K, Ulhoi BP, et al. High expression of karyopherin-alpha2 defines poor prognosis in non-muscle-invasive bladder cancer and in patients with invasive bladder cancer undergoing radical cystectomy. Eur Urol. 2011;59:841–8. doi:10.1016/j.eururo.2011.01.048.

60. Dahl E, Kristiansen G, Gottlob K, Klaman I, Ebner E, Hinzmann B, et al. Molecular profiling of laser-microdissected matched tumor and normal breast tissue identifies karyopherin alpha2 as a potential novel prognostic marker in breast cancer. Clin Cancer Res. 2006;12:3950–60. doi:10.1158/1078-0432.CCR-05-2090.

61. Winkler J, Ori A, Holzer K, Sticht C, Dauch D, Eiteneuer EM, et al. Prosurvival function of the cellular apoptosis susceptibility/importin-α1 transport cycle is repressed by p53 in liver cancer. Hepatology. 2014;60:884–95. doi:10.1002/hep.27207.

62. Singer S, Zhao R, Barsotti AM, Ouwehand A, Fazollahi M, Coutavas E, et al. Nuclear pore component Nup98 is a potential tumor suppressor and regulates posttranscriptional expression of select p53 target genes. Mol Cell. 2012;48:799–810. doi:10.1016/j.molcel.2012.09.020.

63. Desai A, Mitchison TJ. Microtubule polymerization dynamics. Annu Rev Cell Dev Biol. 1997;13:83–117. doi:10.1146/annurev.cellbio.13.1.83.

64. Brouhard GJ, Rice LM. Microtubule dynamics: an interplay of biochemistry and mechanics. Nat Rev Mol Cell Biol. 2018;19:451–63. doi:10.1038/s41580-018-0009-y.

65. Singer S, Ehemann V, Brauckhoff A, Keith M, Vreden S, Schirmacher P, Breuhahn K. Protumorigenic overexpression of stathmin/Op18 by gain-of-function mutation in p53 in human hepatocarcinogenesis. Hepatology. 2007;46:759–68. doi:10.1002/hep.21736.

66. Belletti B, Baldassarre G. Stathmin: a protein with many tasks. New biomarker and potential target in cancer. Expert Opin Ther Targets. 2011;15:1249–66. doi:10.1517/14728222.2011.620951.

67. Gavet O, Ozon S, Manceau V, Lawler S, Curmi P, Sobel A. The stathmin phosphoprotein family: intracellular localization and effects on the microtubule network. Journal of Cell Science. 1998;111 (Pt 22):3333–46.

68. Cassimeris L. The oncoprotein 18/stathmin family of microtubule destabilizers. Current Opinion in Cell Biology. 2002;14:18–24. doi:10.1016/S0955-0674(01)00289-7.

69. Bièche I, Maucuer A, Laurendeau I, Lachkar S, Spano AJ, Frankfurter A, et al. Expression of stathmin family genes in human tissues: non-neural-restricted expression for SCLIP. Genomics. 2003;81:400–10. doi:10.1016/S0888-7543(03)00031-4.

70. Hosoya H, Ishikawa K, Dohi N, Marunouchi T. Transcriptional and Post-transcriptional Regulation of pr22 (Op18) with Proliferation Control. Cell Struct. Funct. 1996;21:237–43. doi:10.1247/csf.21.237.

71. Nemunaitis J. Stathmin 1: a protein with many tasks. New biomarker and potential target in cancer. Expert Opin Ther Targets. 2012;16:631–4. doi:10.1517/14728222.2012.696101.

72. Price DK, Ball JR, Bahrani-Mostafavi Z, Vachris JC, Kaufman JS, Naumann RW, et al. The Phosphoprotein Op18/Stathmin is Differentially Expressed in Ovarian Cancer. Cancer Investigation. 2000;18:722–30. doi:10.3109/07357900009012204.

73. Singer S, Malz M, Herpel E, Warth A, Bissinger M, Keith M, et al. Coordinated expression of stathmin family members by far upstream sequence element-binding protein-1 increases motility in non-small cell lung cancer. Cancer Res. 2009;69:2234–43. doi:10.1158/0008-5472.CAN-08-3338.

74. Alli E, Yang J-M, Hait WN. Silencing of stathmin induces tumor-suppressor function in breast cancer cell lines harboring mutant p53. Oncogene. 2007;26:1003–12. doi:10.1038/sj.onc.1209864.

75. Mahipal A, Malafa M. Importins and exportins as therapeutic targets in cancer. Pharmacol Ther. 2016;164:135–43. doi:10.1016/j.pharmthera.2016.03.020.

76. Livak KJ, Schmittgen TD. Analysis of relative gene expression data using real-time quantitative PCR and the 2(-Delta Delta C(T)) Method. Methods. 2001;25:402–8. doi:10.1006/meth.2001.1262.

77. Conner EA, Lemmer ER, Omori M, Wirth PJ, Factor VM, Thorgeirsson SS. Dual functions of E2F-1 in a transgenic mouse model of liver carcinogenesis. Oncogene. 2000;19:5054–62. doi:10.1038/sj.onc.1203885.

78. Roessler S, Jia H-L, Budhu A, Forgues M, Ye Q-H, Lee J-S, et al. A unique metastasis gene signature enables prediction of tumor relapse in early-stage hepatocellular carcinoma patients. Cancer Res. 2010;70:10202–12. doi:10.1158/0008-5472.CAN-10-2607.

79. Saito F, Araki K, Yokobori T, Ishii N, Tsukagoshi M, Watanabe A, et al. High expression of karyopherin-α2 and stathmin 1 is associated with proliferation potency and transformation in the bile duct and gall bladder epithelia in the cases of pancreaticobiliary maljunction. J Surg Oncol. 2016;114:462–8. doi:10.1002/jso.24330.

80. Neumann O, Kesselmeier M, Geffers R, Pellegrino R, Radlwimmer B, Hoffmann K, et al. Methylome analysis and integrative profiling of human HCCs identify novel protumorigenic factors. Hepatology. 2012;56:1817–27. doi:10.1002/hep.25870.

81. Zhu W, Smith JW, Huang C-M. Mass spectrometry-based label-free quantitative proteomics. J Biomed Biotechnol. 2010;2010:840518. doi:10.1155/2010/840518.

82. Domon B, Aebersold R. Mass spectrometry and protein analysis. Science. 2006;312:212–7. doi:10.1126/science.1124619.

83. Wei J-H, Zhang ZC, Wynn RM, Seemann J. GM130 Regulates Golgi-Derived Spindle Assembly by Activating TPX2 and Capturing Microtubules. Cell. 2015;162:287–99. doi:10.1016/j.cell.2015.06.014.

84. Belletti B, Nicoloso MS, Schiappacassi M, Berton S, Lovat F, Wolf K, et al. Stathmin activity influences sarcoma cell shape, motility, and metastatic potential. Mol Biol Cell. 2008;19:2003–13. doi:10.1091/mbc.E07-09-0894.

85. Yoshimura T, Toyoda S, Kuramochi-Miyagawa S, Miyazaki T, Miyazaki S, Tashiro F, et al. Gtsf1/Cue110, a gene encoding a protein with two copies of a CHHC Zn-finger motif, is involved in spermatogenesis and retrotransposon suppression in murine testes. Dev Biol. 2009;335:216–27. doi:10.1016/j.ydbio.2009.09.003.

86. Gao D-Y, Ling Y, Lou X-L, Wang Y-Y, Liu L-M. GTSF1 gene may serve as a novel potential diagnostic biomarker for liver cancer. Oncol Lett. 2018;15:3133–40. doi:10.3892/ol.2017.7695.

87. Sass G, Barikbin R, Tiegs G. The multiple functions of heme oxygenase-1 in the liver. Z Gastroenterol. 2012;50:34–40. doi:10.1055/s-0031-1282046.

88. Kegelman TP, Das SK, Emdad L, Hu B, Menezes ME, Bhoopathi P, et al. Targeting tumor invasion: the roles of MDA-9/Syntenin. Expert Opin Ther Targets. 2015;19:97–112. doi:10.1517/14728222.2014.959495.

89. Hwangbo C, Tae N, Lee S, Kim O, Park OK, Kim J, et al. Syntenin regulates TGF-β1-induced Smad activation and the epithelial-to-mesenchymal transition by inhibiting caveolin-mediated TGF-β type I receptor internalization. Oncogene. 2016;35:389–401. doi:10.1038/onc.2015.100.

90. Rubin CI, Atweh GF. The role of stathmin in the regulation of the cell cycle. J Cell Biochem. 2004;93:242–50. doi:10.1002/jcb.20187.

91. Cassimeris L. Accessory protein regulation of microtubule dynamics throughout the cell cycle. Current Opinion in Cell Biology. 1999;11:134–41. doi:10.1016/S0955-0674(99)80017-9.

92. Larsson N, Marklund U, Gradin HM, Brattsand G, Gullberg M. Control of microtubule dynamics by oncoprotein 18: dissection of the regulatory role of multisite phosphorylation during mitosis. Mol. Cell. Biol. 1997;17:5530–9. doi:10.1128/MCB.17.9.5530.

93. BRATTSAND G, MARKLUND U, NYLANDER K, ROOS G, GULLBERG M. Cell-cycle-regulated phosphorylation of oncoprotein 18 on Ser16, Ser25 and Ser38. Eur J Biochem. 1994;220:359–68. doi:10.1111/j.1432-1033.1994.tb18632.x.

94. Luo XN, Mookerjee B, Ferrari A, Mistry S, Atweh GF. Regulation of phosphoprotein p18 in leukemic cells. Cell cycle regulated phosphorylation by p34cdc2 kinase. J Biol Chem. 1994;269:10312–8.

95. Huang L, Wang H-Y, Li J-D, Wang J-H, Zhou Y, Luo R-Z, et al. KPNA2 promotes cell proliferation and tumorigenicity in epithelial ovarian carcinoma through upregulation of c-Myc and downregulation of FOXO3a. Cell Death Dis. 2013;4:e745. doi:10.1038/cddis.2013.256.

96. Ma S, Zhao X. KPNA2 is a promising biomarker candidate for esophageal squamous cell carcinoma and correlates with cell proliferation. Oncol Rep. 2014;32:1631–7. doi:10.3892/or.2014.3381.

97. A. Curmi P, Gavet O, Charbaut E, Ozon S, Lachkar-Colmerauer S, Manceau V, et al. Stathmin and its Phosphoprotein Family. General Properties, Biochemical and Functional Interaction with Tubulin. Cell Struct. Funct. 1999;24:345–57. doi:10.1247/csf.24.345.

98. Melander Gradin H, Marklund U, Larsson N, Chatila TA, Gullberg M. Regulation of microtubule dynamics by Ca2+/calmodulin-dependent kinase IV/Gr-dependent phosphorylation of oncoprotein 18. Mol. Cell. Biol. 1997;17:3459–67. doi:10.1128/MCB.17.6.3459.

99. Malz M, Weber A, Singer S, Riehmer V, Bissinger M, Riener M-O, et al. Overexpression of far upstream element binding proteins: a mechanism regulating proliferation and migration in liver cancer cells. Hepatology. 2009;50:1130–9. doi:10.1002/hep.23051.

100. Kinoshita I, Leaner V, Katabami M, Manzano RG, Dent P, Sabichi A, Birrer MJ. Identification of cJun-responsive genes in Rat-1a cells using multiple techniques: increased expression of stathmin is necessary for cJun-mediated anchorage-independent growth. Oncogene. 2003;22:2710–22. doi:10.1038/sj.onc.1206371.

101. Chen Y-L, Uen Y-H, Li C-F, Horng K-C, Chen L-R, Wu W-R, et al. The E2F transcription factor 1 transactives stathmin 1 in hepatocellular carcinoma. Ann Surg Oncol. 2013;20:4041–54. doi:10.1245/s10434-012-2519-8.

102. Mackmull M-T, Klaus B, Heinze I, Chokkalingam M, Beyer A, Russell RB, et al. Landscape of nuclear transport receptor cargo specificity. Mol Syst Biol. 2017;13:962. doi:10.15252/msb.20177608.

103. Attwooll C, Lazzerini Denchi E, Helin K. The E2F family: specific functions and overlapping interests. EMBO J. 2004;23:4709–16. doi:10.1038/sj.emboj.7600481.

104. Verona R, Moberg K, Estes S, Starz M, Vernon JP, Lees JA. E2F activity is regulated by cell cycle-dependent changes in subcellular localization. Mol. Cell. Biol. 1997;17:7268–82. doi:10.1128/MCB.17.12.7268.

105. van der Watt, Pauline J, Ngarande E, Leaner VD. Overexpression of Kpnbeta1 and Kpnalpha2 importin proteins in cancer derives from deregulated E2F activity. PLoS One. 2011;6:e27723. doi:10.1371/journal.pone.0027723.

106. Wang C-I, Chen Y-Y, Wang C-L, Yu J-S, Chang Y-S, Yu C-J. mTOR regulates proteasomal degradation and Dp1/E2F1- mediated transcription of KPNA2 in lung cancer cells. Oncotarget. 2016;7:25432–42. doi:10.18632/oncotarget.8170.

107. Joerger AC, Fersht AR. The p53 Pathway: Origins, Inactivation in Cancer, and Emerging Therapeutic Approaches. Annu Rev Biochem. 2016;85:375–404. doi:10.1146/annurev-biochem-060815-014710.

108. Muller PAJ, Vousden KH. Mutant p53 in cancer: new functions and therapeutic opportunities. Cancer Cell. 2014;25:304–17. doi:10.1016/j.ccr.2014.01.021.

109. Alexandrova EM, Mirza SA, Xu S, Schulz-Heddergott R, Marchenko ND, Moll UM. p53 loss-of-heterozygosity is a necessary prerequisite for mutant p53 stabilization and gain-of-function in vivo. Cell Death Dis. 2017;8:e2661. doi:10.1038/cddis.2017.80.

110. Brosh R, Rotter V. When mutants gain new powers: news from the mutant p53 field. Nat Rev Cancer. 2009;9:701–13. doi:10.1038/nrc2693.

111. Meng X, Franklin DA, Dong J, Zhang Y. MDM2-p53 pathway in hepatocellular carcinoma. Cancer Res. 2014;74:7161–7. doi:10.1158/0008-5472.CAN-14-1446.

112. Kang M-S, Lee H-J, Lee J-H, Ku J-L, Lee KP, Kelley MJ, et al. Mutation ofp53 gene in hepatocellular carcinoma cell lines with HBX DNA. Int. J. Cancer. 1996;67:898–902. doi:10.1002/(SICI)1097-0215(19960917)67:6<898::AID-IJC22>3.0.CO;2-X.

113. Soussi T. HANDBOOK OF p53 MUTATION IN CELL LINES.

114. Chen X, Calvisi DF. Hydrodynamic transfection for generation of novel mouse models for liver cancer research. Am J Pathol. 2014;184:912–23. doi:10.1016/j.ajpath.2013.12.002.

115. Dauch D, Rudalska R, Cossa G, Nault J-C, Kang T-W, Wuestefeld T, et al. A MYC-aurora kinase A protein complex represents an actionable drug target in p53-altered liver cancer. Nat Med. 2016;22:744–53. doi:10.1038/nm.4107.

116. Stelma T, Chi A, van der Watt PJ, Verrico A, Lavia P, Leaner VD. Targeting nuclear transporters in cancer: Diagnostic, prognostic and therapeutic potential. IUBMB Life. 2016;68:268–80. doi:10.1002/iub.1484.

117. Flamini G, Curigliano G, Ratto C, Astone A, Ferretti G, Nucera P, et al. Prognostic significance of cytoplasmic p53 overexpression in colorectal cancer. An immunohistochemical analysis. European Journal of Cancer. 1996;32:802–6. doi:10.1016/0959-8049(95)00625-7.

118. Runnebaum IB, Kieback DG, Mobus VJ, Tong XW, Kreienberg R. Subcellular localization of accumulated p53 in ovarian cancer cells. Gynecol Oncol. 1996;61:266–71. doi:10.1006/gyno.1996.0137.

119. Midorikawa Y, Yamamoto S, Tsuji S, Kamimura N, Ishikawa S, Igarashi H, et al. Allelic imbalances and homozygous deletion on 8p23.2 for stepwise progression of hepatocarcinogenesis. Hepatology. 2009;49:513–22. doi:10.1002/hep.22698.

120. Ji J, Shi J, Budhu A, Yu Z, Forgues M, Roessler S, et al. MicroRNA expression, survival, and response to interferon in liver cancer. N Engl J Med. 2009;361:1437–47. doi:10.1056/NEJMoa0901282.

121. Howell B, Larsson N, GULLBERG M, Cassimeris L. Dissociation of the Tubulin-sequestering and Microtubule Catastrophe-promoting Activities of Oncoprotein 18/Stathmin. MBoC. 1999;10:105–18. doi:10.1091/mbc.10.1.105.

122. Wittmann T, Wilm M, Karsenti E, Vernos I. Tpx2, a Novel Xenopus Map Involved in Spindle Pole Organization. J Cell Biol. 2000;149:1405–18. doi:10.1083/jcb.149.7.1405.

123. Gruss OJ, Carazo-Salas RE, Schatz CA, Guarguaglini G, Kast J, Wilm M, et al. Ran Induces Spindle Assembly by Reversing the Inhibitory Effect of Importin α on TPX2 Activity. Cell. 2001;104:83–93. doi:10.1016/S0092-8674(01)00193-3.

124. Liu Q, Tu K, Zhang H, Zheng X, Yao Y, Liu Q. TPX2 as a novel prognostic biomarker for hepatocellular carcinoma. Hepatol Res. 2015;45:906–18. doi:10.1111/hepr.12428.

125. Cohen-Eliav M, Golan-Gerstl R, Siegfried Z, Andersen CL, Thorsen K, Ørntoft TF, et al. The splicing factor SRSF6 is amplified and is an oncoprotein in lung and colon cancers. J Pathol. 2013;229:630–9. doi:10.1002/path.4129.

126. Philley JV, Kannan A, Dasgupta S. MDA-9/Syntenin Control. J Cell Physiol. 2016;231:545–50. doi:10.1002/jcp.25136.

127. Liu X, Zhang X, Lv Y, Xiang J, Shi J. Overexpression of syntenin enhances hepatoma cell proliferation and invasion: potential roles in human hepatoma. Oncol Rep. 2014;32:2810–6. doi:10.3892/or.2014.3498.

128. Beekman JM, Coffer PJ. The ins and outs of syntenin, a multifunctional intracellular adaptor protein. Journal of Cell Science. 2008;121:1349–55. doi:10.1242/jcs.026401.

129. Franken NAP, Rodermond HM, Stap J, Haveman J, van Bree C. Clonogenic assay of cells in vitro. Nat Protoc. 2006;1:2315–9. doi:10.1038/nprot.2006.339.

130. Noetzel E, Rose M, Bornemann J, Gajewski M, Knüchel R, Dahl E. Nuclear transport receptor karyopherin-α2 promotes malignant breast cancer phenotypes in vitro. Oncogene. 2012;31:2101–14. doi:10.1038/onc.2011.403.

131. Yang Y, Guo J, Hao Y, Wang F, Li F, Shuang S, Wang J. Silencing of karyopherin α2 inhibits cell growth and survival in human hepatocellular carcinoma. Oncotarget. 2017;8:36289–304. doi:10.18632/oncotarget.16749.

132. Wang F, Wang L-X, Li S-L, Li K, He W, Liu H-T, Fan Q-X. Downregulation of stathmin is involved in malignant phenotype reversion and cell apoptosis in esophageal squamous cell carcinoma. J Surg Oncol. 2011;103:704–15. doi:10.1002/jso.21870.

133. Lu Y, Liu C, Cheng H, Xu Y, Jiang J, Xu J, et al. Stathmin, Interacting with Nf-kB, Promotes Tumor Growth and Predicts Poor Prognosis of Pancreatic Cancer. CMM. 2014;14:328–39. doi:10.2174/1566524014666140228120913.

134. Yurong L, Biaoxue R, Wei L, Zongjuan M, Hongyang S, Ping F, et al. Stathmin overexpression is associated with growth, invasion and metastasis of lung adenocarcinoma. Oncotarget. 2017;8:26000–12. doi:10.18632/oncotarget.11006.

135. Ma H-L, Jin S-F, Ju W-T, Fu Y, Tu Y-Y, Wang L-Z, et al. Stathmin is overexpressed and regulated by mutant p53 in oral squamous cell carcinoma. J Exp Clin Cancer Res. 2017;36:109. doi:10.1186/s13046-017-0575-4.

136. Yamaguchi H, Condeelis J. Regulation of the actin cytoskeleton in cancer cell migration and invasion. Biochim Biophys Acta. 2007;1773:642–52. doi:10.1016/j.bbamcr.2006.07.001.

137. Jampel HD. Effect of Brief Exposure to Mitomycin C on Viability and Proliferation of Cultured Human Tenon's Capsule Fibroblasts. Ophthalmology. 1992;99:1471–6. doi:10.1016/S0161-6420(92)31781-6.

138. Wang C-I, Wang C-L, Wang C-W, Chen C-D, Wu C-C, Liang Y, et al. Importin subunit alpha-2 is identified as a potential biomarker for non-small cell lung cancer by integration of the cancer cell secretome and tissue transcriptome. Int J Cancer. 2011;128:2364–72. doi:10.1002/ijc.25568.

139. Watanabe T, Noritake J, Kaibuchi K. Regulation of microtubules in cell migration. Trends Cell Biol. 2005;15:76–83. doi:10.1016/j.tcb.2004.12.006.

140. He L, Weber A, Levens D. Nuclear targeting determinants of the far upstream element binding protein, a c-myc transcription factor. Nucleic Acids Res. 2000;28:4558–65. doi:10.1093/nar/28.22.4558.

141. Fukumoto M, Sekimoto T, Yoneda Y. Proteomic analysis of importin α-interacting proteins in adult mouse brain. Cell Struct. Funct. 2011;36:57–67.

142. Hügel S, Depping R, Dittmar G, Rother F, Cabot R, Sury MD, et al. Identification of importin α 7 specific transport cargoes using a proteomic screening approach. Mol Cell Proteomics. 2014;13:1286–98. doi:10.1074/mcp.M112.026856.

143. Waldmann I, Wälde S, Kehlenbach RH. Nuclear import of c-Jun is mediated by multiple transport receptors. J Biol Chem. 2007;282:27685–92. doi:10.1074/jbc.M703301200.

144. Helin K, Wu CL, Fattaey AR, Lees JA, Dynlacht BD, Ngwu C, Harlow E. Heterodimerization of the transcription factors E2F-1 and DP-1 leads to cooperative trans-activation. Genes Dev. 1993;7:1850–61.

145. Bracken AP, Ciro M, Cocito A, Helin K. E2F target genes: unraveling the biology. Trends Biochem Sci. 2004;29:409–17. doi:10.1016/j.tibs.2004.06.006.

146. Malz M, Bovet M, Samarin J, Rabenhorst U, Sticht C, Bissinger M, et al. Overexpression of far upstream element (FUSE) binding protein (FBP)-interacting repressor (FIR) supports growth of hepatocellular carcinoma. Hepatology. 2014;60:1241–50. doi:10.1002/hep.27218.

147. Kruiswijk F, Labuschagne CF, Vousden KH. p53 in survival, death and metabolic health: a lifeguard with a licence to kill. Nat Rev Mol Cell Biol. 2015;16:393–405. doi:10.1038/nrm4007.

148. Dang CV, Lee WM. Nuclear and nucleolar targeting sequences of c-erb-A, c-myb, N-myc, p53, HSP70, and HIV tat proteins. J Biol Chem. 1989;264:18019–23.

149. Liang S-H, Clarke MF. Regulation of p53 localization. European Journal of Biochemistry. 2001;268:2779–83. doi:10.1046/j.1432-1327.2001.02227.x.

150. Choi M, Lee H, Rho HM. E2F1 Activates the Human p53 Promoter and Overcomes the Repressive Effect of Hepatitis B Viral X Protein (HBx) on the p53 Promoter. IUBMB Life. 2002;53:309–17. doi:10.1080/15216540290106350.

151. Parikh K, Cang S, Sekhri A, Liu D. Selective inhibitors of nuclear export (SINE)--a novel class of anti-cancer agents. J Hematol Oncol. 2014;7:78. doi:10.1186/s13045-014-0078-0.

152. Zheng Y, Gery S, Sun H, Shacham S, Kauffman M, Koeffler HP. KPT-330 inhibitor of XPO1-mediated nuclear export has anti-proliferative activity in hepatocellular carcinoma. Cancer Chemother Pharmacol. 2014;74:487–95. doi:10.1007/s00280-014-2495-8.

153. Azmi AS, Aboukameel A, Bao B, Sarkar FH, Philip PA, Kauffman M, et al. Selective inhibitors of nuclear export block pancreatic cancer cell proliferation and reduce tumor growth in mice. Gastroenterology. 2013;144:447–56. doi:10.1053/j.gastro.2012.10.036.

154. Cheng Y, Holloway MP, Nguyen K, McCauley D, Landesman Y, Kauffman MG, et al. XPO1 (CRM1) inhibition represses STAT3 activation to drive a survivin-dependent oncogenic switch in triple-negative breast cancer. Mol Cancer Ther. 2014;13:675–86. doi:10.1158/1535-7163.MCT-13-0416.

155. Sun H, Hattori N, Chien W, Sun Q, Sudo M, E-Ling GL, et al. KPT-330 has antitumour activity against non-small cell lung cancer. Br J Cancer. 2014;111:281–91. doi:10.1038/bjc.2014.260.

156. Kutay U, Bischoff FR, Kostka S, Kraft R, Görlich D. Export of Importin α from the Nucleus Is Mediated by a Specific Nuclear Transport Factor. Cell. 1997;90:1061–71. doi:10.1016/S0092-8674(00)80372-4.

157. Tian C, Sun R, Liu K, Fu L, Liu X, Zhou W, et al. Multiplexed Thiol Reactivity Profiling for Target Discovery of Electrophilic Natural Products. Cell Chem Biol. 2017;24:1416-1427.e5. doi:10.1016/j.chembiol.2017.08.022.

158. Yi T, Yi Z, Cho S-G, Luo J, Pandey MK, Aggarwal BB, Liu M. Gambogic acid inhibits angiogenesis and prostate tumor growth by suppressing vascular endothelial growth factor receptor 2 signaling. Cancer Res. 2008;68:1843–50. doi:10.1158/0008-5472.CAN-07-5944.

159. Farra R, Grassi G, Tonon F, Abrami M, Grassi M, Pozzato G, et al. The Role of the Transcription Factor E2F1 in Hepatocellular Carcinoma. Curr Drug Deliv. 2017;14:272–81. doi:10.2174/1567201813666160527141742.

160. Zhai J-M, Yin X-Y, Lai Y-R, Hou X, Cai J-P, Hao X-Y, et al. Sorafenib enhances the chemotherapeutic efficacy of S-1 against hepatocellular carcinoma through downregulation of transcription factor E2F-1. Cancer Chemother Pharmacol. 2013;71:1255–64. doi:10.1007/s00280-013-2120-2.

161. Perez EA. Microtubule inhibitors: Differentiating tubulin-inhibiting agents based on mechanisms of action, clinical activity, and resistance. Mol Cancer Ther. 2009;8:2086–95. doi:10.1158/1535-7163.MCT-09-0366.

162. Alli E, Bash-Babula J, Yang J-M, Hait WN. Effect of stathmin on the sensitivity to antimicrotubule drugs in human breast cancer. Cancer Res. 2002;62:6864–9.

163. Malesinski S, Tsvetkov PO, Kruczynski A, Peyrot V, Devred F. Stathmin potentiates vinflunine and inhibits Paclitaxel activity. PLoS One. 2015;10:e0128704. doi:10.1371/journal.pone.0128704.

164. Wang R, Dong K, Lin F, Wang X, Gao P, Wei S-H, et al. Inhibiting proliferation and enhancing chemosensitivity to taxanes in osteosarcoma cells by RNA interference-mediated downregulation of stathmin expression. Mol Med. 2007;13:567–75. doi:10.2119/2007-00046.Wang.

8 LIST OF FIGURES

9 LIST OF TABLES

10 PUBLICATIONS

Publications in peer-reviewed journals

Holzer K, **Drucker E**, Roessler S, Dauch D, Heinzmann F, Waldburger N, Eiteneuer EM, Herpel E, Breuhahn K, Zender L, Schirmacher P, Ori A, Singer S. Proteomic Analysis Reveals GMP Synthetase as p53 Repression Target in Liver Cancer. Am J Pathol. 2017 Feb;187(2):228-235. doi: 10.1016/j.ajpath.2016.09.022.

Winkler J, Roessler S, Sticht C, DiGuilio AL, **Drucker E**, Holzer K, Eiteneuer E, Herpel E, Breuhahn K, Gretz N, Schirmacher P, Ori A, Singer S. Cellular apoptosis susceptibility (CAS) is linked to integrin β1 and required for tumor cell migration and invasion in hepatocellular carcinoma (HCC). Oncotarget. 2016 Apr 19;7(16):22883-92. doi: 10.18632/oncotarget.8256.

Holzer K, **Drucker E**, Oliver S, Winkler J, Eiteneuer E, Herpel E, Breuhahn K, Singer S. Cellular apoptosis susceptibility (CAS) is overexpressed in thyroid carcinoma and maintains tumor cell growth: A potential link to the BRAFV600E mutation. Int J Oncol. 2016 Apr;48(4):1679-87. doi: 10.3892/ijo.2016.3388.

Genov M, Kreiseder B, Nagl M, **Drucker E**, Wiederstein M, Muellauer B, Krebs J, Grohmann T, Pretsch D, Baumann K, Bacher M, Pretsch A, Wiesner C. Tetrahydroanthraquinone Derivative (±)-4-Deoxyaustrocortilutein Induces Cell Cycle Arrest and Apoptosis in Melanoma Cells via Upregulation of p21 and p53 and Downregulation of NF-kappaB. J Cancer. 2016 Mar 12;7(5):555-68. doi: 10.7150/jca.13614.

Krapfenbauer K, **Drucker E**, Thurnher D.Identification of tumour-related proteins as potential screening markers by proteome analysis-protein profiles of human saliva as a predictive and prognostic tool. EPMA J. 2014 Nov 28;5(1):20. doi: 10.1186/1878-5085-5-20.

Drucker E, Krapfenbauer K. Pitfalls and limitations in translation from biomarker discovery to clinical utility in predictive and personalised medicine. EPMA J. 2013 Feb 25;4(1):7. doi: 10.1186/1878-5085-4-7.

11 ACKNOWLEDGMENTS

First of all, I want to thank Prof. Dr. Stephan Singer, Prof. Dr. Kai Breuhahn and Prof. Dr. Peter Schirmacher for the giving me the opportunity to conduct this thesis at the Institute of Pathology Heidelberg. I want to thank Prof. Dr. Ursula Klingmüller and Kai for revising this thesis and Prof. Dr. Stefan Wölfl and Prof. Dr. Ilse Hofmann for being part of my defense committee.

My greatest thank goes to AG Singer: Stephan, Eva and Kerstin. Stephan, thank you so much for your patience and support and for giving me the opportunity to realize my own ideas. Eva, I appreciate your help and support in every day lab work but also for being a friend beyond work life.

I also want to thank the group members of AG Breuhahn and AG Rössler. Kai, thank you for "adopting" me, your support and for understanding my sense of humor – even though I will never be able to say your name correctly. Sofia, I appreciate that you answered my manifold questions. Michaela, thank you for always providing a helpful hand and for all the laughter we shared. Furthermore, I want to thank Steffi and Geli for being there when help was needed. And, of course I want to thank Caro for her professional opinion and critical input, but also for her friendship.

Caro, Eva, Michaela, Sarah, Geli, Jenny, Sarah (the other one), Fabian, Matthias, Maria, Minakshi, Nadine, Andreas: you made my time here in Heidelberg one of the best times of my life.

I want to thank my boyfriend Fredl for loving and supporting me through more than 10 years of different studies at different universities and countries. I want to thank my dog Beluga for her patience with me when I was working instead of playing with her outside. You were the best dog in the world. Hanja, thank you for putting up with me, correcting this thesis and of course for listening to me complaining about doing a PhD. Furthermore, I want to thank my sister Steffi for always being there for me. To know that you are proud on me made me feel strong. Last, I want to thank my mother for telling me I can be whatever I wanted to be and reach whatever goal I wanted to reach. I know you would be proud on me.

And thanks to everybody I forgot to mention here…

APPENDIX

Table A.1: List of most downregulated proteins following KPNA2 depletion as analyzed by quantitative proteomics. adj. p-value: adjusted p-value.

ID	fold change [log_2]	p-value	adj. p-value	short name
P52292	-4.06652799	2.22E-08	3.91E-05	IMA1_HUMAN
Q13247	-2.086579987	0.01177021	0.21331985	SRSF6_HUMAN
Q8WW33	-1.469968789	0.00435593	0.16302233	GTSF1_HUMAN
O00560	-1.390320354	0.00016865	0.0707303	SDCB1_HUMAN
P20700	-1.31021712	5.52E-05	0.04182953	LMNB1_HUMAN
P28074	-1.166164952	0.00298521	0.15727965	PSB5_HUMAN
P62314	-1.094443804	0.05202138	0.36435692	SMD1_HUMAN
Q9Y4E8	-1.062159153	0.03505649	0.33313144	UBP15_HUMAN
Q9Y4Z0	-1.008477528	0.00051366	0.08032323	LSM4_HUMAN
Q10471	-1.007840338	0.00046061	0.08032323	GALT2_HUMAN
P30154	-0.957951503	0.00061188	0.08274524	2AAB_HUMAN
P16949	-0.924246545	0.00347536	0.15727965	STMN1_HUMAN
P29590	-0.918142433	0.04884305	0.36117836	PML_HUMAN
P20618	-0.863252271	0.08238103	0.42518835	PSB1_HUMAN
Q99436	-0.809284713	0.09842096	0.44565474	PSB7_HUMAN
P62847	-0.795179066	0.13272856	0.50303967	RS24_HUMAN
Q9UMY4	-0.79109985	0.01681844	0.26165324	SNX12_HUMAN
Q9Y508	-0.785957085	0.0054811	0.18051136	RN114_HUMAN
Q15269	-0.783813019	0.0207403	0.28120308	PWP2_HUMAN
Q13509	-0.767898445	0.03317723	0.32693324	TBB3_HUMAN
Q53GQ0	-0.761867846	0.04233141	0.34514615	DHB12_HUMAN
P49589	-0.757038963	0.04747328	0.35973287	SYCC_HUMAN
O94905	-0.751309351	0.00585276	0.18051136	ERLN2_HUMAN
P46783	-0.745375832	0.02355126	0.29019833	RS10_HUMAN
Q13620	-0.741820141	0.01586513	0.25355364	CUL4B_HUMAN
Q96PD2	-0.738805068	0.05990561	0.38735155	DCBD2_HUMAN
P17858	-0.726751287	0.0085131	0.19754389	PFKAL_HUMAN
P14174	-0.721575039	0.08319954	0.42518835	MIF_HUMAN
Q9UHD1	-0.712569683	0.00149226	0.12492383	CHRD1_HUMAN
Q9Y617	-0.695984681	0.00020117	0.0707303	SERC_HUMAN
P48449	-0.692810446	0.02387647	0.29149185	ERG7_HUMAN
Q13404	-0.688605589	0.00045027	0.08032323	UB2V1_HUMAN
P16401	-0.687965271	0.05514733	0.37531168	H15_HUMAN
Q9BVP2	-0.681372826	0.03195762	0.32121512	GNL3_HUMAN
P22392	-0.67443197	0.00707494	0.1863338	NDKB_HUMAN

Table A.2: List of most upregulated proteins following KPNA2 depletion as analyzed by quantitative proteomics. adj. p-value: adjusted p-value.

ID	fold change [log_2]	p-value	adj. p-value	short name
P04908	1.167055939	0.0250581	0.29518733	H2A1B_HUMAN
Q9NQW6	1.079326388	0.0395878	0.34283422	ANLN_HUMAN
Q99661	1.028898034	0.01092308	0.20890123	KIF2C_HUMAN
Q9UKA9	0.999421233	0.0045918	0.16817467	PTBP2_HUMAN
P61513	0.983972061	0.0616739	0.39426441	RL37A_HUMAN
Q9BS26	0.971714852	0.00435839	0.16302233	ERP44_HUMAN
P29992	0.91177934	0.07054658	0.40869439	GNA11_HUMAN
O14907	0.84958316	0.00370485	0.16085146	TX1B3_HUMAN
P53814	0.840950498	0.00527634	0.18036487	SMTN_HUMAN
P24928	0.808662706	0.01004873	0.20305363	RPB1_HUMAN
P21980	0.806458348	0.00051554	0.08032323	TGM2_HUMAN
Q9ULW0	0.803453446	7.14E-05	0.04182953	TPX2_HUMAN
O75607	0.783219728	0.00769629	0.19328676	NPM3_HUMAN
O94760	0.782676485	0.00690763	0.1863338	DDAH1_HUMAN
Q15437	0.767441695	0.00101332	0.10478948	SC23B_HUMAN
Q969G3	0.766420203	0.05385049	0.37125163	SMCE1_HUMAN
Q9P035	0.759124722	0.00143272	0.12492383	HACD3_HUMAN
Q9NUQ9	0.755571782	0.00692104	0.1863338	FA49B_HUMAN
Q9Y5J7	0.752409982	0.00232429	0.15715779	TIM9_HUMAN
Q9UI42	0.741567824	0.00854001	0.19754389	CBPA4_HUMAN
Q9BRP1	0.741163495	0.00284629	0.15727965	PDD2L_HUMAN
Q96QD8	0.721004462	0.00872268	0.19914888	S38A2_HUMAN
Q96I24	0.702284924	0.0014667	0.12492383	FUBP3_HUMAN
Q9H501	0.698070824	0.00037662	0.08032323	ESF1_HUMAN
P11388	0.682751058	0.00054828	0.08032323	TOP2A_HUMAN
P14635	0.673542773	0.0150071	0.25000899	CCNB1_HUMAN
O14617	0.668025863	0.10235619	0.45002029	AP3D1_HUMAN
Q9Y312	0.663846976	0.17775453	0.5590205	AAR2_HUMAN
P03956	0.65947673	0.0032367	0.15727965	MMP1_HUMAN
Q92804	0.65794589	0.16252235	0.52812254	RBP56_HUMAN
Q6RFH5	0.656458338	0.15869672	0.52279992	WDR74_HUMAN
Q92879	0.642268976	0.13078413	0.50303967	CELF1_HUMAN
P61204	0.606797204	0.01086535	0.20890123	ARF3_HUMAN
P00367	0.588374932	0.05252546	0.36497926	DHE3_HUMAN
O94973	0.578610725	0.08951013	0.44314581	AP2A2_HUMAN

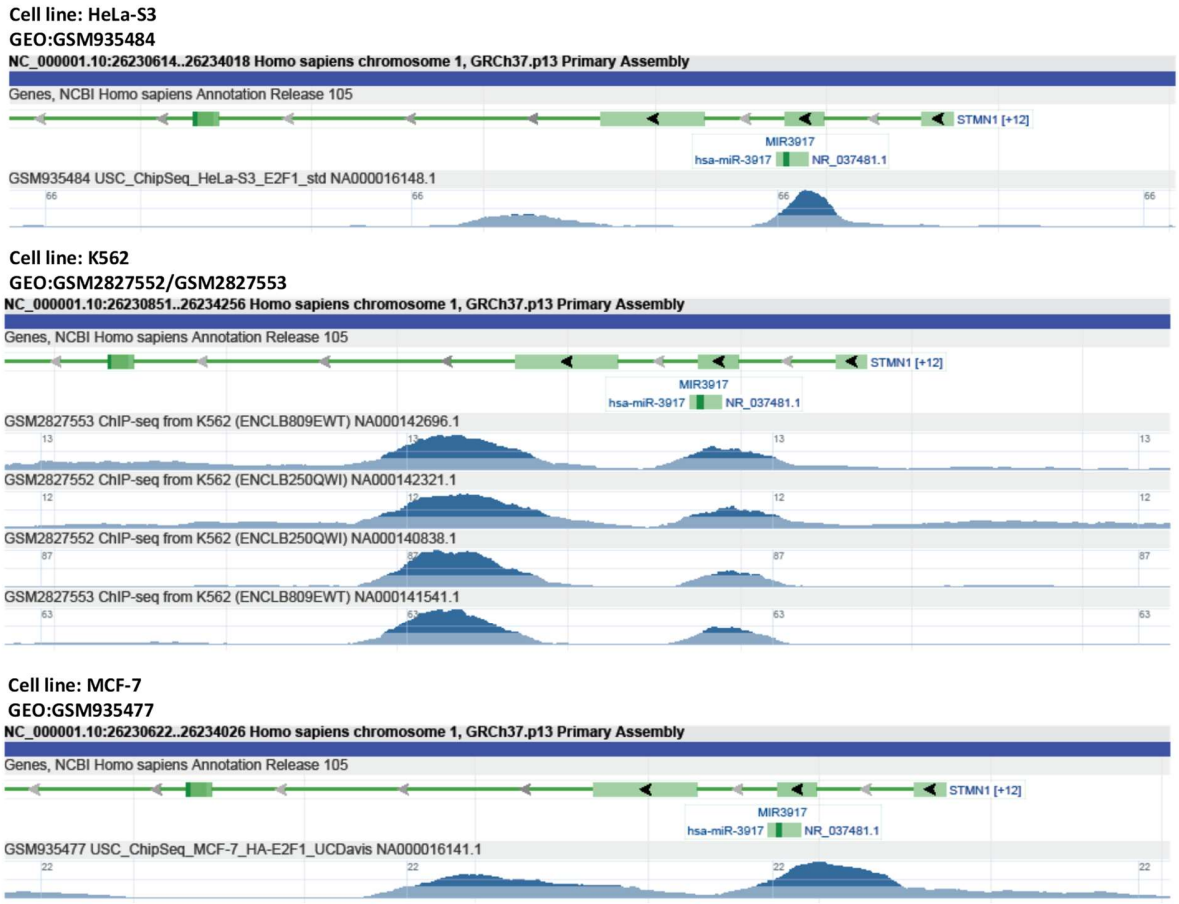

Figure A.1: Publicly available ChIP-Seq datasets reveal binding sites for E2F1 within the STMN1 promoter region. Green line: *STMN1* gene including regulator regions. STMN1 [+12]: start codon plus 12 kbp. GEO: gene omnibus accession number.

ERKLÄRUNG GEMÄß §8 DER PROMOTIONSORDNUNG

Hiermit erkläre ich, dass ich die vorgelegte Dissertation “Functional and mechanistic characterization of the nuclear import receptor karyopherin-α2 in liver cancer“ selbstständig verfasst und keine anderen als die angegebenen Quellen und Hilfsmittel benutzt habe. Des Weiteren bestätige ich, dass ich an keiner anderen Stelle ein Prüfungsverfahren beantragt bzw. die Dissertation in dieser oder einer anderen Form bereits als Prüfungsarbeit verwendet oder einer anderen Fakultät als Dissertation vorgelegt habe.

Heidelberg, den 09.03.2019

Elisabeth Drucker